Departament d'Enginyeria Mecànica

UNIVERSITAT POLITÈCNICA DE CATALUNYA

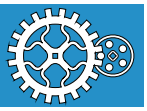

Contributions to dynamic pile-soil interaction modelling

by

Kenny Fernando Conto Quispe

Thesis submitted to obtain the title of
Doctor in Mechanical, Fluids and Aerospace Engineering

by the
Universitat Politècnica de Catalunya (UPC)

16th November 2023

Abstract

The development of more accurate, computationally efficient and practical methodologies for a better understanding of dynamic soil-structure interaction and prediction of ground-borne vibration levels in the vicinity of man-made induced vibration sources is greatly sought-after by practising engineers, as these vibration levels might cause harmful effects on buildings and/or on their occupants. This dissertation aims to develop an approach that requires low computational resources to simulate the response of pile-soil systems accurately and is intended to be simplistic in formulation terms towards a more practical methodology. Thus, an efficient, fully coupled three-dimensional approach for solving pile-soil interaction problems is presented in the current dissertation, as well as its numerical and experimental validation. The proposed approach employs classic rod and Euler-Bernoulli theories to model the pile. The soil, in the presence of the pile's corresponding cavity, is modelled as an elastic half-space using an emerging meshless methodology that approximates the dynamic unknown states of the soil to linear combinations of the fundamental solution of the medium. Thus, this methodology, referred to as the singular boundary method, is adapted in this dissertation to deal with three-dimensional elastodynamic problems. Furthermore, the proposed piled foundation model allows the rotational motions and reaction torques associated with the pile to be accounted for in the pile-soil interaction, and their contribution to the accuracy of the scheme is assessed. To achieve an acceptable trade-off between the accuracy and numerical performance of the methodology, a comprehensive criterion to define the discretization scheme is also proposed. The robustness of the approach is studied in the context of single-pile and pile-group systems, the latter with and without attaching its corresponding pile cap, where the relevance of including torsional motions in the piles-cap coupling is discussed. Comparisons with existing approaches show that the formulation provides strong computational advantages to detailed modelling approaches, such as the ones based on the three-dimensional finite element-boundary element method, as well as overcoming the fundamental limitations of plain-strain and axisymmetric methods. Finally, a set of experimental tests on a full-scale single-pile foundation and a 2×2 pile-group system embedded in layered soil were conducted to validate the modelling strategy for the simulated responses.

Acknowledgements

The work presented in this dissertation was conducted at the Mechanical Engineering Department at the Universitat Politècnica de Catalunya. The research topic was suggested by Dr Robert Arcos and Dr Arnau Clot, who also served as my supervisors. It has been a pleasure to work with them during this period, during which they consistently encouraged me to achieve all the initial goals set for this research. I am grateful for their continuous support and the leisure time we spent together, engaging in endless discussions on the physical significance of the complex mathematical formulations required for this project.

Special thanks are extended to Dr Evangelos Ntotsios and Professor David Thompson of the University of Southampton for their interest in this project and the countless insightful discussions that we had.

My sincere gratitude goes to Dr Jordi Romeu for the opportunity he provided me to be a research member of the Acoustical and Mechanical Engineering Laboratory (LEAM) and for his extensive efforts in funding the implementation of the full-scale piled foundation test facilities, which was a crucial support for the experimental validation of the proposed pile-soil model. I would also like to express my appreciation to my LEAM colleagues, especially Milad, Victor, Guillermo, John, and Behshad, who directly and indirectly made this research possible through their support, suggestions, and valuable friendship.

Last but not least, I would like to express my thanks to my parents and siblings for their continuous emotional support and comfort throughout this research. I also extend my gratitude to Mr Wilfredo Callasi and Mr Ignacio Velasquez for their trust in me and encouragement to undertake this challenging work, and my sincere thanks also go to my friends Andrea Silva and Maria Espinoza, who welcomed me as a member of their family just when I had moved to this part of the world.

This research has been carried out with the financial support of the LEAM and through the scholarship *"Generación del Bicentenario de la República del Perú"* provided by the *"Programa Nacional de Becas y Crédito Educativo"* (PRONABEC).

Dedication

To my beloved parents, Aurélio and Rufina, for the countless lessons, guidance, and, most profoundly, for the unwavering and boundless love they have showered upon me throughout my journey.

To my cherished siblings, David, Patrícia, and Zulema, who transformed my childhood into the most treasured chapter of my existence.

Contents

List of Tables

List of Figures

List of abbreviations

1D	One-dimensional.
2.5D	Two-and-a-half-dimensional.
2D	Two-dimensional.
3D	Three-dimensional
aFE-PML	Approach based on a axisymmetric finite elements & perfectly matched layers.
BE	Boundary element.
BEM	Boundary element method.
FE	Finite element.
FEM	Finite element method.
FRF	Frequency response function.
IPCT	Institut Politècnic del Campus de Terrassa.
LEAM	The acoustical and Mechanical Engineering Laboratory.
MASW	Multichannel analysis of surface waves.
MFS	Method of fundamental solutions.
NPW	Nodes per wavelength.
NRC	No rotational coupling.
OIF	Origin intensity factor.
PiP	Pipe-in-Pipe.
PML	Perfectly matched layers.
PSPI	Pile-soil-pile interaction.
SASW	Spectral analysis of surface waves.
SBM	Singular boundary method.
SMM	Stiffness matrix method.
SSI	Soil-structure interaction.

TLM	Thin-layer method.
UPC	Universitat Politècnica de Catalunya.

List of symbols

i	Index notation for denoting the three Cartesian coordinates $i = x, y, z$.
v	Index notation for denoting the v-th virtual source, $v = 1, 2, ..., N_{\mathrm{v}}$.
c	Index notation for denoting the c-th collocation point, $c = 1, 2, ..., N_{\mathrm{c}}$.
N_{p}	Pile-soil interface represented by N_{p} arbitrary ring-shaped segments along the pile and denoted by points placed at the pile's centroid axis.
N_{s}	Set of N_{s} collocation points uniformly distributed along the pile-soil interface along each N_{p} ring-shaped segment.
i	Imaginary number $\sqrt{-1}$.
ω	Angular frequency.
A_{p}	Cross-sectional area of a single-pile.
L_{p}	Pile length.
E_{p}	Elastic modulus of the pile.
G_{p}	Shear modulus of the pile.
ρ_{p}	Mass density of the pile.
I_{p}	Second moment of area of the pile's cross-section.
$u_{\mathrm{p}i}$	Scalar displacement in the i-direction of the pile in the time domain.
$\phi_{\mathrm{p}i}$	Scalar rotation in the i-direction of the pile in the time domain.
$U_{\mathrm{p}i}$	Scalar displacement in the i-direction of the pile in the frequency domain.
$\theta_{\mathrm{p}i}$	Scalar rotation in the i-direction of the pile in the frequency domain.
f_i	Harmonic force applied in the i-direction to the pile in the time domain.
F_i	Harmonic force applied in the i-direction to the pile in the frequency domain.
m_i	Harmonic moment applied in the i-direction to the pile in the time domain.
M_i	Harmonic moment applied in the i-direction to the pile in the frequency domain.
ε_{ij}	The relative error associated with the FRF of displacements of the coupled pile-soil system in the i-direction induced by forces acting in the j-direction.

$\mathbf{x}$, $\mathbf{y}$	Points in the Euclidean 3D physical space $\mathbb{R}^3$.
$\mathbf{U}(\mathbf{y})$, $\mathbf{T}(\mathbf{y})$	Dynamic unknown states of displacements and traction, respectively, evaluated at the point $\mathbf{y}$.
$\mathbf{U}_\mathrm{b}$, $\mathbf{T}_\mathrm{b}$	Column vectors of the dynamic unknown states of displacements and traction that collect the soil reaction evaluated at the N_c collocation points.
$\mathbf{S}$	Column vector that stores all virtual sources $\mathbf{S}^v$ applied at the collocation points.
$\mathbf{H}(\mathbf{y}, \mathbf{x}^v, \omega)$	Elastodynamic fundamental solution in the frequency-domain for displacement, and its associated traction $\mathbf{H}^\tau(\mathbf{y}, \mathbf{x}^v, \omega)$, evaluated at the point $\mathbf{y}$ and induced by a source located at the point $\mathbf{x}^v$.
$\mathbf{H}_\mathrm{cc}$	The origin intensity factors matrices associated to the Dirichlet's boundary-condition.
$\mathbf{H}^\tau_\mathrm{cc}$	The origin intensity factors matrices associated to the Neumann's boundary-condition.
$\mathbf{H}_\mathrm{bb}$	The FRF matrix of the soil that relates the displacements $\mathbf{U}_\mathrm{b}$ with the virtual sources $\mathbf{S}$.
$\mathbf{H}^\tau_\mathrm{bb}$	The FRF matrix of the soil that relates the traction $\mathbf{T}_\mathrm{b}$ with the virtual sources $\mathbf{S}$.
$\mathbf{F}_\mathrm{p}$	Concentrate external loads vector acting at the pile head(s).
$\mathbf{F}_\mathrm{s}$	Concentrate external loads vector acting anywhere on the soil.
$\mathbf{U}_\mathrm{p}$	The vector that collects the displacement and rotation at the N_p pile centroid points.
$\mathbf{P}_\mathrm{p}$	The vector that collects the interaction forces and moments at the N_p pile centroid points.
$\mathbf{U}^\mathrm{p}_\mathrm{b}$	Pile displacement vector evaluated at the N_c collocation points.
$\mathbf{U}^\mathrm{s}_\mathrm{b}$	Soil-cavity displacement vector evaluated at the N_c collocation points.
$\mathbf{P}^\mathrm{p}_\mathrm{b}$	Pile interaction-force vector evaluated at the N_c collocation points.
$\mathbf{P}^\mathrm{s}_\mathrm{b}$	Soil-cavity interaction-force vector evaluated at the N_c collocation points.
$\mathbf{T}^\mathrm{s}_\mathrm{b}$	Soil-cavity traction vector evaluated at the N_c collocation points.
$\mathbf{W}_\mathrm{A}$	Diagonal matrix that contains the areas of influence of the N_c collocation points.

$\mathbf{W}$	Transformation matrix that relates the six degrees of freedom of the N_p pile centroid points with the three-component motion of the N_c collocation points. Furthermore, its transposed form $\mathbf{W}^\mathrm{T}$ relates the three-component forces acting in the pile-soil interface with the three-component forces and moments acting on the pile's centroid axis.
$\mathbf{U}_\mathrm{h}$	Displacement vector of the coupled pile-soil system evaluated at the pile head.
$\mathbf{U}_\mathrm{s}$	Displacement vector of the coupled pile-soil system evaluated at an arbitrary point in the soil.
$\mathbf{H}_\mathrm{sb}$	The FRF matrix of the soil that relates the displacements $\mathbf{U}_\mathrm{s}$ with the virtual sources $\mathbf{S}$.
$\mathbf{H}_\mathrm{ph}$	The FRF matrix of the pile at the N_p pile centroid points induced by force acting at the pile head.
$\mathbf{H}_\mathrm{pp}$	The FRF matrix of the pile at the N_p pile centroid points.
$\mathbf{H}_\mathrm{hh}$	The FRF matrix of the pile head.
$\mathbf{H}_\mathrm{hp}$	The FRF matrix of the pile head induced by forces acting at the N_p pile centroid points.
$\mathbf{H}^\mathrm{c}_\mathrm{hh}$	The FRF matrix of the coupled pile-soil system that relates the displacements $\mathbf{U}_\mathrm{h}$ with the external force $\mathbf{F}_\mathrm{p}$.
$\mathbf{H}^\mathrm{c}_\mathrm{hf}$	The FRF matrix of the coupled pile-soil system that relates the displacements $\mathbf{U}_\mathrm{h}$ with the external force $\mathbf{F}_\mathrm{s}$.
$\mathbf{H}^\mathrm{c}_\mathrm{sh}$	The FRF matrix of the coupled pile-soil system that relates the displacements $\mathbf{U}_\mathrm{s}$ with the external force $\mathbf{F}_\mathrm{p}$.
$\mathbf{H}^\mathrm{c}_\mathrm{sf}$	The FRF matrix of the coupled pile-soil system that relates the displacements $\mathbf{U}_\mathrm{s}$ with the external force $\mathbf{F}_\mathrm{s}$.
$\mathbf{D}$	Dynamic stiffness matrix of the pile cap.
$\mathbf{K}$	Stiffness matrix of the pile cap.
$\mathbf{M}$	Mass matrix of the pile cap.
$\mathbf{U}^\mathrm{cap}_\mathrm{nb}$	Displacements of the pile cap associated with the 3D FE nodes not located on any of the piles-cap coupling surfaces.
$\mathbf{U}^\mathrm{cap}_\mathrm{b}$	Displacements of the pile cap associated with the 3D FE nodes located on any of the piles-cap coupling surfaces.
$\mathbf{F}^\mathrm{cap}_\mathrm{nb}$	External forces acting on the pile cap at the 3D FE nodes not located on any of the piles-cap coupling surfaces.

$\mathbf{F}_{\mathrm{b}}^{\mathrm{cap}}$	External forces acting on the pile cap at the 3D FE nodes located on any of the piles-cap coupling surfaces.
$\mathbf{P}_{\mathrm{b}}^{\mathrm{cap}}$	Piles-cap interaction-force vector evaluated at the 3D FE nodes located on any of the piles-cap coupling surfaces.
$\mathbf{P}_{\mathrm{h}}^{\mathrm{pile}}$	Piles-cap interaction-force vector evaluated at pile heads.
$\mathbf{W}_{\mathrm{b}}$	Transformation matrix that relates the six degrees of freedom of the pile heads with the three-component motion of the 3D FE nodes located on any of the piles-cap coupling surfaces

Chapter 1

Introduction

> *"There was probably no subject before engineers in the country today, particularly those dealing with road transport, that caused more trouble, or gave rise to more concern than vibration".*
>
> Hyde and Lintern [6], England in 1929.

The rapid growth of the urban population in metropolitan areas often gives rise to challenges regarding urban distribution, especially when geographical constraints such as the limited availability of land for territorial expansion stand. Complications are especially arising in densely populated cities, where urban environments are constantly updating their spatial distribution to implement additional transport links, address the scarcity of residential areas, or provide essential facilities. While these measures aim to enhance people's quality of life and foster urban dynamics, they also give rise to undesirable side effects, with ground-borne noise and vibration being a significant concern. The increasing number of construction activities, denser road traffic, and the operation of the every-day-larger urban railway network contribute to this issue, generating noise and vibration pollution that cause discomfort to residents in nearby buildings and may also affect the functioning of precision machinery or the structural integrity of heritage buildings.

To mitigate these undesired effects, governments have established laws and regulations to limit the exposure of citizens to ground-borne noise and vibration, forcing infrastructure developers and construction managers to prove that the levels of vibration and re-radiated noise in affected buildings (existing or to be constructed) will comply with the particular regulations in place. However, accurately predicting building vibration and re-radiated noise in new scenarios is a

strongly challenging task. The wide range of variables involved in the definition of important subsystems such as the building, the foundations, the soil and the source, as well as the high uncertainty on some of these parameters, especially the ones associated with the soil, are the main causes of this modelling complexity. Thus, engineers and researchers working on this topic face the challenge of achieving accurate predictions with reduced levels of uncertainty and limited computational resources.

In such a sense, developing reliable prediction approaches for ground-borne noise and vibration problems in buildings able to offer a good trade-off between accuracy and computational costs remains an ongoing challenge. Such models would help designers predict noise and vibration levels accurately and adopt countermeasures when these levels exceed the allowed thresholds. Among several complex phenomena involved in such problems, and of particular interest to the present thesis, these methodologies should enable detailed modelling of the three-dimensional dynamic interaction between the building foundations and the soil, especially at high frequencies, where the ground-borne noise and vibration problem takes importance.

1.1 Motivation for the research

From the early days when ground-borne vibration was identified as a harmful effect on buildings and their occupants, researchers have made efforts to develop prediction tools and solutions to this complex structural dynamics problem. Since then, different prediction models have been proposed for modelling the diverse soil-structure interaction scenarios that may be encountered when dealing with the assessment of ground-borne noise and vibration in buildings due to ground vibration sources. However, the existing strategies generally suffer from either limited flexibility/accuracy or high computational costs. The former family of prediction models counts on various alternatives that can provide reliable results with low computational costs but lack the ability to model complex soil-structure scenarios adequately or to account for the full three-dimensional nature of the wave propagation pattern in the soil. On the other side, prediction models based on numerical approaches are considered a good alternative when detailed studies are required or when dealing with non-conventional soil-structure problems. However, the computational efficiency of these models is low, especially when high-frequency responses are intended to be calculated, which is the situation encountered when developing ground-borne noise and vibration assessment studies. The mentioned disadvantages of the different existing prediction models, combined with the increasing amount and complexity of the

problems to be addressed, present a challenge in finding detailed modelling strategies that can effectively handle these engineering problems without becoming impractical due to excessive computational resource requirements. The present dissertation is mainly focused on the case of piled foundations, while the proposed method can be easily adapted to other foundation systems.

1.2 Objectives of the research

This research aims to contribute to the development of practical methodologies to deal with soil-structure interaction problems involving piled foundations in the context of ground-borne noise and vibration assessment studies in buildings. The main objective is to actually develop an approach that requires low computational resources to simulate the response of pile-soil systems accurately. Furthermore, the resulting approach is intended to be simplistic in formulation terms towards a more practical methodology. Thus, the approach to be developed in the framework of this thesis would:

- be able to accurately simulate the three-dimensional dynamic response of pile-soil systems embedded in homogeneous or layered soils;
- offers a suitable trade-off between the accuracy of predicted results and the computational resources required;
- be designed on the basis of a simplistic formulation framework that minimises the complexity of the corresponding algorithm.

In order to reach these goals, the following specific objectives are proposed:

- to develop a pile-soil modelling strategy based on classical linear structural member theories for modelling the pile and an advanced meshless approach to model the soil, offering accuracy, computational efficiency, and a simple formulation;
- to test the importance of detailed pile-soil coupling conditions and to assess in which situations they can be relaxed;
- to develop the method for both single-pile and pile-group systems;

- to numerically verify the proposed approach compared with existing numerical methods;
- to study the limitations of existing simple approaches with respect to the proposed one;
- to experimentally validate the proposed approach.

1.3 Outline of the dissertation

The present thesis dissertation is divided into six chapters. The current Chapter 1 offers a short overview of the ground-borne noise and vibration problem and their negative effects when they reach neighbouring structures through their foundations, as well as the main motivation and the research objectives of this work.

The main body of the dissertation has been divided into four chapters. Chapter 2 is devoted to presenting the phenomenology and sources of ground-borne vibration and the most relevant works proposed to study soil-structure interaction systems under static and, mostly, dynamic loads. Furthermore, the main assumptions, methodologies and capabilities of the different piled foundation models to deal with ground-borne vibration problems are also discussed.

Chapter 3 addresses the formulation for modelling a single-pile system embedded in a half-space model of the soil. The system is under harmonic loads applied at the pile or anywhere on the ground surface. The proposed model employs the classical linear structural member theories to account for the pile reaction, whereas the singular boundary method is adopted to model the soil reaction. The proposed approach is compared with other existing methodologies to verify its correctness and highlight its benefits. Different assumptions that can be adopted for the compatibility conditions at the pile-soil interface are studied.

In Chapter 4, the formulation and assumptions presented in Chapter 3 are extended to the case of pile-group systems with or without pile caps. Pile caps are proposed to be modelled using the finite element method. The significance of the pile cap flexibility and the coupling conditions between the pile cap and the piles themselves are studied. The compatibility conditions at the pile-soil interface are also studied in this chapter for different scenarios to evaluate the influence that these conditions have on the response of pile-group systems.

Chapter 5 presents an experimental validation of the proposed methodology. This validation is carried out with the support of an experimental test site that consists of a single-pile and a 2×2 pile-group system. The soil condition was previously assessed to achieve an accurate

picture of the experimental system in hands. The tests were conducted by hammer testing, and the results have been compared with the ones predicted by the proposed approach.

Finally, Chapter 6 summarises the general findings presented in the dissertation and achieved along the doctoral studies. Further work recommendations are also discussed in detail.

Chapter 2

Literature review

2.1 The problem of ground-borne vibration: phenomenology and sources

Ground-borne vibration problem is mainly considered a man-made problem due to the development of urban roads and rail networks that rarely induce structural integrity failures to surrounding structures. This is not the case with vibration induced by natural sources such as earthquakes that release seismic waves which propagate from the bedrock to the surface and that have the potential to produce structural damage due to high strain levels induced on the building foundation. These aspects have been extensively studied and addressed within the field of earthquake engineering, thus falling outside the scope of this dissertation.

The governing physical mechanism to produce ground-borne vibration generally begins when a dynamic event occurs in which mechanical energy is released in the soil through elastic waves, giving rise to wave fields that travel across the medium and reach the surrounding building foundations. Thus, those vibrations are transmitted through the structure, inducing the building structure (and its walls, windows and furniture) to shake. Consequently, when vibration levels are high enough to turn it perceptible for people, and they are prolonged exposure to this, the ground-borne vibration becomes a harmful effect causing adverse effects on inhabitant health. Similarly, ground-borne vibration can induce malfunction of sensitive equipment (laboratories, recording studios, micro-manufacturing facilities) or discomfort in public facilities (theatres or hospitals) when the vibration levels are high enough.

Although there is a wide range of sources that induce ground-borne vibration, they can be differentiated between those that act on the ground surface, such as heavy machine foundations, at-grade road and railway traffic or construction activities, and those located below the ground, such as tunnelling, blasting or underground road or railway traffic, as shown in Fig. 2.1. In the following, a brief review of the governing physical mechanisms of those sources and the frequency range where their associated excitations present the most significant spectral content is described. However, for a more general overview of ground-borne vibration sources, the interested reader is referred to the books of Thompson [7] and Semblat and Pecker [8].

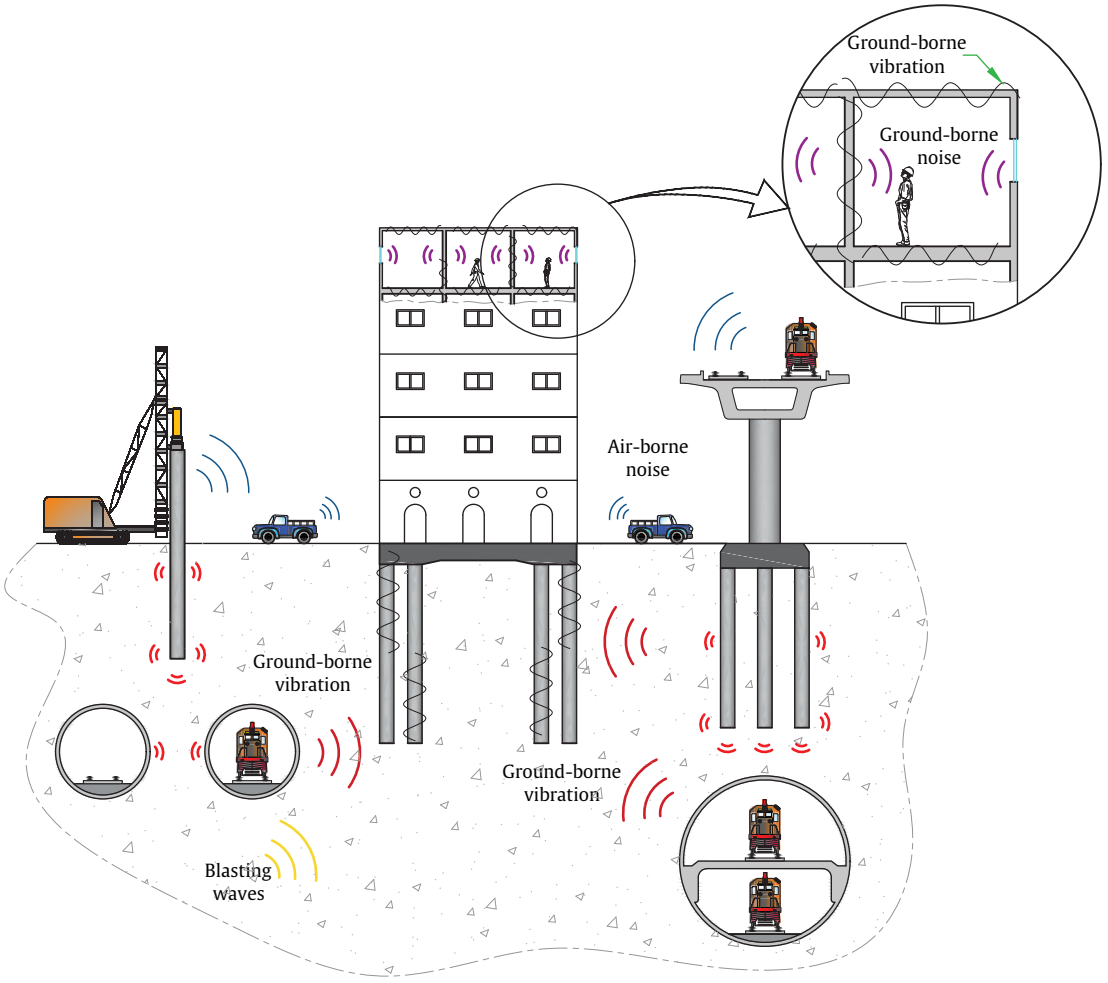

FIGURE 2.1: Sources of ground-borne noise and vibration in urban environments.

Construction activities

Many construction activities, such as vibratory compaction, pavement breaking, building demolition, tunnelling, pile driving or blasting, liberate vibration energy in the soil that can

even structurally damage surrounding buildings. From these sources, blasting has gained considerable attention from the engineering community due to the large amount of mechanical energy realised in the ground. For instance, a numerical study presented in [9] discusses the dynamic fracture mechanism, crack propagation and dynamic stresses at surrounding points where blasting is performed. The prediction of ground vibration generated by pavement breakers has been addressed in [10], where numerical models for predicting the near and far field vibration levels are proposed and validated regarding experimental results, concluding that while non-linear effects govern the near field response and that significant overestimation of vibration levels are expected by neglecting these effects in the numerical model, the far field response can be predicted by linear models. Similar attention has been received on the vibration induced by pile driving activities [11, 12] due to the constantly increasing number of tall buildings constructed in densely populated cities. Empirical prediction methods and their effectiveness in predicting ground-borne vibration levels elicited by construction works and the available options to mitigate problematic vibration levels are described and evaluated in [13].

Roads

Ground-borne vibration induced by traffic roads is generally perceptible in urban zones when roads present an uneven surface. The typical frequency interest ranges from 8-16 Hz and corresponds to the "wheel-hop" and "body-bounce" modes of vibration of the vehicle [14, 15]. Parameters such as the type of vehicle, the type of road [14], and the distance to the building strongly determine the vibration levels. These parameters were accounted for to develop an empiric approach in [15] to deal with road/pavement soil systems under dynamic loads. The model is experimentally validated, and results show that the vibration levels are strongly linked with the soil composition. The results of a more detailed model based on numerical methods have demonstrated that while the pavement type only affects the road-soil frequency response function at small distances and high frequencies, the soil parameters mainly determine the transfer functions. Thus, proper soil characterisation is suggested to obtain accurate results [16]. Recently, the negative effect on heritage buildings due to traffic roads has been an increasing concern because of the cosmetic and minor structural damages to which buildings are exposed. This has been demonstrated in experimental studies that show that, for instance, both the ISO 2631 [17] perception threshold for peak particle velocity (0.14 mm/s) and the Swiss Standard threshold [18] (1.5 mm/s) were exceeded in heritage buildings [19–21].

The vibration of heavy machine foundations

Ground-borne vibration induced by heavy machinery operation has been widely studied over

the years due to the extreme amount of concentrated energy that is delivered to the soil through their foundation. Despite the wide variety of equipment capable of producing such energy amount, the most often heavy machines employed by the industry [22] can be differentiated by their main governing physical mechanisms of operation: machines with rotating components (e.g. electric motors, fans or turbines), those with reciprocating motion (e.g. piston compressors or diesel engines), the ones that generate powerful dynamic forces but very short in duration as, for instance, hydraulic hammers (called shock-producing machines) or those that produce random vibration time history (e.g. pumps, shredders and mills). The frequency content from these sources depends on the particular machine, but it ranges from 5-200 Hz [23]. Although these machines are restricted to being located in a fixed location within an industrial park to prevent vibration/noise pollution within urban zones, they still need to be implemented with vibration isolation (e.g. open and filled trenches) because the released powerful dynamic energy can affect workers, other sensitive equipment and/or sometimes surrounding urban areas.

Railways traffic

The impact of railway-induced ground-borne vibration and noise pollution in densely populated areas is a matter of governmental and public concern nowadays. Recently, a statistical study of a collection of ground-borne vibration and noise reports from 9 countries worldwide has pointed out the alarming increased number of people that, nowadays, complain about vibration and re-radiated noise pollution to what they are exposed for [24]. The study has also shown that more than 44% and 31% of the reports employed have exceeded the vibration and noise thresholds, respectively, allowed by their corresponding national regulations. Furthermore, the same research concludes that more than 50% of the evaluated railway projects have shown the need to account for ground-borne measures.

Traffic-induced vibration has been addressed since the beginning of the previous century when vibration elicited by the traffic of the Central London Railway was studied and measured in 1901. The study was later referred to by Hyde and Lintern [6], who considered improved measured instruments to study the vibration of roads and structures induced by vehicular traffic and machinery. Since then, many studies have been undertaken to identify the possible mechanisms that generate ground vibration when passing trains. These excitation mechanisms, similar to air-borne sources, can be decomposed into supersonic and accelerated motions [25]. The supersonic motion is associated with generating a Mach cone, which occurs when an object moves with greater speed than the wave speed in the surrounding medium. Consequently, the

low pressure behind the object can not be compensated for the high-pressure region in from of the object, so Match cones are generated along with the object. In traffic trains, bending and Rayleigh waves that are associated with the rail and the ground, respectively, are considered as main parameters involved in the generation of ground vibration since they have the lowest wave speed in the train-passing surrounding field. Because bending waves speed in rails lying far away from typical train velocities, high vibration levels induced by this are extremely unlikely. In contrast to the bending waves, the Rayleigh waves do not depend on the frequency and are strongly related to the quasi-static excitation that contributes to generating ground vibration. The quasi-static excitation occurs when the dynamic moving load induced by the repeated passage of axles of the train can be expressed as a superposition of the contribution of different train axles since the wave field that generates the moving load of each train axle is similar to the one of a load at a fixed position when the train moves at speed lower than the surface waves (Rayleigh waves). Consequently, the characteristic peaks and troughs dynamic responses for the quasi-static excitation are obtained, which lie at low frequencies of 1-20 Hz [25, 26]. However, if the moving load speed of the train reaches (or is larger than) the critical surface load speed, vibration amplitudes in the soil and track significantly increase, leading to the formation of Mach cone and, consequently, track stability problems and passenger-safety concerns [27–32].

The second excitation mechanism is associated with accelerated motion or dynamic excitation, which is determined by the train-track interaction, such as wheel and track-unevenness, impact excitation due to rail joints and wheel flats or crossings [7, 26, 33–37]. Parametric excitation is also an important excitation mechanism considered within dynamic excitation. It has been shown that the spatial variation of the train truck stiffness produces ground-borne vibration due to, for instance, the sleeper spacing along the railway track [7, 25, 38, 39]. Furthermore, it has been shown that train speed v and sleeper spacing s determine the sleeper-passing frequency v/s [40–42]. Therefore, for a fixed sleeper spacing $s = 0.6$ m and a conventional urban railway traffic speed (e.g. $v = 80$ km/h), the sleeper-passing frequency appears at 37 Hz that lies within the frequency range of interest for ground-borne noise and vibration. That scenario changes for high-speed trains ($v = 300$ km/h) where the sleeper-passing frequency occurs at 139 Hz in the ground-borne noise frequency range. Another parametric excitation source responsible for the variation of the train track stiffness is the transition zones where the track parameters (geometric or mechanical) change and produce the vehicle to shake [43, 44].

By the previously aforementioned, the peak vibration generated by traffic train lie in the frequency range of 1-80 Hz, [7, 26], in where the building shakes and produces mechanical

vibration perceivable for the human body, whereas, from 16-250 Hz [7, 26, 45], the ground-borne vibration can induce noise pollution (or: re-radiated noise) inside the building.

2.2 Soil-structure interaction

Soil-structure interaction (SSI) is a broad discipline in Applied Mechanics that looks for the development and research of theoretical methods and their computational implementation for the study of the dynamic reaction of structures, taking into account the flexibility and dynamic properties of the surrounding soil. Thus, researchers from multidisciplinary fields (e.g. soil and structural mechanics, soil and structural dynamics, geophysics, geomechanics, earthquakes engineering, computational and numerical methods, and other technical disciplines) have paid attention to developing models capable of predicting the behaviour of structures embedded in the soil, and that can also provide a better understanding of physics within the SSI.

SSI problems where the dynamic excitation acts directly onto the structures (e.g. unbalanced reciprocating machines on elastic foundation, railways track dynamically loaded by passing trains, or tall buildings under wind loads) are known as problems involving external loads. When this external force is applied to the structure, it produces (in conjunction with the resulting inertial load of the structure) an interaction effect in which the loads are transmitted to the ground. This interaction effect is referred to as inertial interaction. Thus, the mechanical energy transferred to the ground is scattered away from the structure in the form of stress waves so that the energy is dissipated. This process is called damping radiation. On the contrary, in structures subjected to forces applied in the medium (e.g. seismic waves induced by blasts or earthquakes), the SSI theory needs to be extended to internal loads in order to deal with the action effect of the stiffer structure that cannot conform to the distortion of the soil elicited by the incident seismic waves. In this case, the foundation or inclusion scatters the seismic waves that lead to modifying the local motion in the vicinity of the foundation. This is known as the kinematic interaction.

Two approaches can basically address these SSI effects. The first one is referred to as the direct approach (based on the superposition theorem [46]), which employs discrete methods to perform the mathematical model of the soil and the structure so that the structure (or structures) and the surrounding soil are analysed together. The principal advantages of this approach are the inclusion of the non-linear soil behaviour, as well as the inclusion of the flexibility of the

mat, and the exact connection to the structure model. However, because many degrees of freedom are involved in the mathematical model to solve the SSI problem, the computational cost is the main disadvantage of the direct approach. The second approach employs a set of springs, dashpots and masses to account for the stiffness or impedance functions of the ground, whereas the structure can be represented by regular linear members or any discrete method, such as finite elements. This approach is normally referred to as the spring method, substructure method, or three-step approach due to the solution of the system involves the following: i) the kinematic interaction (massless structure) for which the structure is treated as a massless rigid system to determine its motion when subjected to input motions, ii) the foundation impedance (massless foundation) where the frequency-dependent subgrade stiffness, which accounts for layering and embedment effects, is determined, and iii) the inertial interaction (dynamic interaction) for which the real model of the structure supported on frequency-dependent soil "springs" (foundation impedance) is calculated when the system is under an input motion computed previously in the kinematic interaction. Although this approach has the advantage of requiring less time consumption, which allows for performing more parametric studies, the assumption of treating the structural foundation as a rigid system is mainly valid at low frequencies (e.g. seismic analysis cases), which is no longer valid for vibration from underground railways. The interested reader is referred to the book of Kausel [46] in which the formulations of these approaches are derived in detail.

As aforementioned, the development of what the SSI is known as nowadays can be tracked since the course of the 19th and early part of the 20th century, by the time a number of scientists developed theoretical frameworks which conform to a cornerstone in the matter (for dealing with SSI problems) such as highly idealised mathematical models (e.g. rigid circular disk resting on halfspace) or the case of the development of fundamental solutions, or Green's functions that are the heart of more sophisticated tools (e.g. the boundary element method) for addressing the reaction of soil cavities of complex geometries. In this regard, a brief review of the most technical developments of the formulation of fundamental solutions and the first SSI approaches are presented in the following sections.

2.2.1 Fundamental solutions

In SSI problems, a fundamental solution is an expression derived analytically (or at least semi-analytically, e.g. Green's functions where numerical solutions are employed for evaluating some integral transforms) for the response anywhere in an elastic or viscoelastic infinite medium (e.g.

soil) due to applying a point force source or distributed load source located at a given, arbitrary fixed position. This fundamental solution, combined with, for instance, the boundary integral theory, provides an excellent alternative for solving complex SSI problems. An earlier pioneer work that addressed the influence of a static concentrate point load acting in an infinite solid was presented by Thomson - better known as Lord Kelvin - in [47] by 1848. In his work, analytic expressions for displacements were presented. Similarly, fundamental solutions for time-varying point loads in a full space were proposed and presented in [48] by Sir George G. Stokes. A modern rendition of these expressions in two and three dimensions using the current mathematical notation employed those days can be found in [49]. It is worth mentioning that those fundamental solutions developed by Stokes are included within the small group of analytical expressions presented in closed forms and solved in both the time and frequency domains, which are widely employed in fields such as SSI, geophysics or acoustic. Subsequently, the solution for a vertical load acting on an elastic half-space was sketched by Boussinesq in [50–52] that was also adopted by Cerruti [53] who addressed the problem employing Betti's principle (integral theorems used in elastostatics) to compute the response within the half-space by prescribing tractions and displacements on the surface (know nowadays as Neumann and Dirichlet boundary value problems, respectively).

A well-detailed explanation for the derivation of fundamental solutions for homogeneous half-space under dynamic loads on the surface was presented by Lamb in [54], where employing an integral transform method gives a solution for far-field responses when the system is under an impulsive load acting in a two-dimensional (2D) system or a suddenly vertical load acting in a three-dimensional (3D) medium. Nowadays, dynamic loads that act on the surface of a half-space are referred to as Lamb's problem [55]. For cases where the dynamic load is applied within the halfspace, Mindlin proposed closed-form equations for computing the response on the ground surface presented in [56]. It should be noted that the solution to those dynamic problems, up to here described, can be evaluated only on the surface or the axis of symmetry below the load but not at interior points without employing numerical approaches. In this regard, Kausel and Kausel and Peek [57, 58] developed the thin-layer method (TLM) to evaluate the responses anywhere in a layered half-space.

2.2.2 Static SSI

One step more to going forward in developing closed-form equations to find the soil response under concentrate loads is to consider a distributed external force instead. However, the

resulting integrals appearing in the formulation have paused its final solution for around 130 years [55]. An initial approach was to consider a rigid, ideally massless disk resting on the soil under a concentrated static vertical load. Closed-form equations were proposed for vertical stiffness and stress distribution underneath the disk under the assumption that the contact interface is not welded but smooth instead [59] (e.g. the interface is lubricated). Later, these solutions were employed to infer the soil reaction [60], which is useful to address foundation problems via the Winkler spring approach. Strip footings and rigid disks under eccentric loads were later attended, and, similar to the previous approach, equations for stress distribution and rocking stiffness underneath the plates were proposed [61]. Subsequent, torsional stiffness for circular disk welded to a half-space were derived in [62, 63], and finally, the lateral stiffness of circular disks subjected to tangential load in the horizontal displacement mode was presented in [64].

Up to this point, the previous closed-form formulations proposed consider static load in the shape of disks and rectangles, but all of them are incapable of predicting the soil reaction within the soil. The first article that attended that inconvenient was presented by Steinbrenner [65] by 1934. In his work, complete formulations (but without giving any technical detail of its derivation, [55]) were presented for predicting displacements and stresses everywhere, including in the soil. It is curious (at least for the writer) that, many years ago, before the Steinbrenner works were published, Terezawa [66] and Love [67] published well detail works addressing soil reaction (even within the medium) induced by circular and rectangle distributed loads. For a complete discussion and more details about this last controversy, the interested reader is referred to the remarkable paper of Kausel [55], which revisits the early history of SSI.

2.2.3 Dynamic SSI

The first dynamic SSI problem involves the study of a rigid circular disk resting on a halfspace subjected to a harmonic load addressed by Reissner in [68], by 1936. In this article, the soil-disk interface was imposed to behave as a frictionless contact, whilst the stresses were assumed to have a uniform distribution at the soil-disk interface to avoid thus the proper solution of a boundary value problem. One year later, the same assumptions regarding frictionless contact and uniform stress distribution were adopted by the same author in [69] for solving the soil response under dynamic torsional loads problem. In that paper, three ways of modelling the load were addressed: concentrate moments, ring moments and distributed torsional loads.

Further investigation on the subject brings Reissner and Sagoci to give the solution to the boundary value problem [62, 63] proving not only the exact formulation for plates dynamically loaded but closed-form solution of the wave equation in spheroidal coordinates. Afterwards, Apsel and Luco [70] adopted the proposed spheroidal coordinates to address oblate ellipsoidal foundation embedded in a half-space under harmonic torsional and propagating shear-horizontal waves coming from arbitrary directions. Similarly, analytic solutions for a rigid sphere embedded in an infinite elastic solid under angular or rectilinear oscillations were developed by Chadwick and Trowbridge in [71, 72] concluding that, for each mode of vibration of the sphere, the character of the solution for rectilinear oscillation has determined by both the density ratio between the sphere and its surrounding medium, and the Poisson's ratio of the elastic medium [72]. Additionally, when the system is under angular oscillations, a free vibration is attenuated due to the density contrast between these two subsystems when the radiation energy is transferred from the sphere toward the medium [71]. It is worth mentioning that all analytical solutions for a dynamically loaded sphere in a full-space provided by Reissner-Sagoci, Apsel-Luco and Chadwick-Throwbidge have been employed in subsequent studies as benchmark solutions for comparison with alternatives method solutions, such as the numerical approaches.

Finally, up to this point, this review has been focused on describing the foundation for giving rise to what the SSI on those days is known for. It is evident that diverse physical and engineering fields own their development (to a greater extent) to the studies previously discussed. Therefore, these highly idealised mathematical models, together with the entry of digital computers and the ever-increasing necessity of developing more realistic models (mainly driven by the nuclear power, offshore industry or earthquakes consequences), have encouraged faster progress in the SSI subjects as well as, to afford particular attention by researchers in creating more than ever predicting models able to account for complex geometries or nonlinear SSI behaviour. In that context, the following sections pay particular attention to reviewing the pile-soil prediction models and the main capabilities of each one.

2.3 Modelling single-pile dynamics

The structural component responsible for the transmission of ground vibration to civil structures is its foundation system. Piled foundation systems are the preferred option among the most common foundation solutions, especially for tall structures or poorly consolidated soils.

Over the years, different approaches have been proposed for estimating the dynamic behaviour of the piled foundation system. These approaches are generally based on three modelling strategies: the dynamic Winkler foundation approach, the elastic continuum theory and mesh-based numerical modelling methods. The reader can find a fully comprehensive review of the existing modelling strategies for pile-soil dynamic interaction in [73]. However, to include some recently proposed methodologies and, more importantly, to make prominent what new contribution the present work offers relative to the existing methods, the main capabilities and assumptions of each modelling approach are briefly outlined in the following paragraphs.

2.3.1 Winkler-foundation approach

In earlier models of foundations, the elastostatic theory was initially employed to estimate the dynamic displacements and stresses response in the soil. This approach was later improved when inertial forces occurring in the soil-structure system and wave propagation through the soil were incorporated to overcome the static-based modelling limitations. Lysmer and Richart [74] were pioneers in adopting this approach for a circular footing. They show that, below the footing, the behaviour of an elastic half-space is similar to that of a simple damped oscillator. Thus, they proposed to model a circular footing as an equivalent mass-spring-damper system to represent the dynamic footing-soil behaviour. This modelling technique, based on the Winkler-foundation approach, was later employed by Lysmer and Kuhlemeyer [75] to represent the infinite soil behaviour through discrete absorbing boundaries in finite element methods. Alternatively, Baranov [76] proposed an analytical methodology to model circular footings based on the hypothesis that the foundation's surrounding soil can be represented by a set of infinitesimally thin horizontal elastic layers that are dynamically uncoupled from each other. As a result, only horizontal waves can be released in the soil so that outward radiation of S-waves (secondary or shear waves) and P-waves (primary or compression waves) is individually accounted for in vertical and lateral footing equations of motion, respectively. Equivalent simple expressions, based on those developments in [76], are later proposed in [77] for vertical motions of footings and in [78] for lateral and rotational motions. In subsequent work, Novak [79] combined Baranov's closed-form expressions for the reactions of the soil with the equations of motion of rod and beam structural elements to obtain vertical and lateral motions of a single-pile embedded in an elastic half-space, respectively. The Novak approach is regarded as the first method that includes the radiation-damping effects of the soil in pile foundation modelling. However, although Novak's approach accurately predicts the vertical dynamic response

of a pile, this methodology presents significant limitations when either horizontal pile-driving response, dynamic interaction between piles or the field response is required.

2.3.2 Elastic continuum approach

The mentioned dynamic Winkler-foundation approach limitations regarding the wave propagation in all directions can be overcome by representing the soil as an elastic continuum. Therefore, by assuming the elastic continuum theory, the soil is modelled as an elastic half-space, whilst the pile is typically modelled as an axial rod for vertical vibrations and as an Euler-Bernoulli beam for lateral vibrations. The earliest works employing this methodology for piles are attributed to Novak and Nogami [80–82], who used mode expansion to model a viscoelastic layer where the pile is embedded. Similarly to [80–82], the resulting vertical and lateral dynamic equivalent stiffnesses of the layer are then introduced into the equations of motion of the pile to account for the pile-soil interaction.

One of the most well-known three-dimensional models for single-pile and pile-group problems was developed by Kaynia and Kausel [1], who discretised the soil-pile interface into an arbitrary number of cylindrical segments, as shown in Fig. 2.2(a), and represented the soil reactions considering the response to two types of loads: barrel and disk loads. While the cylindrical barrel loads are associated with the soil reaction at the lateral surface of the pile, as shown in2.2(b) and (c), the circular disk loads represent the tractions at the pile tip as shown in Fig. 2.2(d) and (e). Therefore, the continuous traction distribution at the pile-soil interface is discretized and replaced by a piecewise-constant distribution over the cylindrical and disk segments. In a similar approach [83], translational and rotational ring line loads at a discrete number of soil-pile interaction layers were proposed to include the traction moments of the coupled system. Other examples of the elastic-continuum-type formulation include Nogami and Novak [80, 81, 84], Pak and Jennings [85], Wolf [86], Rajapakse and Shah [87, 88] , Anoyatis et al. [89, 90] and Di laora et al. [91, 92]. While these analytical elastic-continuum formulations are more accurate than Winkler-type models for modelling pile foundations under harmonic loads or kinematic interactions, soil inhomogeneity can only be included in the form of layers or varying elastic moduli. Moreover, the soil cavity is not explicitly modelled, but rather the pile is treated as reinforcement, with density and elastic modulus equal to the difference between the desired pile and soil values. Kuo and Hunt in [93] have included the soil cavity and proposed a single pile-soil modelling approach which uses the mirror-image method to account for the boundary conditions at the pile head. Nonetheless, that formulation was based

on the Pipe-in-Pipe (PiP) model [94, 95] that for the calculation of the soil-pile interaction tractions considers the soil medium as a full-space with a cavity, downplaying the effect of the soil surface and soil inhomogeneity.

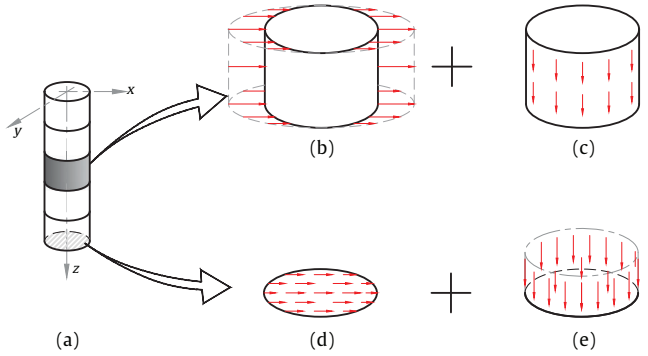

FIGURE 2.2: Soil-pile interface discretization into several cylindrical segments and one disk segment (a) proposed by Kaynia and Kausel [1]. The soil reaction is decomposed into a horizontal (b) and vertical (c) barrel load acting on each cylindrical segment, whilst the soil reaction at the pile tip is decomposed into horizontal (d) and vertical (e) disk loads.

2.3.3 Discrete methods

Finite element method

Up to hear, pile foundation modelling strategies based on analytical solutions involves certain idealised mathematical assumptions, such as a rigid circular body perfectly attached to a homogeneous medium. Such assumptions, together with the fact that many solutions techniques assume some symmetry in the distribution of, for instance, a pile-group, can lead to predicting inaccurate results of the dynamic response of the system. This is particularly true in cases where the soil has to account for non-linear effects such as soil liquefaction or gaps at the pile-soil interface. Modelling strategies based on discrete methods are suitable when the system has a significant degree of complexity.

The first work on modelling piled foundations employing a numerical method is attributed to Kuhlemeyer [96, 97], who took advantage of the finite element method (FEM) versatility in determining the dynamic response of the system under lateral and vertical loads. Syngros [98] presented a single-pile foundation model based on an axisymmetric FE approach to deal

with vertical load applied at the pile head. The model used simplified expressions to represent the soil inhomogeneity in vertical and radial directions induced by, respectively, vertical overburden and pile driving. Other examples of single-pile systems using the axisymmetric FE approach to model impact pile driving include [11, 99]. Because FEM can only deal with finite domains, frequency-dependent [79], or frequency-independent [75] absorbing boundaries were included in FEM models of SSI problems to represent the semi-infinite nature of the soil medium by avoiding wave reflections, as shown in Fig. 2.3(a). Therefore, due to the FE-flexibility offered, intricate geometries depth-dependency of the soil mechanical properties [100, 101], non-linear soil behaviour [102–104] or discontinuity conditions at the pile-soil interface [105] became possible to be addressed . However, the axisymmetric nature of these models limits their applicability to the prediction of radial and vertical responses. Due to the large number of elements required, FEM with absorbing boundaries are not a suitable approach to model the dynamic response of piles or pile-groups, especially at high frequencies

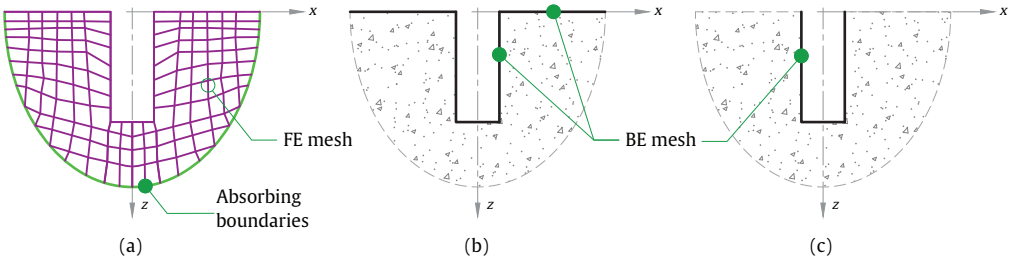

FIGURE 2.3: Comparison between half-space modelling using finite elements (a) against the boundary element approach that uses full-space fundamental solutions (b) or half-space Green's functions (c).

Boundary element method

In contrast with the FEM, the boundary element method (BEM) can naturally deal with infinite or semi-infinite domains. This discrete technique is based on the boundary integral equations, which are discretised along the boundary and computed by enforcing the fundamental solutions (or Green's functions) to be thus evaluated at infinitely many collocation points. Thus, in cases where the BEM employs half-space Green's functions for calculating the soil reaction, only the pile cavity is discretised since the ground surface information is already included in Green's functions. Otherwise, the pile cavity and ground surface should be considered in the mesh discretisation if the fundamental solutions of a full space are used. A review of different BEM-based approaches for 2D and 3D elastodynamic problems in time and frequency domains can be found in [106, 107]. To predict the vibration isolation of a row of piles, Kattis et al. [108]

modelled the piles and the soil using boundary elements and coupled them together through equilibrium and compatibility at their interfaces. Several authors have also proposed the use of hybrid approaches that combine the modelisation of the soil using BEM with other discrete methods or analytical approaches to model the pile. For instance, Padrón et al. [109] proposed a FE-BE approach in which the pile is modelled by employing a one-dimensional (1D) FE model and coupled with a 3D BE model for representing the soil. As their approach considered the fundamental solutions for a full space, both cavity and ground surface were discretised. Talbot and Hunt [5] developed a computationally efficient model for solving a single-pile or a row of piles based on periodic structure theory. In their work, the pile is modelled using the solutions for an elastic bar and Euler beam theory for vertical and lateral motions, respectively. This pile model is coupled with a BE model of the soil that uses constant rectangular elements for meshing the ground surface and the pile cavity, resulting in an accurate and computationally efficient method. In [110], Coulier verified that the improvement obtained by modelling the pile as a Timoshenko beam model was small.

Meshless methods

Meshless methods have emerged as an interesting alternative to mesh-based ones due to their simplicity and computational efficiency. Among them, the singular boundary method (SBM), first proposed by Chen in [111], has gained popularity these recent years due to its robustness with respect to other meshless approaches. The SBM can be seen as a modified version of the method of fundamental solutions (MFS). In brief, the MFS uses a set of virtual sources computed so that they satisfy a prescribed boundary condition. These boundary conditions are evaluated at a set of points called collocation points. While the MFS places the virtual forces outside the domain, the SBM proposes to locate the sources at the physical boundary so that they are superimposed to the collocation points. Like the MFS, the SBM employs the fundamental solutions (or Green's functions) of the governing equation of the problem of interest (e.g. a homogeneous full space or a layered half-space) as the interpolation basis functions. However, singularities of the fundamental solution arise when the collocation points are geometrically coincident with the virtual sources. In those situations, the responses are replaced by the so-called origin intensity factors (OIFs), which overcome the singularity of the fundamental solution for both Neumann and Dirichlet boundary problems. Although this methodology has been extensively employed for solving potential problems in acoustics, few investigations are available on applying the SBM to elastic wave propagation problems. Gu et al. [112] employed the SBM for plane strain elastostatics and later to deal with orthotropic elastostatic problems [113]. This last work also presented a theoretical background for the SBM

formulation, stating that the SBM can be seen as a discrete version of the indirect boundary integral equations based on the single-layer potential formulation. In [114] Sun et al. applied the SBM to 2D dynamic poroelastic problems. Recently, Liravi et al. [115] have proposed a 2.5D FEM-SBM approach for solving SSI problems. In their work, the structure is modelled using the FEM, while the SBM is employed to model the soil system. The authors compare the novel approach with FEM-BEM and FEM-MFS approaches, finding that it offers higher computational efficiency than BEM and more robustness than MFS.

2.4 Modelling pile-group dynamics

In many cases, the bearing capacity of a single-pile is not enough to support the service load required by a column, which needs to transfer such a service load toward its foundation. this could be because, for instance, the building is going to lie on soils that have low bearing capacities (e.g. soft soils), or the pile can not be designed to reach the bedrock (floating pile cases). In these situations, a pile-group foundation is an excellent alternative for increasing the bearing capacity of the foundation. However, when the pile spacing in the pile-group is small, the pile-soil-pile interaction (PSPI) should be considered for predicting its dynamic response at high-frequency ranges. In such a sense, different approaches have been developed to compute the dynamic response of pile-groups efficiently.

The first and most commonly used approach is the use of the "interaction factors" introduced by Poulos [116], who used them to study the static elastostatic response of a laterally loaded two-pile group. In his work, interaction factors are used to express the ratio between the horizontal displacements and rotations of a two-pile system and those obtained for a single-pile. Thus, by using these interaction factors and the superposition principle, a global receptance matrix for a general pile-group can be built up. Later, Novak and Grigg [117] addressed the response of a dynamically loaded pile-group. In their work, the total stiffness and damping values for the pile-group were computed by summing up the stiffness and damping of each pile treated as an isolated system and modelled using the Winkler approach. Additionally, they employed the static interaction factor proposed by Poulos [116], assuming, therefore, that the static and dynamic behaviours of a pile-group should be similar (frequency-independent interaction). This assumption was later tested by Sheta and Novak [118], who, when addressing the vertical vibration of pile-groups, showed that the dynamic group effect differs considerably from the static one. They conclude that the frequency-depend pile-group interaction is much stronger

than the static one when the pile spacing is small. Similar contributions regarding frequency-depend transfer and impedance functions for pile-groups embedded in multilayered soil and subjected to passing seismic waves were discussed by Wolf and Von Arx [119] and Nogami [120]. Dynamic PSPI for lateral vibration was later studied by Nogami [121], who presented a methodology for computing the flexural responses of a pile-group treated as a single-pile. The method employed by Nogami, referred to as Winkler model for pile-groups and developed in his previous works [122–124]), uses the pile-head receptance of two piles to obtain the pile-head receptance of a general pile-group.

Dobry and Gazetas [125] proposed an alternative approach for obtaining the stiffness and damping of floating pile-groups. This method employs asymptotic cylindrical wave expression to simulate the interference of cylindrical wave fields that originated and spread radially out from each pile. By doing this, closed-form equations for computing approximated interaction factors were proposed for pile-groups dynamically loaded with lateral, axial and rocking external forces. Gazeta and Makris performed an extension of this approach in [126, 127] for thus computing the dynamic response of a pile-group embedded in a non-homogeneous half-space and subjected to vertical loads or seismic SV-waves. Milonakis and Gazetas [2] proposed a closed-form expression for the dynamic response of pile-groups embedded in layered soil. In their derivation, the authors considered the Winkler approach to represent the pile-soil interaction system (source pile) under vertical vibration and assumed that the interaction produces cylindrical waves that propagate horizontally to neighbouring pile a surrounding pile (receiver pile), as shown in Fig 2.4. Thus, the axial Winkler stiffness of the receiver and the soil response induced by those cylindrical waves give rise to an interaction between this pile and the surrounding soil, leading to diffraction of the arriving wave field. Consequently, a closed-form expression for computing the interaction factor can be deducted [2].

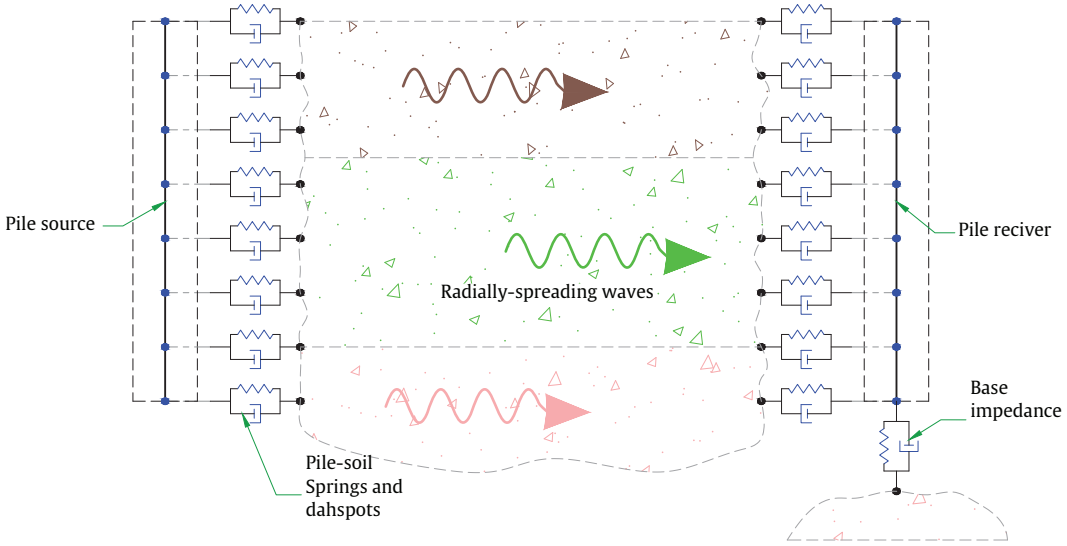

FIGURE 2.4: Schematic representation proposed by Milonakis and Gazetas in [2] to solve pile-group problems based on the Winkler approach.

Cairo et al. [128, 129] proposed a methodology for computing the dynamic response of a vertically loaded pile-group embedded in a layered half-space. The approach employs the stiffness matrix method (SMM) [130] for computing the reaction in points located at the pile-soil interface. The pile-soil-pile interaction of a pile-group is accounted for by assuming that its dynamic response is a function of the pile-soil interaction forces and free-field soil displacements both associated with a single-pile. In their results, a reasonable agreement with theoretical approaches was obtained, especially at low frequencies.

The simplifying assumptions considered by the models presented in the previous paragraphs generally limit their accuracy. More detailed three-dimensional models of pile-group systems can be obtained by considering the displacement compatibility and force equilibrium between the piles and the soil. In this regard, Kaynia and Kausel [1, 3] formulation, previously mentioned in Sec. 2.3, also present the coupling procedure for computing pile-groups. In their work, the responses of several types of pile-groups to dynamic loads or passing seismic waves are calculated. Additionally, a simplified solution scheme based on the superposition method is also presented for cases involving a large number of piles. This simplified approach employs a dynamic interaction factor for a two-pile group without the presence of neighbouring piles, as shown in Fig. 2.5(a). The interaction factor is defined as the ratio between the dynamic displacement of one pile induced by loads acting on the other and the static displacement of the latest when it is considered individually. The comparisons of the results obtained using

the simplified approach against the ones computed using the complete pile-group formulation show a good agreement between them, especially for large pile spacings.

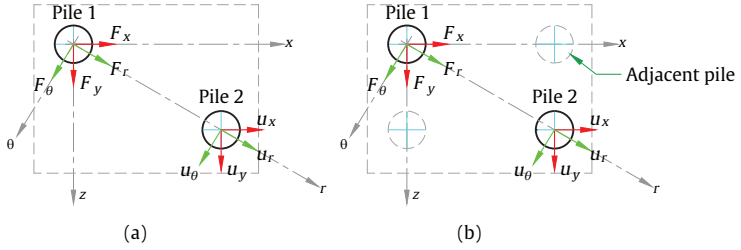

FIGURE 2.5: Two-pile group configuration used for computing the dynamic interaction factor employed by Kaynia [3] (a) and its variant that considers adjacent piles (b) employed by Edirisinghe [4].

The approach presented by Talbot and Hunt [5, 131] employs periodic structure theory for computing a row of an infinite number of identical piles modelled combining Euler-Bernoulli beam and elastic bar formulations with the BEM, as described in Sec. 2.3. In their work, the single-pile model is used to create a repeating unit. The compatibility condition is then applied to vertical meshes located at both ends of the repeating units, as shown in Fig. 2.6. Then, taking advantage of Floquet's theorem [132], the response of a system consisting of an infinite row of identical piles is finally obtained. Comparisons between the results obtained with this approach and those obtained using Kaynia's and Kausel's model [1] showed a good agreement between both formulations.

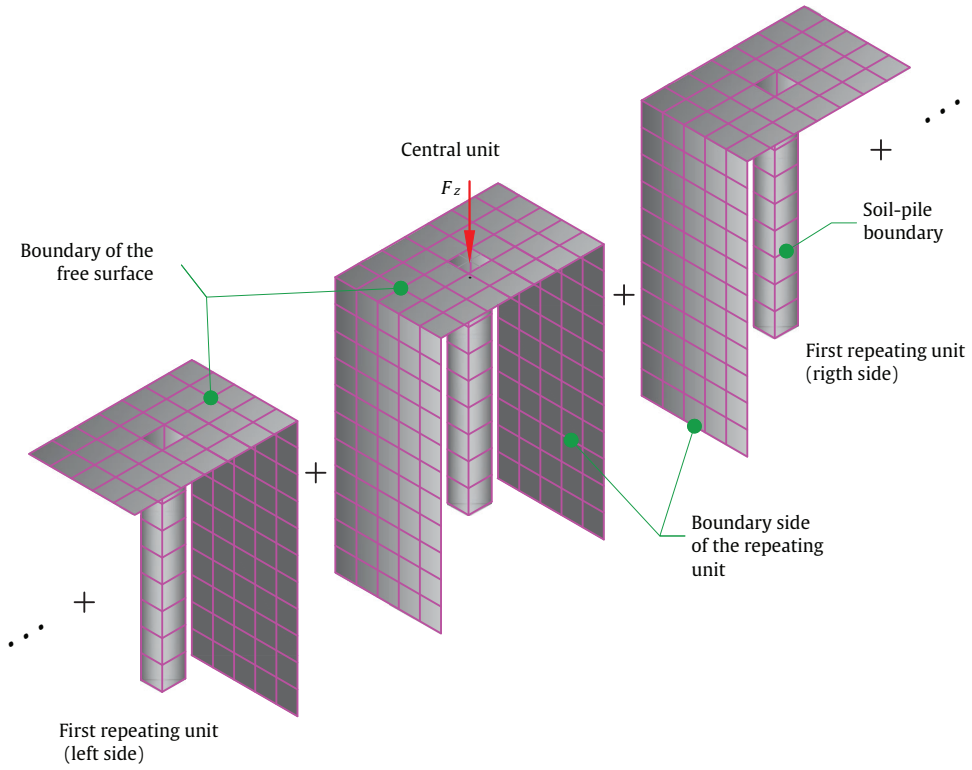

FIGURE 2.6: single-pile repeating units proposed by Talbot in [5] for solving a row pile-group system based on the periodic structure theory.

An extension of the original single-pile model proposed [5] has been developed by Edirisinghe and Talbot [4], who proposed a methodology in which the piles and the soil are considered as two independent subsystems and an iterative wave-scattering approach computes the response of the coupled pile-soil system. The authors show that the results obtained with this methodology are in good agreement with those obtained using the same model in which the subsystems are strongly coupled instead. Furthermore, Edirisinghe and Talbot studied the inertial interaction in pile-groups at high-frequency ranges employing both an iterative wave-scattering approach and a direct method. Parametric studies for different pile-groups show that the results obtained with the two approaches agree very well, thus validating the proposed iterative approach. Further analysis of two-pile models, the authors also show that discrepancies in the dynamic interaction factors arise at high frequencies when adjacent piles are considered in the calculation (Fig. 2.5(b)) rather than neglected, as usually considered in the superposition method (Fig. 2.5(a)).

2.5 Experimental studies of pile dynamics

Single-pile and pile-group dynamics have been investigated by performing tests on both small-scale and full-scale systems. The main benefits of small-scale configurations (or model scale tests) are they usually allow the performing of parametric studies since the tests account for controlled environments, repeatability in the tests, and possess economic advantages. Additionally, because they are used to be conducted in controlled environments, the model scale tests are employed to improve or validate modelling pile-soil methodologies since researchers can address the inertial and kinematic effects in the pile foundation or in piled-building systems. However, because these tests involve setting up a container for the soil, boundary effects may introduce accurate results, mostly in dynamic experimental tests. Therefore, boundary effects and realistic soil-pile stress field representation rise as principal limitations of the scale model testing. In contrast, full-scale tests provide "correct" stress conditions of real pile systems embedded in real soil compositions. This type of pile testing is limited because the testing loads are usually applied at the pile head, concentrating the effects of inertial interaction and neglecting the effects of kinetic interaction. Thus, by combining both the field and laboratory tests on pile foundation systems, valuable global recorded data can be obtained since these two complement each other. A brief resume of pile-soil interaction experimental research focused on only systems under dynamic loads is presented in the following. For a compressive review of full-scale and small experiments conducted to study the seismic soil-pile-structure interactions, the interested reader is referred to the work presented by Meymand [133].

2.5.1 Experimental studies with small-scale systems

Novak and Grigg [117] conducted static and dynamic tests on single small piles and on 2×2 pile-groups. In their work, the pile-soil systems were dynamically loaded through an oscillator placed over a steel test body made of steel flanges, which rested directly on the pile head (for a single-pile case) or the pile cap (for pile-groups). The recorded data is compared with theoretically predicted results [79, 84]. The study shows that resonant amplitudes and natural frequencies could be predicted whether the soil shear modulus, derived from static pile testing, is employed in the formulation of single-piles and when the static interaction factors are accounted for in the pile-group formulation, especially for systems with small pile spacing. El Sharnouby and Novak presented experimental validation for a large group of small piles closely spaced in [134, 135]. The system comprised 102 steel pipes of diameter $d = 26.7$ mm and length

$L = 1.06$ welded to a steel plate and joint with a reinforced concrete cap. An artificial soil mixture with similar properties to the natural deposit was employed in the experimental setup. The recorded data was compared with the ones predicted by other theoretical approaches, such as the one predicted using the dynamic interaction factor proposed by Kaynia and Kausel [1]. By analysing the results, they conclude that the dynamic interaction factor plays an important role in predicting the dynamic response of pile-groups. A similar study is presented by El-Marsafawi et al. in [136] where small- and full-scale pile-groups were dynamically tested under harmonic loads in a frequency range of 6-60 Hz. Results show that linear theories based on dynamic interaction factors to account for pile-group systems can predict the pile-group stiffness well but overestimate its viscous damping when compared with experimental data. The experimental results also showed that the pile-soil system can display moderate nonlinearities in its response. Boominathan and Ayothiraman [137] employ aluminium single-piles, with slender ratios between 10 and 40, embedded in a basket of mild steel and filled with clay. Geomembranes were used to cover the inside basket to act as absorbing boundaries, thus, simulating a semi-infinite medium. The piles were subjected to steady-state sinusoidal lateral excitation in a frequency range of $2-50$ Hz and amplitudes between 7 and 30 N at their pile heads. The study aimed to study the bending behaviour of single-piles. The results showed that linear dynamic responses were obtained for rigid piles even when subjected to large load magnitude. On the contrary, flexible piles only describe linear behaviour when applying low-amplitude loads.

Other pile-soil interaction test approaches used to study the dynamic behaviour of small-scale pile foundations experimentally are the centrifuge testing and the shaking table model test. Centrifuge testing is a widely used method to study the seismic soil-pile-superstructure interaction. Moreover, it provides valuable information to validate and improve pile-soil modelling approaches. A principal advantage of the centrifuge method is that the gravitational stress field in the model can replicate what will occur in a real prototype. This is particularly advantageous to represent cohesionless sands which present a stress-strain behaviour as a function of confining pressure. Because the centrifuge equipment possesses a test container for testing the model, This method presents a boundary limitation to studying pile-soil interaction at high frequencies since reflecting waves are introduced in the result, so then centrifuge tests are usually conducted for a seismic frequency range ($<$10 Hz) [93]. Like the centrifuge testing method, shaking table model tests are also conducted to validate seismic soil-pile-superstructure interaction effects. However, because this technique can not achieve elevated stress fields, it is suitable for testing pile foundations embedded in cohesive soils. The shaking table model test has the advantage of dealing with more realistic shaking conditions than the 1-D shaking

capability offered by centrifuges. Examples of small-scale piles tested on shaking tables under strong shaking can be found in [138] or pile-groups laterally loaded and embedded in two locations with different cohesive soil properties (soft and hard)[139].

2.5.2 Experimetal studies with full-scale systems

Full-scale system tests are typically conducted to ascertain pile-soil stiffness under dynamic loads. Generally, there are three types of full-scale tests which differ from the dynamic excitation: i) the ringdown test, which consists of imposing an initial displacement to the pile to be quickly realised from that subsequently; ii) the impact test in which smaller strain levels are induced to the pile through, for instance, impact hammers to generate lower free vibration than the ringdown tests, and iii) the forced vibration tests in where, for instance, an eccentric mass shaker attached to the pile head induce the pile to vibrate. Although reasonable agreement of experimental and predicted results can be obtained when the system behaves linearly, numerical models become less accurate if dynamic loads are high enough to genera nonlinear soil-pile dynamic response. In contrast to small-scale system tests, which typically employ artificial soil mixtures to simulate natural deposits, full-scale system tests necessitate significant efforts to characterise the soil composition surrounding and beneath the pile foundation. Moreover, soil properties exhibit spatial dependence (e.g. presence of boulders, sand or clay sediments, soft layers), temporal variability (e.g. structural settlement or soil consolidation), and are influenced by the employed characterisation techniques—such as laboratory analysis of samples or in-situ seismic testing (e.g. cross hole). Consequently, full-scale system tests are considered an expensive experimental investigation since parametric studies cannot be performed. Nevertheless, they yield invaluable insights into the performance of pile foundation systems under realistic soil and pile stress conditions. In the following, a brief review of some experimental studies on full-scale systems is presented. The interested reader is referred to the work presented by Meymand [133] for a more detailed review of the subject.

Both pile and field responses were evaluated by Masoumi et al. in [140]. In this work, two cast-in-situ concrete piles with a diameter of 0.46 m were partially embedded in dry sand, which was characterised by a spectral analysis of surface waves (SASW) test and the information was used in a prediction model based on the coupled FE-BE method. The piles are excited at their heads using a 5.5 kg instrumented hammer to evaluate pile and soil low-strain vibrations. A good agreement was obtained between the time history and the frequency content of the measured and predicted pile head response, respectively when compared. Additionally, A reasonable

agreement between the predicted and experimental results at far distances is found regarding the free-field response, but significant discrepancies were found when evaluated at closer ones. Masoumi et al. concluded that the soil response is more sensitive at closer distances rather than longer ones, so a careful characterisation of the damping ratio of the soil is crucial to predict thus free-field vibration levels accurately. Elkasabgy and El Naggar performed a full-scale test on a double-helix helical pile and a driven steel pile of the same length and shaft geometry [141]. Elkasabgy and El Naggar aimed to study the dynamic performance of the piles when subjected to harmonic (quadratic) loading of different force intensities and the influence of the consolidation settlement in the dynamic response. Predicted results, based on linear and nonlinear theories computed using the DYNA 6 software [142], are compared with the measured ones, which were tested twice: two weeks and nine months after the installation. The comparison of experimental results showed that the dynamic response of helical piles is essentially the same as that of driven steel piles. Additionally, it has shown that free-field response is mainly induced by the soil-pile shaft interaction rather than by the presence of that double-helix in the helical pile. By comparing the data recorded two weeks after installation with the predicted results, the linear theory tends to overestimate the stiffness and damping of the piles since the model assumes perfect pile-soil contact. On the contrary, the nonlinear model, which accounted for the weak boundary zone and the pile-soil separation in their formulation, provided reasonable estimations. However, the discrepancies between these results increased when the comparison accounts for the data recorded nine months after installation, concluding that the weak boundary zone's influence has reduced due to the soil's stiffening. Capatti et al. [143] present data recorded in extensive experimental tests on full-scale vertical-injected (grouted at high pressures) and not injected (simply grouted) micropiles embedded in alluvial soils. Three experimental setups were considered consisting of ambient vibration and impact load tests to investigate the system's dynamic response and snap back (ringdown) test to investigate its nonlinear behaviour. The fundamental frequency of the micropile with injections was found to be higher than the simply grouted. Additionally, the radial driving response of the injected micropile is no longer the same along two investigated orthogonal directions. Regarding the ambient vibration test, although this method provides reliable dynamic properties of the systems concerning the impact test load, this requires more demanding post-processing techniques. The snap-back tests showed that the injected micropile develops several nonlinear behaviours due to the resulting opening of radial cracks in the soil-micropile interface.

Han and Vaziri [144] tested the dynamic response of six cast-in-place reinforced concrete piles

subjected to a lateral harmonic excitation generated by counterrotating eccentric mass, which was placed on the pile cap. The experiment conducted in winter time aimed to evaluate the influence of frozen soil layer on the dynamic behaviour of the pile-group, as well as to investigate the viability of theoretical approaches based on dynamic interaction factors in predicting pile-group system. The experimental results showed that the presence of a frozen soil layer induces the dynamic response to a significant displacement reduction regarding experimental data acquired in the summertime. Moreover, although the pile-group formulation based on the dynamic interaction can predict reasonably good results, introducing weak boundary zones in its formulation improves the agreement between the calculated and measured results. Biswas and Manna [145] employed a mechanical oscillator to produce lateral harmonic loads of different excitation intensities to test the dynamic response on pile and pile-group systems. The systems accounted for pressure sensors along the pile length to thus investigate the distance from the ground level up to the point of no contact between the pile and soil (pile-soil separation length). Biswas and Manna employed the computational tool DYNA 6, which accounted for the separation length and weak boundary zones around the pile-soil interface in the formulation, to predict pile-soil responses and compared it with experimental results. Good agreements are presented in the comparison of results. An extension of this work using pile-groups with different pile spacing was presented in [146]. Recently, Theland et al. [147] have presented an experimental study of the dynamic response of end-bearing single and multi piles foundations embedded in soft clay. This study addresses the dynamic response of a single-pile, the dynamic interaction factors of the pile-group without casting the pile cap, and the global behaviour of the 2x2 pile-group connected by a concrete cap. The system has been instrumented with accelerometers along the centerline of each pile, and the soil properties for small and large-strain excitations have been measured using non-destructive tests. The dynamic load was induced by an impact hammer with a mass of 5.5 kg. The authors have compared the experimental results against predictions performed using a FE model of the system provided with perfectly matched layers to attenuate any outgoing waves. The comparison shows that while the numerical model tends to overestimate the dynamic response of the single-pile, a good agreement is obtained in the pile-group case.

Chapter 3

A single-pile foundation model based on the singular boundary method

An efficient three-dimensional approach for solving pile-soil interaction problems is proposed in this chapter. In the approach, the soil is modelled as an elastic half-space, and its response in the presence of the pile's corresponding cavity is computed by employing the singular boundary method (SBM). The pile is modelled analytically using the classic rod and Euler-Bernoulli beam theories. For the coupling with the soil, the pile is divided into a set of rigid segments that interact along their circumference with the soil. The methodology allows the rotational motions and reaction torques at these segments to be accounted for, and their contribution to the accuracy of the scheme is assessed. A criterion to define the minimum number of collocation points that offers an acceptable trade-off between accuracy and numerical performance is also proposed. For radiation problems, the method is verified against well-established methodologies. In contrast, the reciprocity principle, which relates the wave radiation from the pile to the ground field with the incident wave problem due to a load on the ground surface, is employed to verify the system response under incident wave fields. Results are shown for different soil stiffnesses and different pile length to diameter ratios. The employment of the singular boundary method is shown to provide strong computational advantages with respect to detailed modelling approaches such as the three-dimensional (3D) finite element-boundary element (FE-BE) method, as well as overcoming the fundamental limitations of plain-strain and axisymmetric methods.

3.1 Single-pile foundation modelling

The system under investigation consists of a single-pile embedded in a homogeneous half-space, as shown schematically in Fig. 3.1, with the origin of the Cartesian coordinate system placed on the ground surface and coincident with the pile axis. In the formulation, lowercase letters denote variables in the time domain, and uppercase letters relate to scalar variables in the frequency domain. Bold lowercase letters and bold uppercase letters denote vectors or matrices in the time domain and frequency domain, respectively. A modelling strategy is presented that aims to compute the dynamic response of the system, at the pile head and at the ground surface, due to loads applied at the pile head and/or at the ground surface. The pile is assumed to be purely elastic and is modelled as a rod to account for axial and torsional motions, whilst the Euler-Bernoulli beam theory is considered for the flexural response of the pile. The soil is considered as an elastic homogeneous half-space; however, the proposed methodology can be applied to layered soils as well. Non-linear effects associated with pile-soil contact interactions, high strain levels or soil liquefaction are not accounted for. The coupled pile-soil model is formulated in the frequency domain and constructed employing the dynamic substructuring technique; the response of each subsystem is separately derived and they are coupled considering force equilibrium and displacement compatibility conditions. The mathematical formulation of the proposed model is presented in the following subsections.

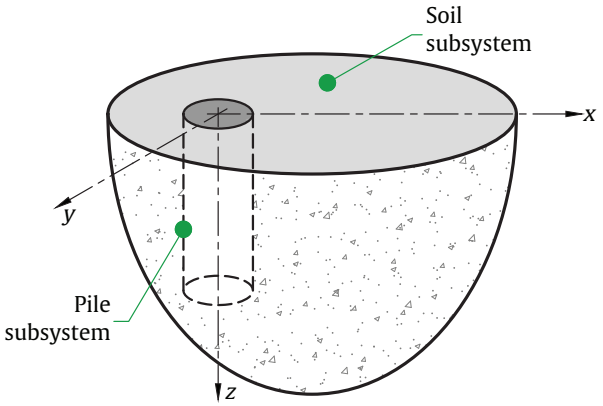

FIGURE 3.1: Schematic drawing of the pile-soil system.

3.1.1 Model of the pile subsystem

As mentioned above, the pile subsystem is modelled analytically using axial rod and Euler-Bernoulli beam theories. Thus, the model accounts for the 3D deformation of the pile, represented by displacements $u_{\mathrm{p}i}= (u_{\mathrm{p}x}, u_{\mathrm{p}y}, u_{\mathrm{p}z})$ and rotations $\phi_{\mathrm{p}i}= (\phi_{\mathrm{p}x}, \phi_{\mathrm{p}y}, \phi_{\mathrm{p}z})$ along the three Cartesian coordinates (x, y, z), respectively. Free-free boundary conditions are adopted for both rod and beam models. In this section, the expressions that determine the response of the pile model when subjected to loads applied to an arbitrary position along the pile axis z are outlined.

First, consider the differential equations of motion of a rod for axial and torsional deformations before applying any external excitation, which are given by the expressions

$$\rho_{\mathrm{p}} \frac{\partial^2 u_{\mathrm{p}z}(z,t)}{\partial t^2} - E_{\mathrm{p}} \frac{\partial^2 u_{\mathrm{p}z}(z,t)}{\partial z^2} = 0, \tag{3.1a}$$

$$\frac{\partial^2 \phi_{\mathrm{p}z}(z,t)}{\partial t^2} - C_{\mathrm{s}}^2 \frac{\partial^2 \phi_{\mathrm{p}z}(z,t)}{\partial z^2} = 0, \tag{3.1b}$$

where E_{p} is the elastic modulus of the pile. The shear wave speed of the pile is given by $C_{\mathrm{s}} = \sqrt{G_{\mathrm{p}}/\rho_{\mathrm{p}}}$, being G_{p} the shear modulus and ρ_{p} its density. For the bending motion of the pile, the differential equation of an Euler-Bernoulli beam

$$\rho_{\mathrm{p}} A_{\mathrm{p}} \frac{\partial^2 u_{\mathrm{p}x}(z,t)}{\partial t^2} + E_{\mathrm{p}} I_{\mathrm{p}} \frac{\partial^4 u_{\mathrm{p}x}(z,t)}{\partial z^4} = 0, \tag{3.2}$$

is employed, where A_{p} is the cross-sectional area of a pile, and I_{p} is the second moment of area of the pile's cross-section. The same expression is also valid for $u_{\mathrm{p}y}(z,t)$ that describes the bending in the y direction.

The pile is excited at an arbitrary position z_1 along the pile axis, as illustrated in Fig. 3.2, by an arbitrary set of harmonic forces and moments of the form $f_i(z,t) = F_i(z)\exp(\mathrm{i}\omega t)$ and $m_i(z,t) = M_i(z)\exp(\mathrm{i}\omega t)$, respectively, with $i = x, y, z$; ω is the angular frequency and $\mathrm{i} = \sqrt{-1}$ represents the unit imaginary number. The resulting displacements and rotations of the pile take the form $u_{\mathrm{p}i}(z,t) = U_{\mathrm{p}i}(z)\exp(\mathrm{i}\omega t)$ and $\phi_{\mathrm{p}i}(z,t) = \theta_{\mathrm{p}i}(z)\exp(\mathrm{i}\omega t)$, respectively, where $\theta_{\mathrm{p}i}$ is used to represent the rotational motion $\phi_{\mathrm{p}i}$ in the frequency domain. As a result, the axial response of the free-free pile along its neutral axis due to a unit point load can be expressed in the frequency domain as

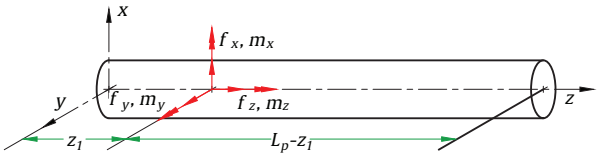

FIGURE 3.2: Pile subsystem (illustrated horizontally for convenience) subjected to arbitrary loads at an arbitrary position along the pile axis.

$$U_{pz}(z) = A_1 \cos(\alpha z) + A_2 \sin(\alpha z), \qquad 0 \le z \le z_1, \tag{3.3a}$$

$$U_{pz}(z) = A_3 \cos(\alpha z) + A_4 \sin(\alpha z), \qquad z_1 \le z \le L_p, \tag{3.3b}$$

where L_p is the pile length and $\alpha^2 = (\rho_p \omega^2)/E_p$.

Similarly, the expressions for the torsional response are given by

$$\theta_{pz}(z) = B_1 \cos(\gamma z) + B_2 \sin(\gamma z), \qquad 0 \le z \le z_1, \tag{3.4a}$$

$$\theta_{pz}(z) = B_3 \cos(\gamma z) + B_4 \sin(\gamma z), \qquad z_1 \le z \le L_p, \tag{3.4b}$$

where $\gamma^2 = (\rho_p \omega^2)/G_p$. The expressions for the coefficients A_j in Eqs. (3.3) and B_j in Eqs. (3.4) can be found in Appendix A.

Finally, the lateral displacements induced by lateral loads or bending moments can be determined using the following expressions:

$$U_{px}(z) = C_1 \cos(\beta z) + C_2 \sin(\beta z) + C_3 \cosh(\beta z) + C_4 \sinh(\beta z), \quad 0 \le z \le z_1, \tag{3.5a}$$

$$U_{px}(z) = C_5 \cos(\beta z) + C_6 \sin(\beta z) + C_7 \cosh(\beta z) + C_8 \sinh(\beta z), \quad z_1 \le z \le L_p, \tag{3.5b}$$

where $\beta^4 = (\rho_p A_p \omega^2)/(E_p I_p)$. The coefficients C_j are again defined in Appendix A, whilst the cross-sectional rotation induced by lateral loads or bending moments can be obtained applying $\theta_{py} = \partial U_{px}/\partial z$ in Eq. (3.5). These expressions are associated with the bending in the y direction: analogous expressions can be used for the bending of the pile in the x direction.

3.1.2 Model of the soil subsystem

The soil subsystem is modelled as an elastic half-space that includes the cavity corresponding to the pile using the SBM [113, 115, 148]. In order to describe the SBM-based model of the soil presented in this work, consider the general case of a 3D cavity in an elastic medium $\Omega \in \mathbb{R}^3$, as shown in Fig. 3.3(a), where $\partial\Omega$ represents the boundary (for simplicity, the key elements of the SBM are represented in a 2D scheme in the figure). The variables $\mathbf{x}$, $\mathbf{y}$ denote the position in a Cartesian system of coordinates of points located at $\partial\Omega$ and Ω, respectively. As a radial basis function method, the SBM assumes that the dynamic unknown states of the medium (the displacement and traction fields for the case of the soil) can be approximated by a linear combination of a set of virtual sources with the fundamental solution (or Green's function) of the medium evaluated at the virtual sources locations, which are placed over the physical boundary $\partial\Omega$. Red circles in Fig. 3.3(b) and Fig. 3.3(c) represent this set of virtual forces. This leads to a system of equations that can be expressed as

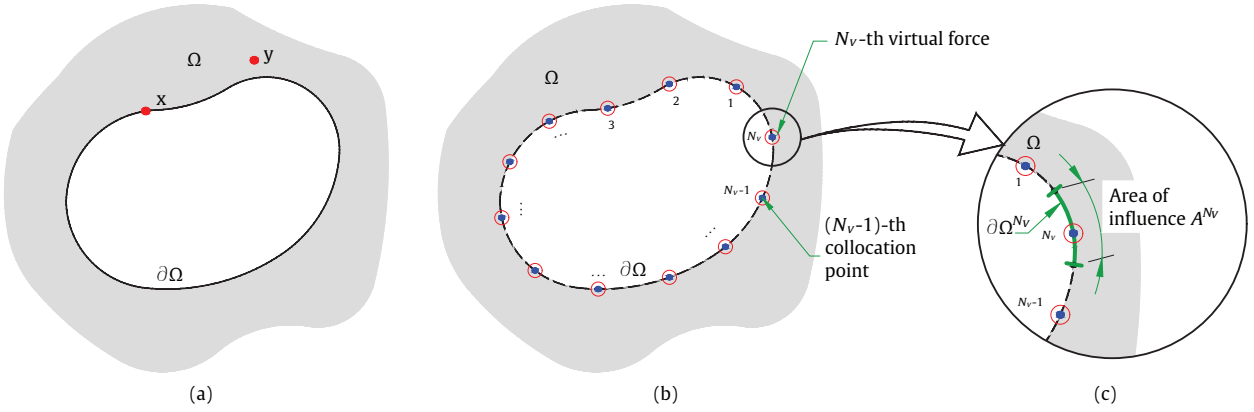

FIGURE 3.3: Schematic of the generic problem (a); distribution of the collocation points (marked by blue dots) and the virtual sources (marked by red circles) over the boundary (b); and generic description of the area of influence associated with a particular virtual source (c).

$$\mathbf{U}(\mathbf{y}) = \sum_{v=1}^{N_v} \mathbf{H}(\mathbf{y}, \mathbf{x}^v, \omega)\mathbf{S}^v, \tag{3.6a}$$

$$\mathbf{T}(\mathbf{y}) = \sum_{v=1}^{N_v} \mathbf{H}^T(\mathbf{y}, \mathbf{x}^v, \omega)\mathbf{S}^v, \tag{3.6b}$$

where the vectors $\mathbf{U}(\mathbf{y})$, $\mathbf{T}(\mathbf{y})$ contain the three components of the displacements and tractions of the medium, respectively, at the point $\mathbf{y}$. These are induced by a set of virtual sources in which the v-th virtual force of the set is defined by the three-component complex vectors $\mathbf{S}^v$ for amplitude and $\mathbf{x}^v$ for position. The displacement and traction elastodynamic fundamental solutions in the frequency domain evaluated at the point $\mathbf{y}$ caused by a point load placed at $\mathbf{x}^v$ are represented by the matrices $\mathbf{H}(\mathbf{y}, \mathbf{x}^v, \omega)$ and $\mathbf{H}^\tau(\mathbf{y}, \mathbf{x}^v, \omega)$, respectively. Eq. (3.6) can be seen as a discrete version of the indirect boundary integral equation in the form of a single-layer potential, as discussed in detail by Gu et al. [113]. Thus, the set of virtual sources can be interpreted as a discretization of the flux discontinuity, which is used as auxiliary sources in the indirect boundary integral equations in the form of a single-layer potential [149]. It is worth mentioning that the fundamental solution notation in this dissertation is based on a function with three input variables: the first representing the receiver location, the second the source location and the third the angular frequency at which the fundamental solution is evaluated and that it has been explicitly included to ease the differentiation between elastodynamic and elastostatic fundamental solutions in what follows. In the case of the traction fundamental solution, the vector normal to the plane at which the traction is evaluated is a variable not explicitly stated in the notation of the fundamental solutions but also required in its calculation.

It is important to note that, as for the BEM, the SBM naturally allows for using Green's functions of more complex problems than the case of a full-space, for instance, homogeneous or layered half-spaces (both employed in [115]). In this dissertation, the soil is assumed to be a homogeneous elastic half-space. The corresponding Green's functions to this problem are computed on the basis of the direct stiffness matrix method proposed by Kausel [150]. However, the adoption of layered models of the soil can be carried out simply by replacing those Green's functions with the corresponding ones of the adopted layered half-space configuration, which can also be obtained based on the direct stiffness matrix method [150].

To determine the virtual sources due to the prescribed boundary conditions, the collocation method is commonly used in boundary domain methods, which proposes to discretize those boundary conditions at a set of collocation points distributed along the physical boundary. For the particular SBM approach presented in this work, a set of collocation points, defined by the positions $\mathbf{x}^c$, is established for $c = 1, 2, ..., N_\mathrm{c}$. This set of collocation points is assumed to be geometrically coincident with the set of virtual sources, having $N_\mathrm{c} = N_\mathrm{v}$. Both sets of collocation and source points are shown in Fig. 3.3(b). A linear system of equations results by the evaluation of Eq. (3.6) at all the collocation points of the set. Due to geometrical coincidence between collocation and source sets, singularities arise from the fundamental solutions in Eq.

(3.6) when $c = v$. To overcome those singularities, the SBM proposes to employ the origin intensity factors (OIFs) [115]. When considered, the resulting linear systems of equations for Dirichlet and Neumann boundary conditions, respectively, are

$$\mathbf{U}(\mathbf{x}^c) = \sum_{v=1, v\neq c}^{N_\mathrm{v}} \mathbf{H}(\mathbf{x}^c, \mathbf{x}^v, \omega)\mathbf{S}^v + \mathbf{H}_{\mathrm{cc}}\mathbf{S}^c, \quad \text{for } c = 1, 2, ..., N_\mathrm{v}, \tag{3.7a}$$

$$\mathbf{T}(\mathbf{x}^c) = \sum_{v=1, v\neq c}^{N_\mathrm{v}} \mathbf{H}^\tau(\mathbf{x}^c, \mathbf{x}^v, \omega)\mathbf{S}^v + \mathbf{H}^\tau_{\mathrm{cc}}\mathbf{S}^c, \quad \text{for } c = 1, 2, ..., N_\mathrm{v}, \tag{3.7b}$$

where $\mathbf{H}_{\mathrm{cc}}$ and $\mathbf{H}^\tau_{\mathrm{cc}}$ represent the matrices of the OIFs associated with the Dirichlet and Neumann boundary conditions, respectively.

The fundamental solutions $\mathbf{H}^\tau(\mathbf{x}^c, \mathbf{x}^v, \omega)$ behaves as a singular function of the type $|\mathbf{x}^c - \mathbf{x}^v|^{-2}$ when $\mathbf{x}^c$ tends to $\mathbf{x}^v$ [149]. Thus, to derive the corresponding OIFs, a regularization strategy similar to the one used in standard BEM is considered. The procedure involves the application of the subtracting and adding-back technique in Eq. (3.7b) and using the rigid-body identity. This procedure is thoroughly explained in [113, 115] for the elastostatics and elastodynamic problems, respectively. Here, the formulation presented in [115] for determining the OIFs associated with the Neumann boundary condition is adopted. A three-dimensional version of that formulation results in

$$\mathbf{H}^\tau_{\mathrm{cc}} = \frac{1}{A^c}\left[\mathbf{I} + \mathbf{B}_{\mathrm{cc}} - \sum_{v=1, v\neq c}^{N_\mathrm{v}} A^v \mathbf{H}^\tau(\mathbf{x}^v, \mathbf{x}^c, 0)\right], \tag{3.8}$$

where the terms A^v and A^c represent the area of influence associated with the v-th and c-th sources, respectively, as shown in Fig. 3.3(c). $\mathbf{I}$ is the identity matrix, $\mathbf{H}^\tau(\mathbf{x}^v, \mathbf{x}^c, 0)$ is the matrix of static fundamental solutions for the tractions and $\mathbf{B}_{\mathrm{cc}}$ is given by

$$\mathbf{B}_{\mathrm{cc}} = \int_{\partial\Omega^c} \left[\mathbf{H}^\tau(\mathbf{x}^c, \mathbf{x}, 0) - \mathbf{H}^\tau(\mathbf{x}, \mathbf{x}^c, 0)\right] \mathrm{d}S_x, \tag{3.9}$$

where $\mathrm{d}S_x$ is a differential of area along the boundary portion $\partial\Omega^c$, which is the portion of influence of the c-th source, with a total area of A^c. Note that the integration in Eq. (3.9) is performed componentwise (i.e. the integration is performed for each component of the matrix). For arbitrarily smooth boundaries, by assuming that the considered source point moves gradually close to the considered collocation point along a line segment, the term $\mathbf{B}_{\mathrm{cc}}$

becomes zero [151, 152]. For general boundaries, $\mathbf{B}_{cc}$ is still regular and can be numerically integrated using standard Gaussian quadrature [113].

Regarding the OIFs for the Dirichlet boundary condition, the fundamental solution $\mathbf{H}(\mathbf{x}^c, \mathbf{x}^v, \omega)$ undergoes a singular of behaviour of the form $|\mathbf{x}^c - \mathbf{x}^v|^{-1}$ [149] when $\mathbf{x}^c$ tends to $\mathbf{x}^v$. In this case, the associated OIFs $\mathbf{H}_{cc}$ can be directly computed by averaging the fundamental solution over the boundary portion of influence where the virtual source is applied [113, 115, 152].

The linear systems of equations associated with Eqs. (3.7a, 3.7b) can be written in matrix form as

$$\mathbf{U}_b = \mathbf{H}_{bb}\mathbf{S}, \quad \mathbf{T}_b = \mathbf{H}^{\tau}_{bb}\mathbf{S}, \tag{3.10}$$

where $\mathbf{U}_b$, $\mathbf{T}_b$ are the vectors that contain the three components of the displacements and tractions, respectively, at the boundary for all collocation points. The vector $\mathbf{S}$ contains the source intensities of all virtual sources, and $\mathbf{H}_{bb}$ and $\mathbf{H}^{\tau}_{bb}$ are the corresponding matrices of frequency response functions of the soil for the displacement and traction, respectively, which are composed of Green's functions and OIFs. A unit vector normal to the boundary pointing outwards to the soil medium is considered when constructing $\mathbf{H}^{\tau}_{bb}$. In a similar way, displacements $\mathbf{U}_s$ at an arbitrary point in the soil medium can be computed using the matrix form Eq. (3.6a), which can be written as

$$\mathbf{U}_s = \mathbf{H}_{sb}\mathbf{S}, \tag{3.11}$$

where $\mathbf{H}_{sb}$ is the matrix of fundamental solutions that relates the set of forces $\mathbf{S}$ with the responses at the particular arbitrary point.

3.1.3 Pile-soil coupling formulation

The pile-soil dynamic coupling is carried out by employing the dynamic substructuring technique considering the two subsystems presented in the previous two subsections, the pile and the soil with the pile's cavity inclusion. When coupling two elastic solids, this technique enforces compatibility of the strain and stress fields at their interface. In the proposed method for pile-soil problems presented in this work, these conditions are met by ensuring displacement and interaction forces compatibility at a set of collocation points distributed along the pile-soil interface. Interaction forces seen by the cavity at the collocation points are determined considering a constant distribution of the traction field in the vicinity of each particular collocation

point, whilst these forces are transferred to the pile as point forces.

A detailed description of the collocation point distribution employed is presented in Fig. 3.4(a). A uniformly distributed set of N_{p} ring-shaped distributions of collocation points are defined along the lateral pile-soil interface. Each ring-shaped distribution has a total of N_{s} uniformly distributed collocation points. Also, an additional collocation point is located at its centre in the bottom circular pile-soil interface. Therefore, this implies that the dynamic fields at the pile-soil interface are represented at $N_{\mathrm{c}} = N_{\mathrm{s}}N_{\mathrm{p}} + 1$ collocation points. As shown in Fig. 3.4(a), a set of uniformly distributed pile centroid points constitutes the discretization scheme for the pile. Each of them is associated with a pile segment and also with a ring of collocation points. Based on the assumption that each of these pile segments is rigid, the corresponding responses at the collocation points at the pile-soil interface can be related with the responses of the pile at the centroid points. The derivation of this relation is presented in the next paragraphs. Additionally, the areas of influence associated with each collocation point have also been depicted in Fig. 3.4(b). These areas are important in the application of the SBM to model the soil, as described in the previous section, as well as for the determination of the interaction forces applied to the pile from the tractions at the pile-soil interface.

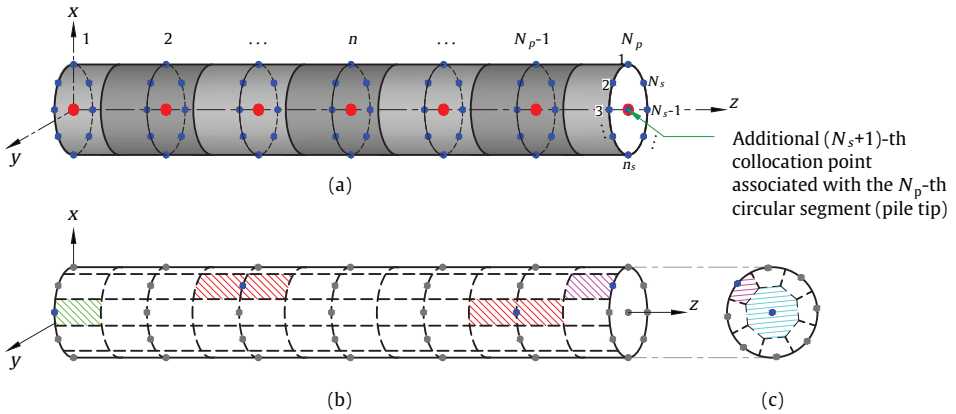

FIGURE 3.4: Discretization schemes adopted in this work (illustrated horizontally for convenience). In (a), the distribution of collocation points (blue dots) over the pile-soil interface, together with the corresponding pile centroid points (red dots) is displayed. In (b) and (c), the four distinct types of areas of influence are presented: In green, the area of influence of a collocation point located at the ground surface is shown; in red, the one for a collocation point located in an intermediate position along the lateral interface is illustrated; in magenta, the influence area for one point of the ring-shaped distribution at the pile tip is represented; and finally, in cyan, the area of influence of the collocation point located at the centre of the bottom pile-soil interface is displayed.

The displacements at all collocation points along the pile-soil interface are collected by the vectors $\mathbf{U}_{\mathrm{b}}^{\mathrm{s}}$ and $\mathbf{U}_{\mathrm{b}}^{\mathrm{p}}$ for the soil and pile subsystems, respectively. Displacement compatibility at the interface leads to $\mathbf{U}_{\mathrm{b}}^{\mathrm{s}} = \mathbf{U}_{\mathrm{b}}^{\mathrm{p}}$. Due to the assumption that each pile segment acts as a rigid body, the displacements $\mathbf{U}_{\mathrm{b}}^{\mathrm{p}}$ can be expressed in terms of the rigid body translation and rotation of the cylindrical segments defined at the corresponding pile centroid points displacements as

$$\mathbf{U}_{\mathrm{b}}^{\mathrm{p}} = \mathbf{W}\mathbf{U}_{\mathrm{p}}, \tag{3.12}$$

where the $\mathbf{U}_{\mathrm{p}}$ vector collects the displacements and rotations at all pile centroid points, and $\mathbf{W}$ is the transformation matrix that relates the six degrees of freedom of all pile centroid points with the three-component motion of all collocation points. Details of this transformation and the definition of $\mathbf{W}$ are given in Appendix B. The compatibility of the reaction forces at the interface is expressed as $\mathbf{P}_{\mathrm{b}}^{\mathrm{s}} = -\mathbf{P}_{\mathrm{b}}^{\mathrm{p}}$, with $\mathbf{P}_{\mathrm{b}}^{\mathrm{s}}$ and $\mathbf{P}_{\mathrm{b}}^{\mathrm{p}}$ being the interaction forces to which the soil and the pile are subjected, respectively, at all collocation points. As mentioned above, the present methodology assumes that the traction field in the pile-soil interface is constant along each influence area and equal to the value evaluated at its corresponding collocation point. Thus, the interaction forces to which the soil is subjected are given by

$$\mathbf{P}_{\mathrm{b}}^{\mathrm{s}} = \mathbf{W}_{\mathrm{A}}\mathbf{T}_{\mathrm{b}}^{\mathrm{s}}, \tag{3.13}$$

where $\mathbf{W}_{\mathrm{A}}$ is a diagonal matrix that contains the areas of influence associated with all collocation points and $\mathbf{T}_{\mathrm{b}}^{\mathrm{s}}$ is the vector that contains the tractions at all collocation points along the pile-soil interface. Regarding the pile interaction forces, their summation for each rigid pile segment results in equivalent three-component forces and moments applied to the corresponding pile centroid point. This transformation is analogous to the one presented for the translational and rotational motions: $\mathbf{P}_{\mathrm{p}} = \mathbf{W}^{\mathrm{T}}\mathbf{P}_{\mathrm{b}}^{\mathrm{p}} = -\mathbf{W}^{\mathrm{T}}\mathbf{P}_{\mathrm{b}}^{\mathrm{s}}$ (see Appendix B for more details). Thus, tractions at the pile-soil interface are related with the interaction forces and moments at the pile centroid as

$$\mathbf{P}_{\mathrm{p}} = -\mathbf{W}^{\mathrm{T}}\mathbf{W}_{\mathrm{A}}\mathbf{T}_{\mathrm{b}}^{\mathrm{s}}. \tag{3.14}$$

As discussed above, the transformations of motions and forces from the pile centroid points to the collocation points consider both translational and rotational motions, as well as forces and moments. A simplified approach has been considered in previous works about dynamic pile-soil interaction, for which the rotations and the moments are neglected in the coupling procedure [4, 5]. This assumption can also be applied in the context of the present formulation, as discussed in Appendix B. The accuracy of such simplification are studied in Section 3.2.

The pile-soil system is considered to be subjected to external forces at the pile head and at an arbitrary point in the soil, represented by the three-component vectors $\mathbf{F}_\mathrm{p}$ and $\mathbf{F}_\mathrm{s}$, respectively. Based on the superposition principle, the dynamic unknown states of the soil can be written as the summation of the motion induced by the external load $\mathbf{F}_\mathrm{s}$ and the motion induced by the traction boundary condition at the pile-soil interface. Thus, based on Eqs. (3.10) and (3.11), the response at the collocation points $\mathbf{U}_\mathrm{b}^\mathrm{s}$ and at an arbitrary point in the soil $\mathbf{U}_\mathrm{s}$ can be written as

$$\mathbf{U}_\mathrm{b}^\mathrm{s} = \mathbf{H}_\mathrm{bb}(\mathbf{H}_\mathrm{bb}^\tau)^{-1}\mathbf{T}_\mathrm{b}^\mathrm{s} + \mathbf{H}_\mathrm{bf}^\mathrm{cav}\mathbf{F}_\mathrm{s}, \tag{3.15a}$$

$$\mathbf{U}_\mathrm{s} = \mathbf{H}_\mathrm{sb}(\mathbf{H}_\mathrm{bb}^\tau)^{-1}\mathbf{T}_\mathrm{b}^\mathrm{s} + \mathbf{H}_\mathrm{sf}^\mathrm{cav}\mathbf{F}_\mathrm{s}, \tag{3.15b}$$

with $\mathbf{H}_\mathrm{bf}^\mathrm{cav}$ and $\mathbf{H}_\mathrm{sf}^\mathrm{cav}$ being the receptance matrices relating the response at the collocation points and at an arbitrary point in the soil subsystem, respectively, due to the external force $\mathbf{F}_\mathrm{s}$. The superindex cav is used to denote that these receptance matrices of the soil should be determined by accounting for the inclusion of the cavity. They can be expressed in terms of the Green's functions of an elastic half-space with no inclusions as

$$\mathbf{H}_\mathrm{bf}^\mathrm{cav} = \mathbf{H}_\mathrm{bf} - \mathbf{H}_\mathrm{bb}(\mathbf{H}_\mathrm{bb}^\tau)^{-1}\mathbf{H}_\mathrm{bf}^\tau \quad \text{and} \quad \mathbf{H}_\mathrm{sf}^\mathrm{cav} = \mathbf{H}_\mathrm{sf} - \mathbf{H}_\mathrm{sb}(\mathbf{H}_\mathrm{bb}^\tau)^{-1}\mathbf{H}_\mathrm{bf}^\tau, \tag{3.16}$$

where the matrices $\mathbf{H}_\mathrm{bf}$ and $\mathbf{H}_\mathrm{sf}$ contain the Green's functions associated with the source point of $\mathbf{F}_\mathrm{s}$ and the receivers at the collocation points or at the arbitrary point in the soil, respectively. The matrix $\mathbf{H}_\mathrm{bf}^\tau$ is analogous to $\mathbf{H}_\mathrm{bf}$ but for traction response. In Eq. (3.16), the second terms of the right-hand side simulates the existence of the cavity by enforcing a traction-free field along the surface where the pile-soil interface should be.

Similar expressions can be derived for the pile subsystem, for which its responses at the collocation points $\mathbf{U}_\mathrm{b}^\mathrm{p}$ and at the pile head $\mathbf{U}_\mathrm{h}$ are given by

$$\mathbf{U}_\mathrm{b}^\mathrm{p} = \mathbf{W}\left(\mathbf{H}_\mathrm{ph}\mathbf{F}_\mathrm{p} - \mathbf{H}_\mathrm{pp}\mathbf{W}^\mathrm{T}\mathbf{W}_\mathrm{A}\mathbf{T}_\mathrm{b}^\mathrm{s}\right), \tag{3.17a}$$

$$\mathbf{U}_\mathrm{h} = \mathbf{H}_\mathrm{hh}\mathbf{F}_\mathrm{p} - \mathbf{H}_\mathrm{hp}\mathbf{W}^\mathrm{T}\mathbf{W}_\mathrm{A}\mathbf{T}_\mathrm{b}^\mathrm{s}, \tag{3.17b}$$

in which $\mathbf{H}_\mathrm{ph}$, $\mathbf{H}_\mathrm{pp}$, $\mathbf{H}_\mathrm{hh}$ and $\mathbf{H}_\mathrm{hp}$ are the matrices of receptance functions that relate the response at all pile centroid points or at the pile head (represented by p and h, respectively, as the first subscript) due to forces along the pile or at the pile head (represented by the same nomenclature for the second subscript).

By applying the compatibility of displacements and using Eqs. (3.15a) and (3.17a), the tractions at the pile-soil interface can be determined and subsequently substituted to Eqs. (3.15b) and (3.17b) to find the final expressions for the coupled pile-soil system which allow for calculating the responses of an arbitrary point in the soil or the pile head, respectively. These responses of the coupled system can be written as a function of the external loads as

$$\mathbf{U}_{\mathrm{s}} = \mathbf{H}^{\mathrm{c}}_{\mathrm{sh}}\mathbf{F}_{\mathrm{p}} + \mathbf{H}^{\mathrm{c}}_{\mathrm{sf}}\mathbf{F}_{\mathrm{s}}, \tag{3.18a}$$

$$\mathbf{U}_{\mathrm{h}} = \mathbf{H}^{\mathrm{c}}_{\mathrm{hh}}\mathbf{F}_{\mathrm{p}} + \mathbf{H}^{\mathrm{c}}_{\mathrm{hf}}\mathbf{F}_{\mathrm{s}}, \tag{3.18b}$$

where $\mathbf{H}^{\mathrm{c}}_{\mathrm{sh}}$, $\mathbf{H}^{\mathrm{c}}_{\mathrm{sf}}$, $\mathbf{H}^{\mathrm{c}}_{\mathrm{hh}}$ and $\mathbf{H}^{\mathrm{c}}_{\mathrm{hf}}$ are the receptance matrices of the coupled system that provide the relationship between the response of an arbitrary point in the soil or the pile head (identified in the first subscript by s and h, respectively) due to forces applied to the soil at another arbitrary point or forces applied to the pile head (identified by the second subscripts f and h, respectively). These matrices are given by the following expressions

$$\mathbf{H}^{\mathrm{c}}_{\mathrm{sh}} = \mathbf{H}_{\mathrm{sb}}(\mathbf{H}^{\tau}_{\mathrm{bb}})^{-1}\boldsymbol{\Upsilon}\mathbf{W}\mathbf{H}_{\mathrm{ph}}, \tag{3.19a}$$

$$\mathbf{H}^{\mathrm{c}}_{\mathrm{sf}} = \mathbf{H}^{\mathrm{cav}}_{\mathrm{sf}} - \mathbf{H}_{\mathrm{sb}}(\mathbf{H}^{\tau}_{\mathrm{bb}})^{-1}\boldsymbol{\Upsilon}\mathbf{H}^{\mathrm{cav}}_{\mathrm{bf}}, \tag{3.19b}$$

$$\mathbf{H}^{\mathrm{c}}_{\mathrm{hh}} = \mathbf{H}_{\mathrm{hh}} - \mathbf{H}_{\mathrm{hp}}\mathbf{W}^{\mathrm{T}}\mathbf{W}_{\mathrm{A}}\boldsymbol{\Upsilon}\mathbf{W}\mathbf{H}_{\mathrm{ph}}, \tag{3.19c}$$

$$\mathbf{H}^{\mathrm{c}}_{\mathrm{hf}} = \mathbf{H}_{\mathrm{hp}}\mathbf{W}^{\mathrm{T}}\mathbf{W}_{\mathrm{A}}\boldsymbol{\Upsilon}\mathbf{H}^{\mathrm{cav}}_{\mathrm{bf}}, \tag{3.19d}$$

with

$$\boldsymbol{\Upsilon} = \left[\mathbf{H}_{\mathrm{bb}}(\mathbf{H}^{\tau}_{\mathrm{bb}})^{-1} + \mathbf{W}\mathbf{H}_{\mathrm{pp}}\mathbf{W}^{\mathrm{T}}\mathbf{W}_{A}\right]^{-1}. \tag{3.20}$$

Eqs. (3.18a) and (3.18b) inherently contain the solution to both radiation and scattering problems for the system under study, which can be extracted by enforcing $\mathbf{F}_{\mathrm{s}} = \mathbf{0}$ or $\mathbf{F}_{\mathrm{p}} = \mathbf{0}$, respectively.

Finally, note that the formulation of the proposed model is not limited to single-piles and/or homogeneous soils. While the case of a multi-pile foundation can be directly considered by considering displacement compatibility and force equilibrium on each pile (as described in detail in Chapter 4), considering horizontally layered soils instead of homogeneous ones only requires using the corresponding Green's functions in the calculation.

3.2 Numerical assessment of the single-pile model

A numerical assessment of the single-pile foundation model is presented in this section. For this purpose, a convergence study is initially performed to define suitable values for N_{p} and N_{s} that ensure an acceptable degree of convergence that allows for defining a general criterion to select the number of collocation points required for a specific problem. Although the study presented in Section 3.2.1 only focuses on the convergence of the method itself, it is worth mentioning that the accuracy of the converged results has also been verified for each one of the calculation cases considered. The accuracy of the proposed method is discussed in detail in Section 3.2.2 in which the method is compared with other existing state-of-the-art methodologies. The aim is to demonstrate the accuracy of the method and discuss its numerical efficiency in the framework of two problems: the radiation problem, for which the response of the pile-soil system due to the force $\mathbf{F}_{\mathrm{p}}$ on the pile is calculated; and the scattering problem, in which the system response to a load $\mathbf{F}_{\mathrm{s}}$ on the soil is evaluated. These numerical studies are performed in the context of three different pile-soil systems: a short pile embedded in soft soil (Case 1); a short pile embedded in stiff soil (Case 2); and a long pile embedded in soft soil (Case 3). The soil is modelled as a homogeneous elastic half-space for all these cases.

The specific geometrical and mechanical parameters considered for the three cases are presented in Table 3.1. The dimensions of the piles and the soil properties have been selected to assess the performance of the proposed methodology in very different situations rather than attempting to represent realistic scenarios. Therefore, while the pile aspect ratio of the short pile case ($L_p/r_p = 33.4$) is similar to those considered other works in the field [3, 4], the long pile $L_p/r_p = 100$ has been chosen to assess the performance of the method for a very slender pile. The material damping is introduced in the soil by considering complex Lamé constants λ^* and ν^* given by $\lambda^* + 2\nu^* = (\lambda + 2\nu)(1 + \mathrm{i}2D)$ and $\nu^* = \nu(1 + \mathrm{i}2D)$ for positive-valued frequencies, where D represents the hysteretic material damping ratio of the soil. The frequency range of interest is selected to be $1 - 100$ Hz in accordance with the frequency range in which ground-borne vibration is typically significant [153]. For the comparison of results, three observation points are considered: O_1, O_2 and O_3, located at positions $(0, 0, 0)$, $(5, 0, 0)$ m and $(20, 0, 0)$ m, respectively; the first one is collecting the pile head response and the other two are collecting the response of the soil surface at the near and far field. Furthermore, the results are presented in terms of magnitude of the free-field and pile-head frequency response functions receptances in dB with 1 m/N as reference. This form of presentation is particularly adequate to compare the performance of various numerical models, as it does not involve any additional assumption

or source of inaccuracy, such as the ones that could arise when dynamic stiffness results are normalised by their static counterparts [93]. Moreover, as the free-field and pile-head responses depend on the pile-soil interaction forces, the obtention of accurate results strongly suggests that the model adequately captures any dynamic unknown state at the pile-soil boundary.

Description	**Units**	**Soft soil**	**Hard soil**	**Short pile**	**Long pile**
Density (ρ)	kg/m^3	1950	2000	2860	2860
Young's modulus (E)	MPa	151.2	445.5	40000	40000
Poisson's ratio (ν)	-	0.35	0.40	0.25	0.25
Hysteretic damping ratio (D)	-	0.05	0.02	0.01	0.01
Speed of the P-waves (C_p)	m/s	352.8	703.6	-	-
Speed of the S-waves (C_s)	m/s	169.5	287.2	-	-
Pile length (L_p)	m	-	-	10	35
Pile radius (r_p)	m	-	-	0.3	0.35

TABLE 3.1: Pile and soil parameters used in the considered numerical examples.

Regarding the computation details, the elastic half-space Green's functions required in the proposed approach, as well as for the 3D FE-BE approach employed for verification purposes, are computed with the EDT toolbox [154]. Algorithms for all methods have been implemented in MATLAB, and the simulations have been carried out on a 40-core high-performance cluster with 2 GHz Intel® Xeon® Gold 6138 CPU.

Finally, the term $\mathbf{B}_\mathrm{cc}$ presented in Eq. (3.9) has been neglected from the calculations to enhance thus the computational efficiency of the proposed method since, as discussed in Section 3.1.2 and reported in [115, 151, 152], this term has almost no impact on the accuracy of the results in the case of smooth boundaries. This fact has also been verified numerically for each one of the considered examples.

3.2.1 Convergence analysis of the proposed approach

This subsection aims to provide a criterion for defining N_p and N_s values that ensure an acceptable trade-off between accuracy and numerical performance. In the context of the BEM, it is usually stated that element size should be between six and ten times smaller than the minimum wavelength of the problem [155]. This statement may not be representative of the SBM, taking into account the meshless nature of the method. In this sense, a convergence study to determine appropriate N_p and N_s values is presented in this section. For this analysis, only the radiation problem for the Case 1 is presented; however, similar results have been derived

for the other two cases (not included here). The response of this case has been computed for values of N_p ranging between 5 and 60, and for N_s between 4 and 40. The excitation frequency is set to the maximum of the frequency range, being 100 Hz. The convergence analysis is performed by comparing the results obtained for the different values of N_p and N_s with those obtained for a reference case with $N_\mathrm{p}^\mathrm{ref} = 70$ and $N_\mathrm{s}^\mathrm{ref} = 40$. The discrepancies between each case and the reference one are presented in terms of a relative error, which is given by

$$\varepsilon_{ij} = \frac{\left| H_{k\mathrm{h}}^{\mathrm{c},ij} - H_{k\mathrm{h,ref}}^{\mathrm{c},ij} \right|}{\left| H_{k\mathrm{h,ref}}^{\mathrm{c},ij} \right|}, \tag{3.21}$$

where ε_{ij} is the relative error of the receptance component $H_{k\mathrm{h}}^{\mathrm{c},ij}$ with respect to the reference one $H_{k\mathrm{h,ref}}^{\mathrm{c},ij}$. The first superscript i denotes the response direction, while j is referred to the force direction. The subscript k is defined as $k = \mathrm{h}$ or $k = \mathrm{s}$ according to whether the response is evaluated on the pile head or at the ground surface, respectively.

Fig. 3.5 shows the convergence analysis results at the three observation points. For clarity, the results are presented in logarithmic scale. As expected, the relative errors decrease as the values of N_p and N_s increase. Very small relative errors are observed for values of N_p and N_s above 50 and 18, respectively, suggesting that the results of the proposed method have numerically converged. The vertical driving-point response at the pile head (associated with ε_{zz}) in Figs. 3.5(a-i), (b-i) and (c-i) converges for smaller values of N_p and N_s than the lateral driving-point response (associated with ε_{xx}, ε_{yy}). Moreover, the lateral driving-point responses are more sensitive with respect to N_s than the vertical driving-point responses, which are almost insensitive to changes in N_s. These trends are less prominent for soil response. The convergence analysis shows that the difference between the reference results and the results obtained when considering at least eight collocation points per wavelength in the longitudinal direction are below -1.25 in the logarithmic scale used in Fig. 3.5, which corresponds to differences below 0.2 dB with respect to the reference solution. Thus, N_p is suggested to be defined based on this criterion. For the specific problem under investigation, where the minimum wavelength is $\lambda_\mathrm{min} = 1.695$ m, this criterion indicates that N_p should be at least 47 (see vertical dashed green lines in Fig. 3.5). Regarding the discretization scheme for the collocation points within the ring-shaped distributions along the perimeter of the pile segments, the convergence study demonstrated that a practical rule for defining an appropriate value for N_s is $N_\mathrm{s} \geq 32\pi r_\mathrm{p}/\lambda_\mathrm{min}$, in which λ_min stands for the minimum wavelength of the problem. Consequently, the minimum number of collocation points per wavelength along each ring-shaped distribution is 16. This

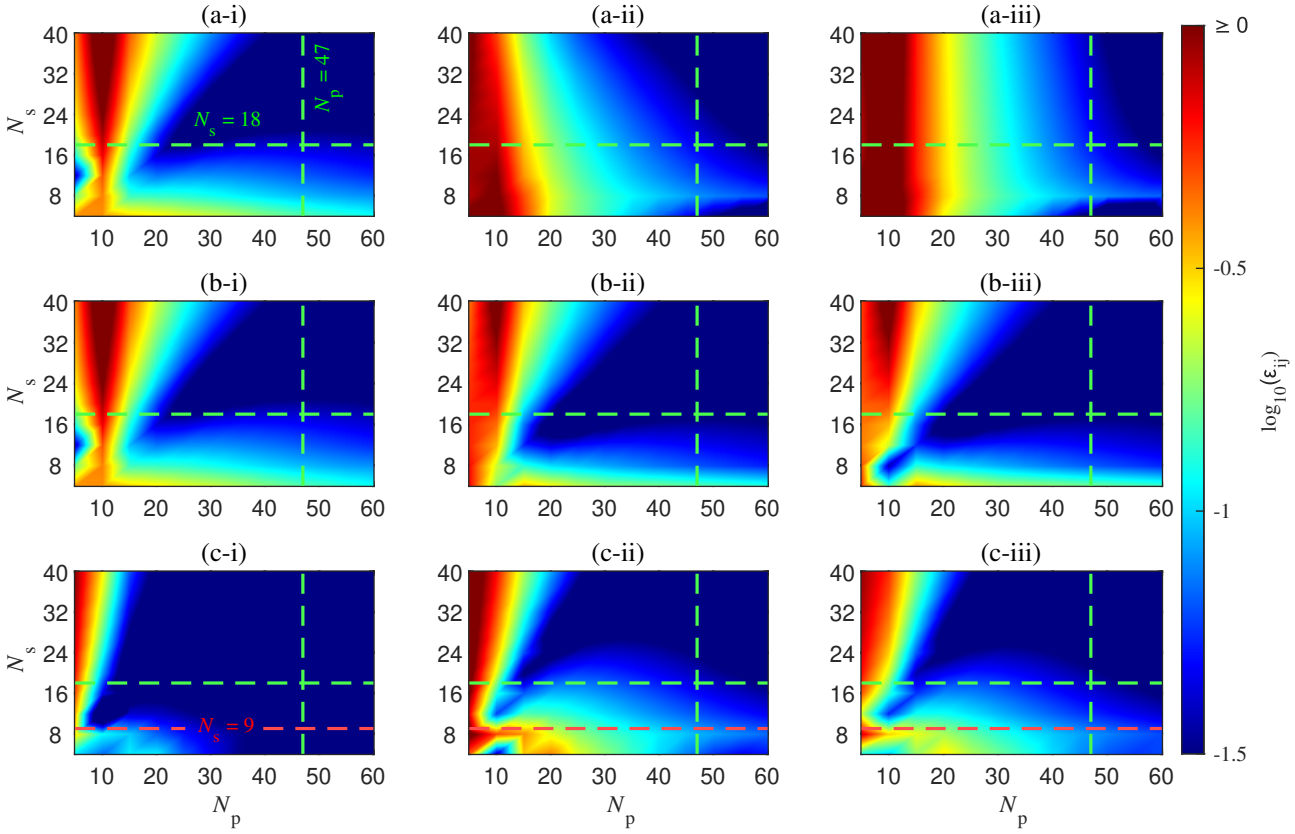

FIGURE 3.5: Relative errors (depicted in logarithmic scale) ε_{xx} (a), ε_{yy} (b) and ε_{zz} (c) associated with the response at the observation points O_1 (i), O_2 (ii), O_3 (iii), respectively, for the case of a short pile embedded in soft soil.

rule is especially important to be complied when the lateral driving-point response at the pile head is computed. Following this criterion, the suggested value for N_s is 18 (see horizontal dashed green lines in Fig. 3.5). When only the vertical response due to vertical loading is computed, this criterion can be significantly relaxed and a value $N_s \geq 16\pi r_p/\lambda_{min}$ is found to be working well in this situation. For the specific problem under investigation, the N_s value suggested for computing ε_{zz} is 9 (see horizontal dashed red lines in Figs. 3.5(c-i), (c-ii) and (c-iii)).

Furthermore, the efficacy of the proposed discretization rules has been studied by comparing the results for four discretization schemes, which are: $N_p = 70$ and $N_s = 40$; $N_p = 50$ and $N_s = 32$; $N_p = 35$ and $N_s = 8$; and $N_p = 15$, $N_s = 8$. The resulting frequency response functions (FRFs) are presented in Fig. 3.6 and show that, as suggested by the relative error results, there is almost no difference between the cases that consider N_p and N_s values that comply with the previously stated criteria. It should be noticed that, as shown by the relative

errors, vertical responses due to a vertical load on the pile head are predicted with reasonable accuracy by the proposed approach, even for low N_p and N_s values, as shown in Fig. 3.6(c-i), (c-ii) and (c-iii), where differences of less than 1 dB are found, occurring at 100 Hz. On the contrary, the responses related to lateral motions and/or loading are more sensitive to such changes.

The proposed criterion for defining the N_s and N_p values has been tested in other scenarios proving its correctness in all those situations. The mechanical and geometry parameters employed for testing these criteria ranged between the ones described for piled foundation Case 1 and Case 3. Therefore, for the sake of brevity, only the convergence analysis for the case associated with the minimum wave speed (Case 1) is shown since it is the one requiring the highest density of collocation and source points.

3.2.2 Comparison with existing approaches

In this section, the proposed modelling approach is compared with other well-established approaches in terms of its accuracy. This study serves to verify the approach and to test the discretization criteria discussed in the previous section. Furthermore, the need to account for rotational motion and torques when coupling both pile and soil subsystems has been also assessed. This study is performed for the radiation problem of Case 1, Case 2 and Case 3 scenarios.

The methods considered for comparison in this validation study are Novak's approach [79]; an axisymmetric FE-based approach that uses perfectly matched layers (PML) to avoid wave reflections at the borders of the model referred to as aFE-PML [11]; and a 3D FE-BE approach consisting of a 3D BE-based approach developed on the basis of [149]. Table 3.2 summarises the discretization schemes adopted for the proposed method, the aFE-PML and the FE-BE methodologies, particularly defining the number of nodes per wavelength (NPW) considered and the resulting discretization or mesh parameters. Additionally, Table 3.3 provides the number of collocation points or nodes, as well as the number of elements N_E, used in the different numerical models considered in this study. The 3D FE-BE approach has been implemented using four-noded quadrilateral BEs and eight-noded hexahedral FEs, whilst the aFE-PML method uses six-noded triangular elements to construct its meshes.

Although a detailed description of the aFE-PML approach is not in the scope of the present dissertation, it is worth mentioning some general information about the PML formulation.

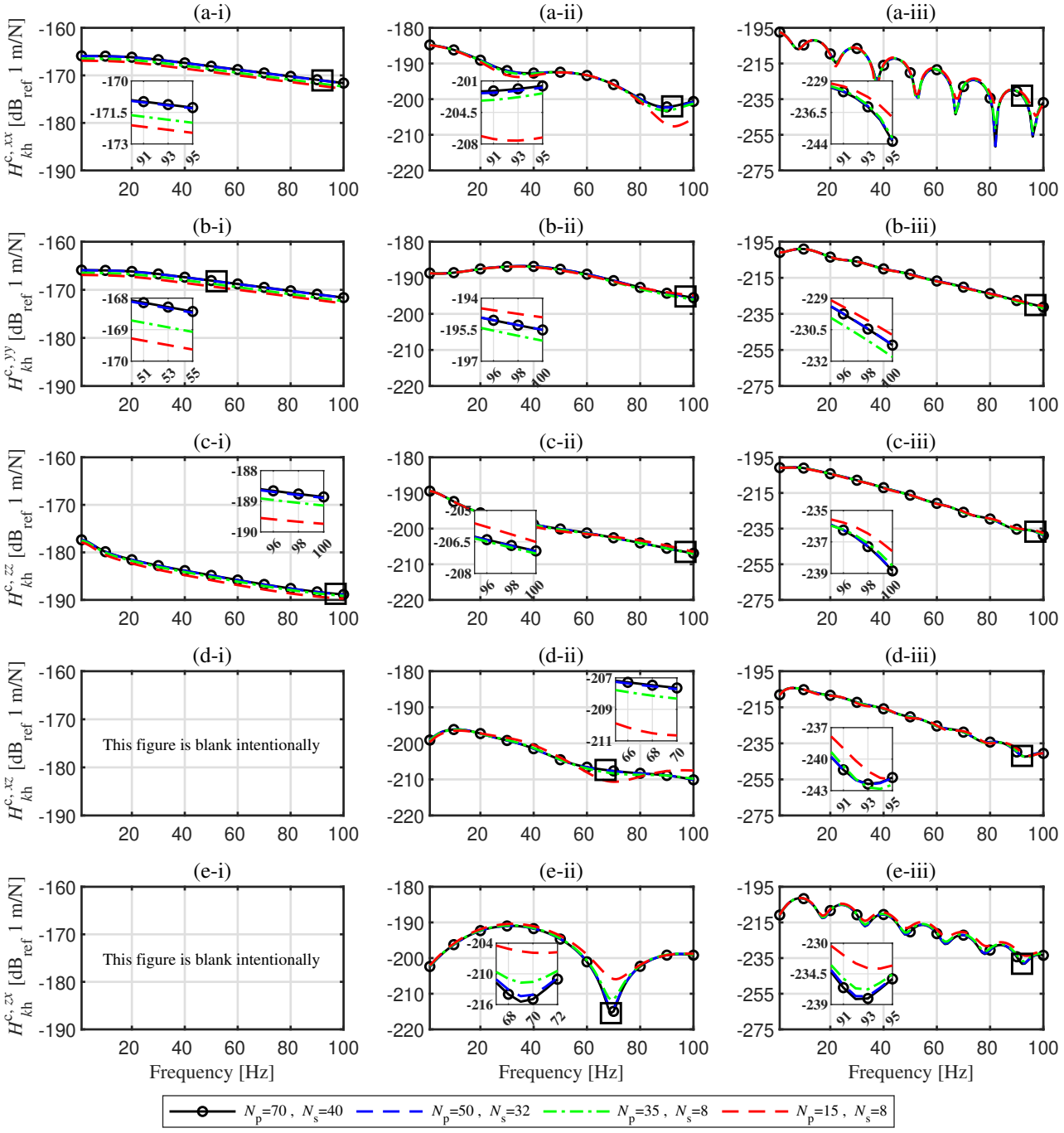

FIGURE 3.6: Displacement FRFs (receptances) for the radiation problem in the context of Case 1 scenario considering different discretization schemes. Components of the FRFs matrices shown are xx (a), yy (b), zz (c), xz (d) and zx (e) and observation points considered are O_1 (i), O_2 (ii), O_3 (iii). Results in dB using $20\log_{10}(|H|)$, with 1 m/N as reference.

For the three pile cases computed with the aFE-PML approach, a stretching function with a constant value of 20 for the attenuation function is considered, as suggested in [156, 157], the

thickness of the PML layer has been set to be 1 m in the radial and vertical direction, dividing the layer into six sub-layers. Regarding Novak's approach, the soil lateral reaction equation described in [79] does not correspond to the one proposed by Baranov in his original work [76]. This imprecise transcription of the original Baranov's formula could lead to inaccurate results for lateral driving-point responses. Corrected closed-form expressions for the soil reaction, originally proposed by Baranov, have been detailed in Appendix C. Additionally, the equation for obtaining the lateral response of the pile proposed in [79], which considers either the pile with both ends fixed or the pile head fixed and the pile tip pinned, is adapted to the case where both ends are free.

Although Novak's approach is generally a suitable and extremely efficient approach for modelling pile driving cases, the method does not perform well at low frequencies and cannot predict the free-field response. Additionally, due to its axisymmetric nature, the aFE-PML approach can only be used to predict the system's dynamic vertical and radial responses to vertical excitations applied on the pile axis. However, both methods are included in the comparison study to highlight the proposed method's potential and increase the validation process's merit. Regarding the latter, since the FE-BE model was developed within this study to validate the proposed method and assess its computational efficiency, it was also considered necessary to verify the FE-BE results by including the comparison against results from other available tools. It is worth mentioning that although there are several alternative pile-soil interaction models based on analytical elastic-continuum formulations to deal with single-pile foundations [89–92], these models have not been considered in the presented comparisons since they involve assumptions that are not considered in the presented numerical approaches, as discussed in Section 2.3 and reported in [73].

Description	**Proposed approach**				**3D FE-BE**		**aFE-PML**	
Case study	NPW	d [cm]	N_p	N_s	NPW	d [cm]	NPW	d [cm]
Case 1: Short pile - soft soil	8	21	47	28	9	20	7	25
Case 2: Short pile - stiff soil	9	32	32	18	14	20	6	45
Case 3: Long pile - soft soil	8	21	165	32	4	50	7	25

TABLE 3.2: Discretization schemes adopted for the proposed 3D FE-BE and aFE-PML approaches. The variable d represents the distance between collocation points along the longitudinal direction of the pile in the proposed approach and the element size in the mesh-based approaches.

Fig. 3.7 to 3.9 show the displacement FRF (receptance) at each one of the observation points to forces applied on the pile head obtained by the different approaches mentioned above. An alternative version of the proposed approach that does not account for rotations and torques in

Description	**Proposed approach**	**3D FE-BE**				**aFE-PML**	
Case study	SB points	FE mesh		BE mesh		FE mesh	
	N_c	Nodes	N_E	N_c	N_E	Nodes	N_E
Case 1: Short pile - soft soil	1317	3723	3000	1273	1260	125685	62464
Case 2: Short pile - stiff soil	577	3723	3000	1273	1260	85890	42605
Case 3: Long pile - soft soil	5281	5183	4200	1740	1753	125685	62464

TABLE 3.3: Number of collocation points (or nodes) and elements used in the different numerical models considered in the numerical assessment.

the coupling between the pile and the soil is also included in the comparison. It can be seen that the responses due to vertical loads simulated by all the considered methods demonstrate a good agreement between them. Some differences between the methods can be seen in the results of the responses due to lateral loading. This is particularly clear for the Novak approach, which is found to be inaccurate at low frequencies for the lateral driving-point responses. Results show that the Novak method underestimates the lateral stiffness of the pile in a range of frequencies that mainly depends on the mechanical properties of the soil rather than the pile geometry, having inaccurate results arising below 20 Hz for the soft soil cases and below 40 Hz in the stiff soil case. On the contrary, a good agreement over the whole frequency range is observed when comparing the results of the proposed methodology with those obtained with the other two numerical approaches. The results also show that when rotations and bending moments are not included in the coupling procedure, the proposed methodology may predict inaccurate responses to lateral loads. This effect can be observed in Figs. 3.7 to 3.9, that show discrepancies between the two coupling assumptions for the x and z soil responses due to lateral forces in the x-direction, especially at high frequencies. However, the impact of neglecting rotations and bending effects is much smaller for the remaining lateral loading responses.

Overall, the results from the comparison study presented in this section demonstrate the high accuracy of the proposed approach due to the agreement of its corresponding results with the ones delivered by the 3D FE-BE methodology, which is expected to provide highly detailed results.

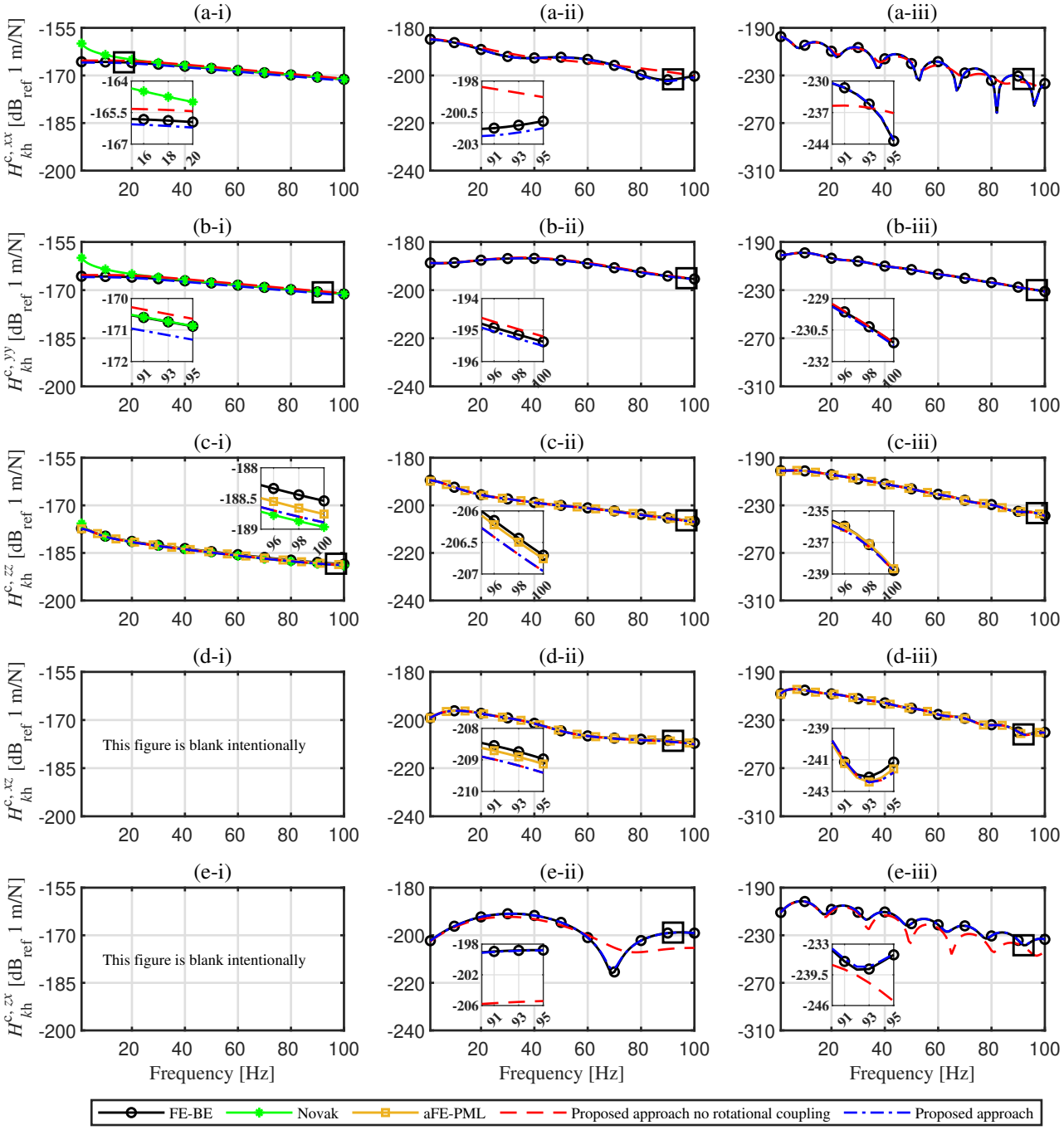

FIGURE 3.7: FRFs for the radiation problem in the framework of Case 1 (short pile & soft soil) scenario considering different approaches. Components of the FRFs matrices shown are xx (a), yy (b), zz (c), xz (d) and zx (e) and observation points considered are O_1 (i), O_2 (ii), O_3 (iii). Results in dB using $20\log_{10}(|H|)$, with 1 m/N as reference.

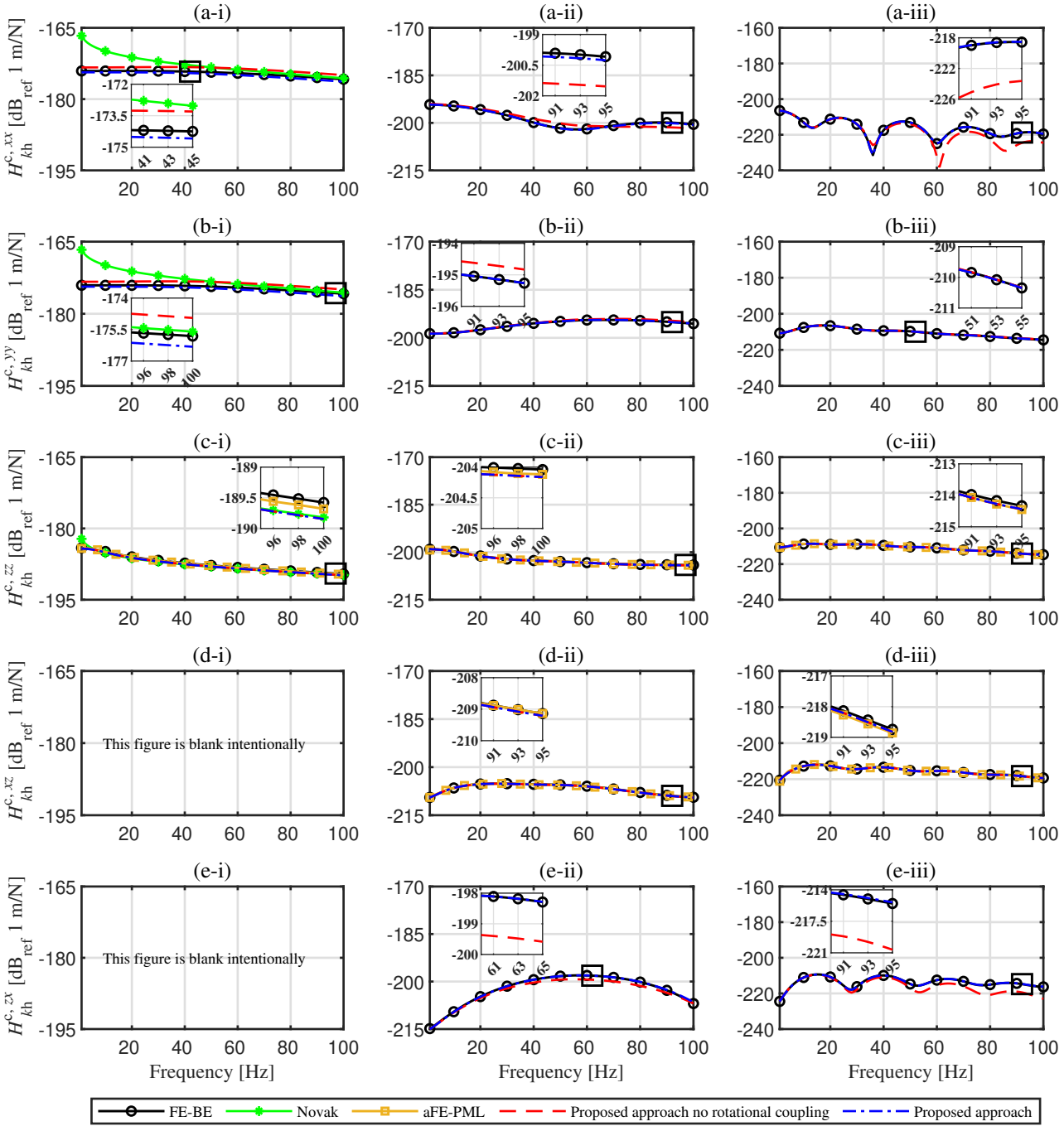

FIGURE 3.8: FRFs for the radiation problem in the framework of Case 2 (short pile & stiff soil) scenario considering different approaches. Components of the FRFs matrices shown are xx (a), yy (b), zz (c), xz (d) and zx (e) and observation points considered are O_1 (i), O_2 (ii), O_3 (iii). Results in dB using $20\log_{10}(|H|)$, with 1 m/N as reference.

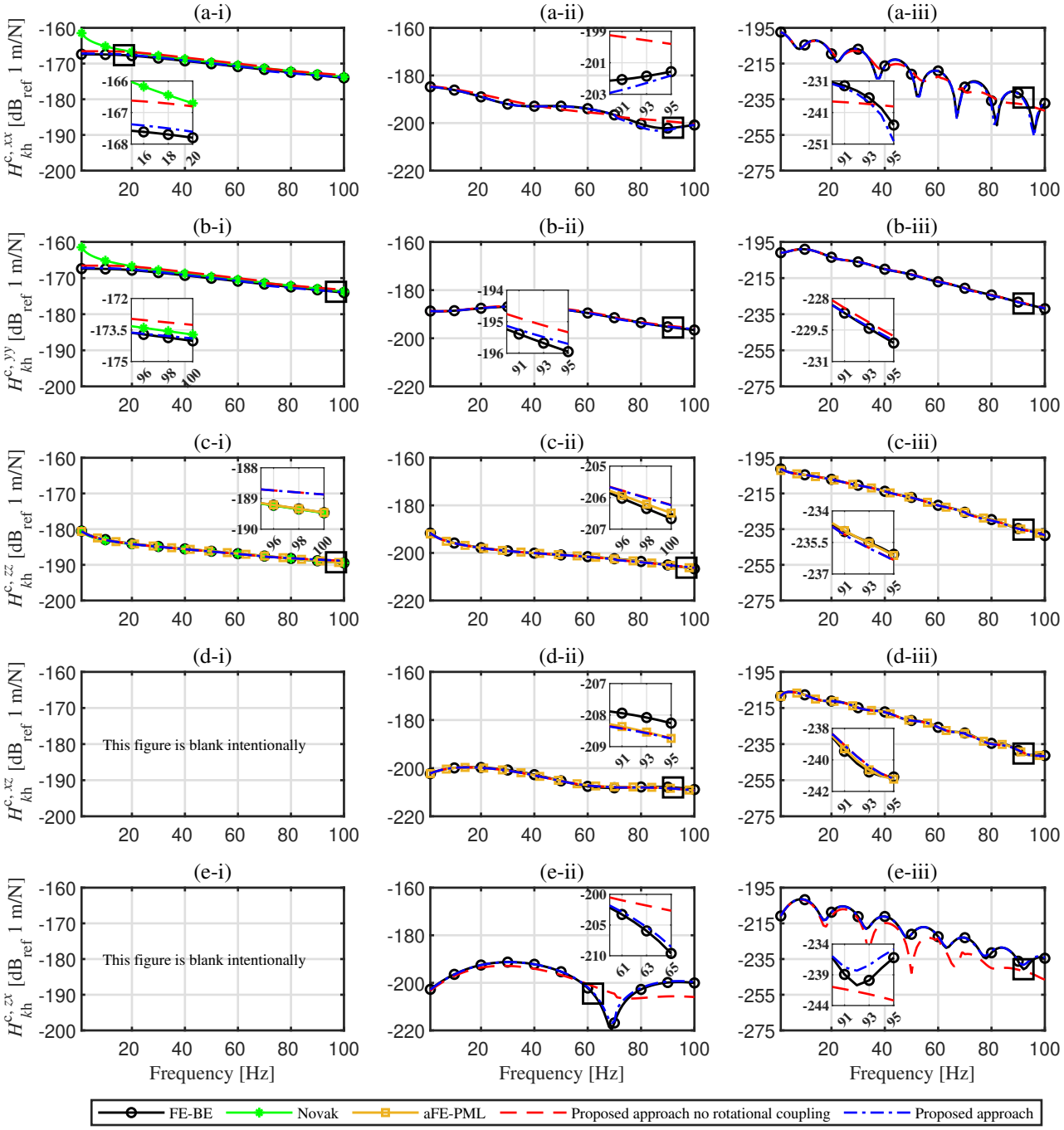

FIGURE 3.9: FRFs for the radiation problem in the framework of Case 3 (long pile & soft soil) scenario considering different approaches. Components of the FRFs matrices shown are xx (a), yy (b), zz (c), xz (d) and zx (e) and observation points considered are O_1 (i), O_2 (ii), O_3 (iii). Results in dB using $20\log_{10}(|H|)$, with 1 m/N as reference.

3.2.3 Verification of the dynamic reciprocity of the proposed approach

In the context of ground-borne vibration problems, the response of the pile due to a dynamic load applied on the ground is the most interesting problem to study since it allows for determining the response of buildings or structures with piled foundations to the action of incident elastic wave fields. This problem can be referred to as a travelling wave problem (or kinematic excitation problem) for which the pile foundation is induced to shake by the incident wave fields from a source. However, employing the dynamic reciprocity theorem, this result can be obtained by solving the radiation problem for the case that the response is determined at the position where the load in the original scattering problem is intended to be placed.

In this section, a numerical study to verify that the proposed approach fulfils the dynamic reciprocity theorem is presented, which states the following property of the fundamental or Green's function of an elastic system as $\mathbf{H}(\mathbf{x},\mathbf{y},\omega) = \mathbf{H}^{\mathrm{T}}(\mathbf{y},\mathbf{x},\omega)$, which also applies for any FRF of the system. Due to the special assumptions taken into consideration in the proposed approach, it is worth checking the correctness for the proposed approach and for the alternative version that only considers translational coupling when dealing with the pile-soil interaction. Thus, the radiation problem of a force applied at the pile head and the response evaluated at the point O_2, governed by Eq. (3.19a), is compared to the scattering problem where the force is applied at the point O_2 and the response is evaluated at the pile head, governed by Eq. (3.19d). Results are shown in Fig. 3.10, from which it can be observed that the reciprocity for the proposed approach is satisfied. Therefore, it can be deduced that the dynamic reciprocity is fulfilled over the frequency range of interest in all situations for both studied coupling strategies employed within the proposed approach.

3.2.4 Computational efficiency of the proposed approach

In the cases studied in the previous subsections, it was shown that the proposed approach offers several advantages over the other methods. Compared with Novak's method, although significantly more computationally demanding, it can perform with better accuracy and include the results in the free field. Similarly, compared with the aFE-PML method, the proposed method overcomes the fundamental limitation on obtaining the results due to excitations at the free field (incident wave fields) and lateral excitations at the pile. Also, it avoids the high

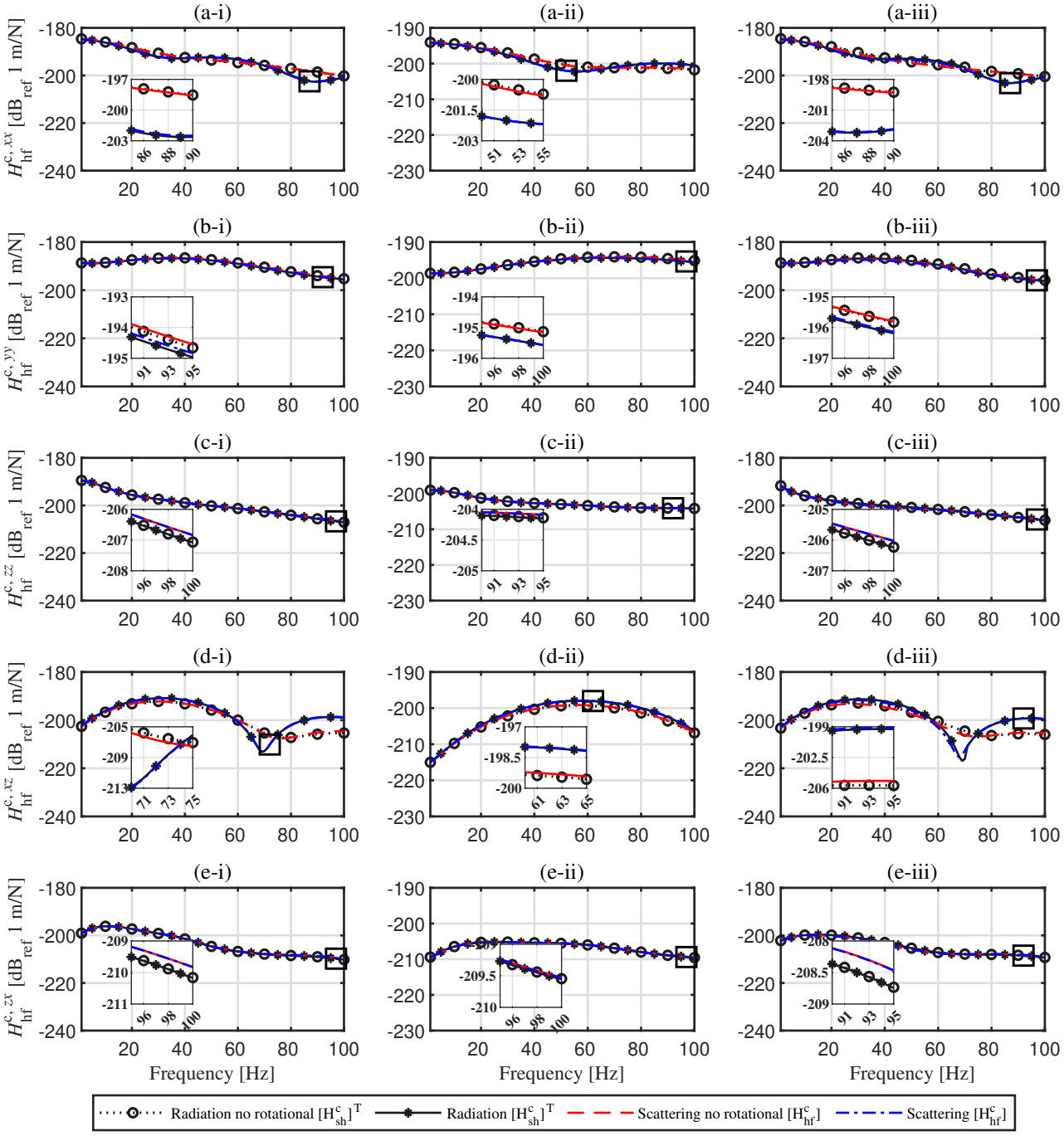

FIGURE 3.10: Response of the radiation and corresponding scattering problems in the context of the Case 1 (i), Case 2 (ii) and Case 3 (iii) scenarios. Components of the FRFs matrices shown are xx (a), yy (b), zz (c), xz (d) and zx (e). Results in dB using $20\log_{10}(|H|)$, with 1 m/N as reference.

computational cost of dealing with far evaluation points and the requirements for a large mesh of the soil (a similar issue can be extrapolated for a 3D FE-PML model).

The 3D FE-BE methodology can provide accurate results in all directions; however, an inherent disadvantage of this method is associated with the computational effort. This is because the 3D FE-BE model requires a significant number of Green's function evaluations for solving the numerical integration over each of the BEs of the constructed mesh. This computational effort increases rapidly when the mesh density increases, either to fulfil high-frequency range requirements or to include multiple piles. The current work does not include a detailed computational efficiency comparison, particularly against the FE-BE approach because such an effort would depend (to some extent) on the programmer's skill in the computational implementation of the two methods. Furthermore, as described in Table 3.3, the SBM and BEM have modelled the pile cavity with different numbers and arrangements of collocation points so that a quantitative comparison of the computational times between them appears to be unfair. However, a general overview of the computational benefits of the SBM over the BEM is included here. Previous work in the fields of elastostatics [113] and acoustics [158] showed that the SBM can outperform the BEM in terms of accuracy when considering the same number of collocation points. Having that in mind, consider, for instance, a generic BE mesh consisting of N_{E} boundary elements and N_{c} collocation points and assuming a moderate number of Gaussian points $GP = 2 \times 2$ for a bilinear interpolation function of elements that are not severely distorted, as suggested in [149]. The BEM would require at least $n = GP \times N_{\mathrm{E}} \times N_{\mathrm{c}}$ Green's functions evaluations to obtain the unknown states of the system. In contrast, a corresponding SBM model considering the same number of collocation points would require $n = N_{\mathrm{c}}^2$ computations. Therefore, considering the BEM and SBM employing the same collocation point distribution to characterize the unknown states of the cavity, the inequality $N_{\mathrm{c}}^2 < GP \times N_{\mathrm{E}} \times N_{\mathrm{c}}$ holds and demonstrates the SBM to be more computationally efficient than the BEM, generally speaking. Moreover, although different numbers and arrangements of collocation points are employed to model the soil sub-system with the BEM and the SBM, the differences in computational requirements between these two approaches were observed when computing the results included in this dissertation. This difference was particularly significant for the pile foundation Case 3 when, even utilizing a discretization scheme incorporating six NPW, considerable computational efforts in terms of processor speed and rapid access memory was required for calculating the response of that pile-soil system. For these reasons, only four nodes per wavelength were employed in the modelling, as reported in Table 3.2, which has induced some inaccuracies at higher frequencies in the semi-analytical response, as shown in Fig. 3.9(a-ii), (a-iii), or (e-iii). Due to the meshless nature of the proposed approach, a significantly smaller number of Green's function evaluations are required to obtain the response of the targeted pile-soil system using

the proposed method, resulting in a large reduction of the computation resources employed in the simulation.

3.3 Conclusions

A computationally efficient 3D approach for predicting pile-soil interaction problems is presented in this chapter. The proposed method models the soil as a half-space and represents the pile as an Euler-Bernoulli beam to capture its flexural motion and as a rod to account for axial deformations. Regarding the coupling, the soil reaction is modelled using the SBM, an emerging meshless numerical method with computational efficiency and formulation simplicity merits exploited in the proposed scheme. The pile is divided into circular segments, each of them involving a set of collocation points placed at the soil-pile interface, in which the compatibility of displacements and tractions between the two sub-systems is enforced. A transformation matrix is introduced to relate the pile response at the collocation points in the pile-soil interface with the pile response computed at the pile's centroid. This matrix is constructed assuming each pile segment to be rigid and considering both translational and rotational motions of the pile segments, as well as forces and bending moments.

The outcomes of the present chapter can be summarised in the following list of findings:

- The convergence analysis conducted for the proposed approach has provided a criterion for defining the number of pile segments and the number of collocation points per segment that ensures an acceptable trade-off between robustness, accuracy and numerical performance of the scheme.

- The proposed methodology has been verified against a 3D FE-BE methodology, an axisymmetric aFE-PML approach and compared with the Novak's method. Moreover, the reciprocity principle has also been verified for the proposed methodology in order to assess the correctness of the formulation presented. In the calculation examples considered, the method is found to yield a comparable level of accuracy with respect to the FE-BE approach when employing a similar number of collocation points for both methods. This, combined with the fact that SBM typically involves less Green's function evaluations with respect to BEM per collocation point, allows for concluding that the method is more computationally efficient than a standard 3D FE-BE.

- The verification study also shows that the rotational motions and bending moments must be considered in the pile-soil coupling scheme to obtain accurate results, especially when estimating the lateral response of the free field due to lateral or vertical loading patterns. The discrepancies appearing when only translational motions and forces are considered to establish the coupling conditions are more pronounced at high frequencies.

Given the robustness of the proposed method as well as its computational efficiency merits, it conforms as an interesting alternative to deal with ground vibration problems involving single-piled foundations. Moreover, the current methodology can be employed to model multi-pile foundation systems by considering displacement compatibility and force equilibrium on each pile. The formulation for pile-group system is described in detail in the following Chapter 4.

Chapter 4

A multi-pile foundation model based on the singular boundary method

In many practical situations, the number of piles required to support a foundation is determined by factors such as the amplitude of columns' service loads, the soil's bearing capacity, or the pile spacing. The dynamic response of pile-groups can typically be modelled by employing the governing equations and soil-pile coupling assumptions used in single-pile models. An example of a pile-group model based on elastic continuum theory is the one developed by Kaynia and Kausel [1, 3] and, examples of pile-group models based on numerical methods have been presented in [4, 5, 96, 97, 109, 131]. As in single-pile models, accurate predictions of a pile-group's dynamic response require realistic coupling assumptions. However, 3D fully coupled approaches become impractical in terms of computational effort when dealing with pile-groups comprising many piles. An alternative method to overcome the computational challenges associated with fully coupled approaches is the use of the superposition method proposed by Poulos [116] to study the static behaviour of a pile-group system employing the response of two isolated piles only. This methodology is also employed by Kaynia [3] to compare the dynamic response of a generic pile-group predicted by a fully coupled model with the ones obtained using the superposition method, which employs the dynamic interaction factors of two isolated piles as entries to construct a global flexibility matrix that solely relates force and displacement at the pile heads. While this method offers some advantages in terms of computational effort when foundations comprise many piles, inaccurate results can be predicted at high-frequency ranges since the calculation of the dynamic interaction factors does not account for neighbouring or intermediate piles [4].

This chapter employs the previously proposed single-pile formulation, which considered Euler-Bernoulli beam and elastic rod theories to model the pile, and the SBM to model the soil, described in detail in Section 3.1.1 and 3.1.2, respectively, to develop a fully-coupled 3D multi-pile foundation model. In the proposed model, the piles and soil are coupled using the procedure and formulations for a single-pile presented in Chapter 3. Furthermore, by employing the method of joining subsystems presented in Section 3.1.3, the formulation for coupling a pile-group with a pile cap (or slab) is also obtained. The proposed approach is validated by comparing the results obtained against the ones given by a 3D FE-BE method. The proposed methodology is also employed to study the influence of including neighbouring piles in the calculation of the interaction factors in the context of three pile-group cases.

4.1 Pile-group model formulation

A modelling strategy is presented in this section that aims to compute the dynamic response of pile-group systems. In the formulation developed below, uppercase letters relate to scalar variables in the frequency domain, and bold uppercase letters denote vectors or matrices in the frequency domain. The system under investigation is a pile-group comprising of M identical piles in an arbitrary arrangement, as shown in 4.1(b), and embedded in M cavities in the soil modelled by a set of collocation points, as illustrated in 4.1(a). Similar to the single-pile case, the piles and the soil are dynamically coupled by ensuring displacement compatibility and force equilibrium at a set of collocation points distributed uniformly along each pile-soil interface. The dynamic fields at the piles-soil interfaces for the pile-group are represented by a total set of $N_c = M(N_s N_p + 1)$ collocation points, where N_p represent the generic number of cylindrical segments of each pile and N_s a set of collocation points distributed along the pile-soil interface of each cylindrical segment. A detailed description of the collocation points distribution and their corresponding area of influence is presented in Section 3.1.3.

Assuming that each pile is identified by the superscript notation $m = 1, 2, ..., M$, the vector that contains the three-component displacements and rotations at the piles' centroid points can be expressed by $\mathbf{U}_\mathrm{p} = [\mathbf{U}_\mathrm{p}^{(1)}\ \mathbf{U}_\mathrm{p}^{(2)} \cdots \mathbf{U}_\mathrm{p}^{(m)} \cdots \mathbf{U}_\mathrm{p}^{(M)}]^\mathrm{T}$. Moreover, by considering that each cylindrical segment acts as a rigid body, the displacements at all the N_c collocation points of

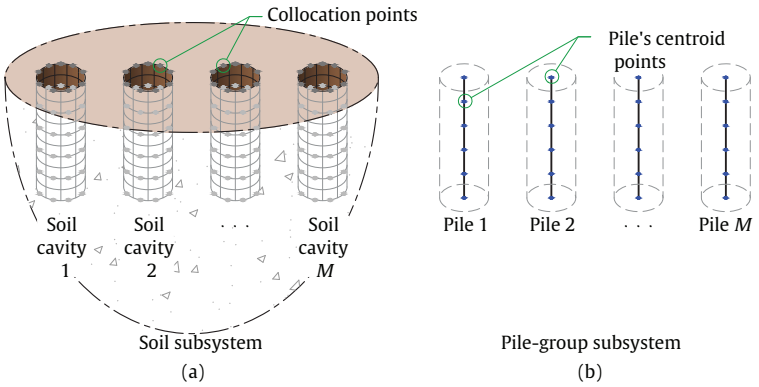

FIGURE 4.1: Schematic drawing of soil (a) and pile (b) subsystems comprising the multi-pile foundation.

all pile subsystems $\mathbf{U}_{\mathrm{p}}$ can be expressed in terms of $\mathbf{U}_{\mathrm{p}}$ as

$$\mathbf{U}_{\mathrm{b}}^{\mathrm{p}} = \begin{bmatrix} \mathbf{U}_{\mathrm{b}}^{\mathrm{p}(1)} \\ \mathbf{U}_{\mathrm{b}}^{\mathrm{p}(2)} \\ \vdots \\ \mathbf{U}_{\mathrm{b}}^{\mathrm{p}(M)} \end{bmatrix} = \begin{bmatrix} \mathbf{W}^{(1)} & \mathbf{0} & \cdots & \mathbf{0} \\ \mathbf{0} & \mathbf{W}^{(2)} & \cdots & \mathbf{0} \\ \vdots & \cdots & \ddots & \vdots \\ \mathbf{0} & \mathbf{0} & \cdots & \mathbf{W}^{(M)} \end{bmatrix} \begin{bmatrix} \mathbf{U}_{\mathrm{p}}^{(1)} \\ \mathbf{U}_{\mathrm{p}}^{(2)} \\ \vdots \\ \mathbf{U}_{\mathrm{p}}^{(M)} \end{bmatrix} = \mathbf{W}\mathbf{U}_{\mathrm{p}}, \tag{4.1}$$

where $\mathbf{W}^{(m)}$ represents the transformation matrix of the m-th pile that relates the vector $\mathbf{U}_{\mathrm{p}}^{(m)}$ with the vector $\mathbf{U}_{\mathrm{b}}^{\mathrm{p}(m)}$ that contains the three-component displacements at its corresponding collocation points. Note that for a pile-group system comprised of identical pile geometries and similar collocation points distribution, the transformation matrices are also identical since the construction of each of them is a function of the local coordinates of each pile rather than the global coordinates of the system, so then $\mathbf{W}^{(1)} = \mathbf{W}^{(2)} = \cdots = \mathbf{W}^{(m)}$. Details of this transformation and the definition of $\mathbf{W}^{(m)}$ are given in Appendix B.

Similar to the single-pile formulation, the coupling is performed by assuming displacement compatibility and force equilibrium conditions at each pile-soil interface. Thus, the displacement compatibility condition between the two subsystems leads to $\mathbf{U}_{\mathrm{b}}^{\mathrm{p}} = \mathbf{U}_{\mathrm{b}}^{\mathrm{s}}$, where the vector $\mathbf{U}_{\mathrm{b}}^{\mathrm{s}} = [\mathbf{U}_{\mathrm{b}}^{\mathrm{s}(1)}\ \mathbf{U}_{\mathrm{b}}^{\mathrm{s}(2)} \cdots \mathbf{U}_{\mathrm{b}}^{\mathrm{s}(m)} \cdots \mathbf{U}_{\mathrm{b}}^{\mathrm{s}(M)}]^{\mathrm{T}}$, contains the soil displacements at the N_c collocation points.

The compatibility of the reaction forces at the piles-soil interfaced is expressed by $\mathbf{P}_{\mathrm{b}}^{\mathrm{s}} = -\mathbf{P}_{\mathrm{b}}^{\mathrm{p}}$, with $\mathbf{P}_{\mathrm{b}}^{\mathrm{s}}$ and $\mathbf{P}_{\mathrm{b}}^{\mathrm{p}} = [\mathbf{P}_{\mathrm{b}}^{\mathrm{p}(1)}\ \mathbf{P}_{\mathrm{b}}^{\mathrm{p}(2)} \cdots \mathbf{P}_{\mathrm{b}}^{\mathrm{p}(m)} \cdots \mathbf{P}_{\mathrm{b}}^{\mathrm{p}(M)}]^{\mathrm{T}}$ being the interaction forces to which the soil and the piles are subjected, respectively, at the N_c collocation points.

As discussed in Section 3.1.3, the traction field in the pile-soil interface is assumed to be constant along each influence area and equal to the value at its corresponding collocation point. Thus, the interaction forces to which the soil is subjected are given by

$$\mathbf{P}_{\mathrm{b}}^{\mathrm{s}} = \begin{bmatrix} \mathbf{P}_{\mathrm{b}}^{\mathrm{s}(1)} \\ \mathbf{P}_{\mathrm{b}}^{\mathrm{s}(2)} \\ \vdots \\ \mathbf{P}_{\mathrm{b}}^{\mathrm{s}(M)} \end{bmatrix} = \begin{bmatrix} \mathbf{W}_{\mathrm{A}}^{(1)} & \mathbf{0} & \cdots & \mathbf{0} \\ \mathbf{0} & \mathbf{W}_{\mathrm{A}}^{(2)} & \cdots & \mathbf{0} \\ \vdots & \cdots & \ddots & \vdots \\ \mathbf{0} & \mathbf{0} & \cdots & \mathbf{W}_{\mathrm{A}}^{(M)} \end{bmatrix} \begin{bmatrix} \mathbf{T}_{\mathrm{b}}^{\mathrm{s}(1)} \\ \mathbf{T}_{\mathrm{b}}^{\mathrm{s}(2)} \\ \vdots \\ \mathbf{T}_{\mathrm{b}}^{\mathrm{s}(M)} \end{bmatrix} = \mathbf{W}_{\mathrm{A}} \mathbf{T}_{\mathrm{b}}^{\mathrm{s}}, \tag{4.2}$$

where $\mathbf{W}_{\mathrm{A}}^{(m)}$ is a diagonal matrix that contains the areas of influence associated with all the collocation points of the m-th soil cavity and $\mathbf{T}_{\mathrm{b}}^{\mathrm{s}(m)}$ is a vector that contains the traction field at these collocation points.

Because each cylindrical segment is assumed to behave as a solid rigid, the pile interaction forces $\mathbf{P}_{\mathrm{b}}^{\mathrm{p}}$ acting on the pile-soil interface of each segment can be expressed in terms of equivalent forces and moments acting on their corresponding pile centroid point. This transformation leads to $\mathbf{P}_{\mathrm{p}} = \mathbf{W}^{\mathrm{T}} \mathbf{P}_{\mathrm{b}}^{\mathrm{p}} = -\mathbf{W}^{\mathrm{T}} \mathbf{P}_{\mathrm{b}}^{\mathrm{s}}$, where the vector $\mathbf{P}_{\mathrm{p}} = [\mathbf{P}_{\mathrm{p}}^{(1)}\ \mathbf{P}_{\mathrm{p}}^{(2)} \cdots \mathbf{P}_{\mathrm{p}}^{(m)} \cdots \mathbf{P}_{\mathrm{p}}^{(M)}]^{\mathrm{T}}$ contains the equivalent interaction forces applied at the piles' centroid points. Thus, the traction at the piles-soil interfaces $\mathbf{T}_{\mathrm{b}}^{\mathrm{s}}$ is related with the vector $\mathbf{P}_{\mathrm{p}}$ as

$$\mathbf{P}_{\mathrm{p}} = -\mathbf{W}^{\mathrm{T}} \mathbf{W}_{\mathrm{A}} \mathbf{T}_{\mathrm{b}}^{\mathrm{s}}. \tag{4.3}$$

As in Chapter 3, the system is considered to be subjected to forces applied at the soil and on the pile heads, represented by $\mathbf{F}_{\mathrm{s}}$ and $\mathbf{F}_{\mathrm{p}} = [\mathbf{F}_{\mathrm{p}}^{(1)}\ \mathbf{F}_{\mathrm{p}}^{(2)} \cdots \mathbf{F}_{\mathrm{p}}^{(m)} \cdots \mathbf{F}_{\mathrm{p}}^{(M)}]^{\mathrm{T}}$, respectively. Based on the superposition principle, the dynamic unknown states of the soil cavities can be written as the summation of the motion induced by the piles-soil interaction forces, which are elicited by $\mathbf{F}_{\mathrm{s}}$ and $\mathbf{F}_{\mathrm{p}}$. Thus, the soil response is given by equivalent expressions to the ones described in Eqs. (3.15) but now accounting for the M pile cavities, therefore, the soil response at all the N_c collocation points $\mathbf{U}_{\mathrm{b}}^{\mathrm{s}}$ and at an arbitrary point on the soil $\mathbf{U}_{\mathrm{s}}$ can be written as

$$\mathbf{U}_{\mathrm{b}}^{\mathrm{s}} = \mathbf{H}_{\mathrm{bb}} \left[\mathbf{H}_{\mathrm{bb}}^{\tau}\right]^{-1} \mathbf{T}_{\mathrm{b}}^{\mathrm{s}} + \mathbf{H}_{\mathrm{bf}}^{\mathrm{cav}} \mathbf{F}_{\mathrm{s}}, \tag{4.4a}$$

$$\mathbf{U}_{\mathrm{s}} = \mathbf{H}_{\mathrm{sb}} \left[\mathbf{H}_{\mathrm{bb}}^{\tau}\right]^{-1} \mathbf{T}_{\mathrm{b}}^{\mathrm{s}} + \mathbf{H}_{\mathrm{sf}}^{\mathrm{cav}} \mathbf{F}_{\mathrm{s}}, \tag{4.4b}$$

with

$$\mathbf{H}_{\mathrm{bb}}^{\tau} = \begin{bmatrix} \mathbf{H}_{\mathrm{bb}}^{\tau(11)} & \mathbf{H}_{\mathrm{bb}}^{\tau(12)} & \cdots & \mathbf{H}_{\mathrm{bb}}^{\tau(1M)} \\ \mathbf{H}_{\mathrm{bb}}^{\tau(21)} & \mathbf{H}_{\mathrm{bb}}^{\tau(22)} & \cdots & \mathbf{H}_{\mathrm{bb}}^{\tau(2M)} \\ \vdots & \cdots & \ddots & \vdots \\ \mathbf{H}_{\mathrm{bb}}^{\tau(M1)} & \mathbf{H}_{\mathrm{bb}}^{\tau(M2)} & \cdots & \mathbf{H}_{\mathrm{bb}}^{\tau(MM)} \end{bmatrix}, \mathbf{H}_{\mathrm{bb}} = \begin{bmatrix} \mathbf{H}_{\mathrm{bb}}^{(11)} & \mathbf{H}_{\mathrm{bb}}^{(12)} & \cdots & \mathbf{H}_{\mathrm{bb}}^{(1M)} \\ \mathbf{H}_{\mathrm{bb}}^{(21)} & \mathbf{H}_{\mathrm{bb}}^{(22)} & \cdots & \mathbf{H}_{\mathrm{bb}}^{(2M)} \\ \vdots & \cdots & \ddots & \vdots \\ \mathbf{H}_{\mathrm{bb}}^{(M1)} & \mathbf{H}_{\mathrm{bb}}^{(M2)} & \cdots & \mathbf{H}_{\mathrm{bb}}^{(MM)} \end{bmatrix}, \tag{4.5}$$

where $\mathbf{H}_{\mathrm{bb}}^{(ij)}$ is the corresponding FRF matrix of displacements at the collocation points of cavity i induced by unit loads applied at the collocation points of cavity j, and the matrix $\mathbf{H}_{\mathrm{bb}}^{\tau(ij)}$ is analogous to $\mathbf{H}_{\mathrm{bb}}^{(ij)}$ but for the FRF of traction. Moreover, $\mathbf{H}_{\mathrm{sb}}$ contains the soil receptance due to unit loads applied at all the collocation points N_c, and expressions $\mathbf{H}_{\mathrm{bf}}^{\mathrm{cav}}$ and $\mathbf{H}_{\mathrm{sf}}^{\mathrm{cav}}$ are given by

$$\mathbf{H}_{\mathrm{bf}}^{\mathrm{cav}} = \mathbf{H}_{\mathrm{bf}} - \mathbf{H}_{\mathrm{bb}} \left[\mathbf{H}_{\mathrm{bb}}^{\tau}\right]^{-1} \mathbf{H}_{\mathrm{bf}}^{\tau} \quad \text{and} \quad \mathbf{H}_{\mathrm{sf}}^{\mathrm{cav}} = \mathbf{H}_{\mathrm{sf}} - \mathbf{H}_{\mathrm{sb}} \left[\mathbf{H}_{\mathrm{bb}}^{\tau}\right]^{-1} \mathbf{H}_{\mathrm{bf}}^{\tau}, \tag{4.6}$$

where the matrices $\mathbf{H}_{\mathrm{bf}}$ and $\mathbf{H}_{\mathrm{sf}}$ contain the Green's functions associated with all the collocation points and an arbitrary point in the soil, respectively, both induced by the external force $\mathbf{F}_{\mathrm{s}}$. The matrix $\mathbf{H}_{\mathrm{bf}}^{\tau}$ is analogous to $\mathbf{H}_{\mathrm{bf}}$ but for traction response.

Similar expressions can be derived for the pile-group subsystem for which its responses at the collocation points $\mathbf{U}_{\mathrm{b}}^{\mathrm{p}}$ and at the pile heads $\mathbf{U}_{\mathrm{h}}$ are given by

$$\mathbf{U}_{\mathrm{b}}^{\mathrm{p}} = \mathbf{W} \left[\mathbf{H}_{\mathrm{ph}} \mathbf{F}_{\mathrm{p}} - \mathbf{H}_{\mathrm{pp}} \mathbf{W}^{\mathrm{T}} \mathbf{W}_{\mathrm{A}} \mathbf{T}_{\mathrm{b}}^{\mathrm{s}}\right], \tag{4.7a}$$

$$\mathbf{U}_{\mathrm{h}} = \mathbf{H}_{\mathrm{hh}} \mathbf{F}_{\mathrm{p}} - \mathbf{H}_{\mathrm{hp}} \mathbf{W}^{\mathrm{T}} \mathbf{W}_{\mathrm{A}} \mathbf{T}_{\mathrm{b}}^{\mathrm{s}}, \tag{4.7b}$$

in which $\mathbf{H}_{\mathrm{ph}}$, $\mathbf{H}_{\mathrm{pp}}$, $\mathbf{H}_{\mathrm{hh}}$ and $\mathbf{H}_{\mathrm{hp}}$ are the matrices of receptance functions that relate the response at all piles' centroid points or at the pile heads (represented by p and h, respectively, as the first subscript) due to forces along the pile or at the pile head (represented by the same nomenclature for the second subscript). It should be noted that, as the pile-group subsystem is composed of independent piles, the matrices of receptance functions are block diagonal matrices.

Finally, by applying the compatibility of displacements and using Eqs. (4.7a) and (4.4a), the traction at the piles-soil interfaces can be determined and subsequently substituted in Eqs. (4.7b) and Eqs. (4.4b) to find the following expressions for the response at the soil soil or at

the pile heads

$$\mathbf{U}_{\mathrm{s}} = \mathbf{H}^{\mathrm{c}}_{\mathrm{sh}}\mathbf{F}_{\mathrm{p}} + \mathbf{H}^{\mathrm{c}}_{\mathrm{sf}}\mathbf{F}_{\mathrm{s}}, \tag{4.8a}$$

$$\mathbf{U}_{\mathrm{h}} = \mathbf{H}^{\mathrm{c}}_{\mathrm{hh}}\mathbf{F}_{\mathrm{p}} + \mathbf{H}^{\mathrm{c}}_{\mathrm{hf}}\mathbf{F}_{\mathrm{s}}, \tag{4.8b}$$

where

$$\mathbf{H}^{\mathrm{c}}_{\mathrm{sh}} = \mathbf{H}_{\mathrm{sb}}\left[\mathbf{H}^{\tau}_{\mathrm{bb}}\right]^{-1}\boldsymbol{\Upsilon}\mathbf{W}\mathbf{H}_{\mathrm{ph}}, \tag{4.9a}$$

$$\mathbf{H}^{\mathrm{c}}_{\mathrm{sf}} = \mathbf{H}^{\mathrm{cav}}_{\mathrm{sf}} - \mathbf{H}_{\mathrm{sb}}\left[\mathbf{H}^{\tau}_{\mathrm{bb}}\right]^{-1}\boldsymbol{\Upsilon}\mathbf{H}^{\mathrm{cav}}_{\mathrm{bf}}, \tag{4.9b}$$

$$\mathbf{H}^{\mathrm{c}}_{\mathrm{hh}} = \mathbf{H}_{\mathrm{hh}} - \mathbf{H}_{\mathrm{hp}}\mathbf{W}^{\mathrm{T}}\mathbf{W}_{\mathrm{A}}\boldsymbol{\Upsilon}\mathbf{W}\mathbf{H}_{\mathrm{ph}}, \tag{4.9c}$$

$$\mathbf{H}^{\mathrm{c}}_{\mathrm{hf}} = \mathbf{H}_{\mathrm{hp}}\mathbf{W}^{\mathrm{T}}\mathbf{W}_{\mathrm{A}}\boldsymbol{\Upsilon}\mathbf{H}^{\mathrm{cav}}_{\mathrm{bf}}, \tag{4.9d}$$

with

$$\boldsymbol{\Upsilon} = \left[\mathbf{H}_{\mathrm{bb}}\left[\mathbf{H}^{\tau}_{\mathrm{bb}}\right]^{-1} + \mathbf{W}\bar{\mathbf{H}}_{\mathrm{pp}}\mathbf{W}^{\mathrm{T}}\mathbf{W}_{\mathrm{A}}\right]^{-1}. \tag{4.10}$$

Eqs. (4.8a) and (4.8b) inherently contain the solution to both radiation and scattering problems for the system under study, which can be recovered by enforcing $\mathbf{F}_{\mathrm{s}} = \mathbf{0}$ or $\mathbf{F}_{\mathrm{p}} = \mathbf{0}$, respectively.

4.2 Modelling a dynamic pile-cap foundation model

As discussed in Chapter 2, ground-borne vibrations are transmitted to the building through its foundation, usually composed of a pile-group system attached to a large concrete slab, referred to as a pile cap, that joins the pile heads. The pile cap is a thick concrete block that rests on a pile-group foundation and distributes the service load from the column onto the piles so that, as far as possible, the load is shared between the piles. Thus, the pile cap, usually designed to behave as a rigid block, supports axial and bending loads induced by the column and the piles. Particular care is taken by designers in selecting a pile cap thickness that ensures its resistance to shear stresses. It is beyond the scope of this dissertation to discuss construction specifications, such as pile spacing, pile arrangement distribution or pile and pile cap design under specific service loads. The interested reader is referred to foundation design handbooks such as Tomlinson [159, 160], Eurocode 2 [161] and Eurocode 7 [162, 163].

Although the pile cap is assumed to behave as a rigid body in seismic analysis, this assumption may no longer be valid for ground-borne vibrations induced by man-made activities, for which

the range of frequencies of interest is much higher. Hence, a dynamic pile-cap model based on the FE method is proposed in this section. Thus, the governing equation for the pile cap subsystem is given by

$$\mathbf{D}\mathbf{U}^{\text{cap}} = \mathbf{F}^{\text{cap}}, \tag{4.11}$$

where $\mathbf{U}^{\text{cap}}$ contains the displacements of each FE node induced by the external nodal forces $\mathbf{F}^{\text{cap}}$, and where the dynamic stiffness matrix of the pile cap is represented by $\mathbf{D}$ and given by the expression

$$\mathbf{D} = -\omega^2\mathbf{M} + \mathbf{K}, \tag{4.12}$$

where $\mathbf{M}$ and $\mathbf{K}$ are the mass and stiffness matrices of the pile. The structural damping is introduced in Eq. (4.12) by considering a complex stiffness matrix given by $\mathbf{K}^* = \mathbf{K}(\mathbf{I}+\mathrm{i}2D\mathbf{K})$, where D is the hysteretic damping ratio of the pile cap.

The pile heads and the pile cap are coupled by assuming force equilibrium and displacement compatibility. This joining procedure is performed by meeting these compatibility conditions between the pile heads and their corresponding coupling surfaces of the pile cap, which are represented by a set of FE nodes located at the same z-plane as the pile heads and within the pile head surfaces, as shown in Fig. 4.2. Thus, Eq. (4.11) can be expressed in terms of FE nodes employed for coupling and the free ones. The resulting expression is given by

$$\begin{bmatrix} \mathbf{D}^{11} & \mathbf{D}^{12} \\ \mathbf{D}^{21} & \mathbf{D}^{22} \end{bmatrix} \begin{bmatrix} \mathbf{U}_{\text{nb}}^{\text{cap}} \\ \mathbf{U}_{\text{b}}^{\text{cap}} \end{bmatrix} = \begin{bmatrix} \mathbf{F}_{\text{nb}}^{\text{cap}} \\ \mathbf{F}_{\text{b}}^{\text{cap}} \end{bmatrix} + \begin{bmatrix} \mathbf{0} \\ \mathbf{P}_{\text{b}}^{\text{cap}} \end{bmatrix}, \tag{4.13}$$

where subscripts nb and b denote, respectively, the subset of FE nodes not located on any of the coupling surfaces and the subset of FE nodes located on these surfaces. Therefore, $\mathbf{U}_{\text{nb}}^{\text{cap}}$ and $\mathbf{U}_{\text{b}}^{\text{cap}}$ are the displacements induced by the external forces $\mathbf{F}_{\text{nb}}^{\text{cap}}$ and $\mathbf{F}_{\text{b}}^{\text{cap}}$, as well as by the interaction forces $\mathbf{P}_{\text{b}}^{\text{cap}}$ to which the pile cap is subjected.

As detailed in Section 3.1, it is assumed that, to model the dynamics of the piles, these can be divided into small rigid cylindrical segments (see Fig. 3.4). This assumption implies that the displacement of any point of the pile can be expressed in terms of the displacements and rotations associated with each one of the corresponding rigid segments. Therefore, the displacement compatibility condition relates the displacement of the FE nodes belonging to each coupling surface to the displacement and rotations associated with each pile head. The

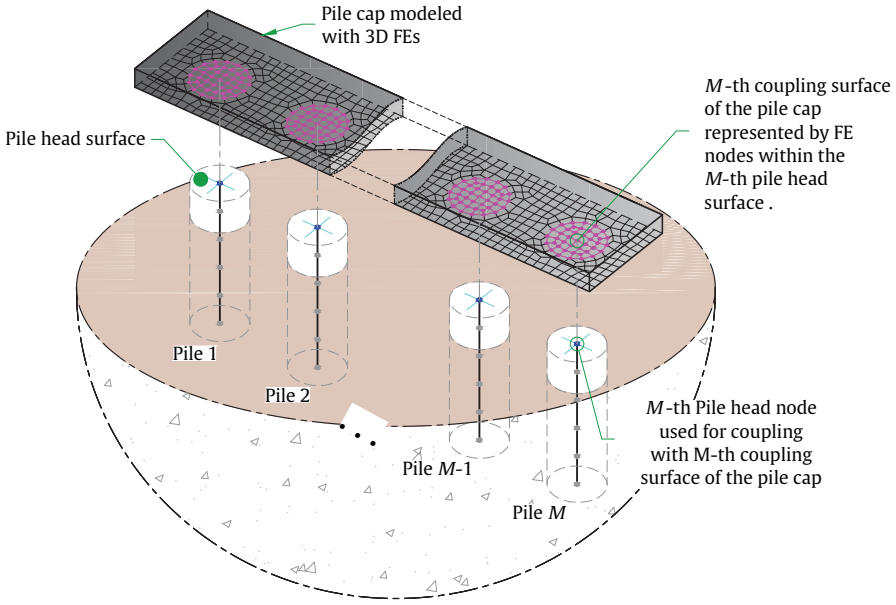

FIGURE 4.2: Schematic drawing of the joining procedure of the piles and the pile cap. The M pile heads are coupled with their corresponding coupling surface of the pile cap modelled by FE nodes, which are within the pile head surfaces.

relation can be expressed as

$$\mathbf{U}_{\mathrm{b}}^{\mathrm{cap}} = \begin{bmatrix} \mathbf{U}_{\mathrm{b}}^{\mathrm{cap}(1)} \\ \mathbf{U}_{\mathrm{b}}^{\mathrm{cap}(2)} \\ \vdots \\ \mathbf{U}_{\mathrm{b}}^{\mathrm{cap}(M)} \end{bmatrix} = \begin{bmatrix} \mathbf{W}_{\mathrm{b}}^{(1)} & \mathbf{0} & \cdots & \mathbf{0} \\ \mathbf{0} & \mathbf{W}_{\mathrm{b}}^{(2)} & \cdots & \mathbf{0} \\ \vdots & \cdots & \ddots & \vdots \\ \mathbf{0} & \mathbf{0} & \cdots & \mathbf{W}_{\mathrm{b}}^{(M)} \end{bmatrix} \begin{bmatrix} \mathbf{U}_{\mathrm{h}}^{(1)} \\ \mathbf{U}_{\mathrm{h}}^{(2)} \\ \vdots \\ \mathbf{U}_{\mathrm{h}}^{(M)} \end{bmatrix} = \mathbf{W}_{\mathrm{b}}\mathbf{U}_{\mathrm{h}} \tag{4.14}$$

where $\mathbf{W}_{\mathrm{b}}^{(m)}$ relates the displacements of those FE nodes belonging to the m-th coupling surface $\mathbf{U}_{\mathrm{b}}^{\mathrm{cap}(m)}$ with the displacement and rotation of the m-th pile head $\mathbf{U}_{\mathrm{h}}^{(m)}$. The procedure to obtain $\mathbf{W}_{\mathrm{b}}^{(m)}$ is similar to the one considered for $\mathbf{W}^{(m)}$ and can be found in Appendix B.

As each pile has been discretised into small cylindrical rigid segments, the interaction forces and moments acting on the pile-heads $\mathbf{P}_{\mathrm{h}}^{\mathrm{pile}(m)}$ can be expressed in terms of the resulting forces acting on the FE nodes of the pile cap in contact with the m-th pile-head surface $\mathbf{P}_{\mathrm{b}}^{\mathrm{cap}(m)}$.

Thus, the expression that describes the force equilibrium condition can be expressed by

$$\mathbf{P}_{\mathrm{h}}^{\mathrm{pile}} = \begin{bmatrix} \mathbf{P}_{\mathrm{h}}^{\mathrm{pile}(1)} \\ \mathbf{P}_{\mathrm{h}}^{\mathrm{pile}(2)} \\ \vdots \\ \mathbf{P}_{\mathrm{h}}^{\mathrm{pile}(M)} \end{bmatrix} = - \begin{bmatrix} \mathbf{W}_{\mathrm{b}}^{\mathrm{T}(1)} & \mathbf{0} & \cdots & \mathbf{0} \\ \mathbf{0} & \mathbf{W}_{\mathrm{b}}^{\mathrm{T}(2)} & \cdots & \mathbf{0} \\ \vdots & \cdots & \ddots & \vdots \\ \mathbf{0} & \mathbf{0} & \cdots & \mathbf{W}_{\mathrm{b}}^{\mathrm{T}(M)} \end{bmatrix} \begin{bmatrix} \mathbf{P}_{\mathrm{b}}^{\mathrm{cap}(1)} \\ \mathbf{P}_{\mathrm{b}}^{\mathrm{cap}(2)} \\ \vdots \\ \mathbf{P}_{\mathrm{b}}^{\mathrm{cap}(M)} \end{bmatrix} = -\mathbf{W}_{\mathrm{b}}^{\mathrm{T}} \mathbf{P}_{\mathrm{b}}^{\mathrm{cap}}. \tag{4.15}$$

Introducing Eq. (4.14) into Eq. (4.13) and multiplying the resulting expression by $\mathbf{W}_{\mathrm{b}}^{\mathrm{T}}$ the following matrix equation is obtained

$$\begin{bmatrix} \mathbf{I} & \mathbf{0} \\ \mathbf{0} & \mathbf{W}_{\mathrm{b}}^{\mathrm{T}} \end{bmatrix} \begin{bmatrix} \mathbf{D}^{11} & \mathbf{D}^{12} \\ \mathbf{D}^{21} & \mathbf{D}^{22} \end{bmatrix} \begin{bmatrix} \mathbf{I} & \mathbf{0} \\ \mathbf{0} & \mathbf{W}_{\mathrm{b}} \end{bmatrix} \begin{bmatrix} \mathbf{U}_{\mathrm{nb}}^{\mathrm{cap}} \\ \mathbf{U}_{\mathrm{h}} \end{bmatrix} = \begin{bmatrix} \mathbf{I} & \mathbf{0} \\ \mathbf{0} & \mathbf{W}_{\mathrm{b}}^{\mathrm{T}} \end{bmatrix} \left(\begin{bmatrix} \mathbf{F}_{\mathrm{nb}}^{\mathrm{cap}} \\ \mathbf{F}_{\mathrm{b}}^{\mathrm{cap}} \end{bmatrix} + \begin{bmatrix} \mathbf{0} \\ \mathbf{P}_{\mathrm{b}}^{\mathrm{cap}} \end{bmatrix} \right). \tag{4.16}$$

Introducing the expression $\mathbf{P}_{\mathrm{h}}^{\mathrm{pile}} = -\mathbf{W}_{\mathrm{b}}^{\mathrm{T}} \mathbf{P}_{\mathrm{b}}^{\mathrm{cap}}$ described in Eq. (4.15) in the right-hand side of Eq. (4.16), and imposing $\mathbf{F}_{\mathrm{b}}^{\mathrm{cap}} = \mathbf{0}$, the resulting matrix equation is given by

$$\begin{bmatrix} \mathbf{D}^{11} & \mathbf{D}^{12}\mathbf{W}_{\mathrm{b}} \\ \mathbf{W}_{\mathrm{b}}^{\mathrm{T}}\mathbf{D}^{21} & \mathbf{W}_{\mathrm{b}}^{\mathrm{T}}\mathbf{D}^{22}\mathbf{W}_{\mathrm{b}} \end{bmatrix} \begin{bmatrix} \mathbf{U}_{\mathrm{nb}}^{\mathrm{cap}} \\ \mathbf{U}_{\mathrm{h}} \end{bmatrix} = \begin{bmatrix} \mathbf{F}_{\mathrm{nb}}^{\mathrm{cap}} \\ \mathbf{0} \end{bmatrix} + \begin{bmatrix} \mathbf{0} \\ -\mathbf{P}_{\mathrm{h}}^{\mathrm{pile}} \end{bmatrix}. \tag{4.17}$$

The pile and field responses for the pile-group subsystem considered in this section are obtained by adding to Eqs. (4.8) the interaction forces $\mathbf{P}_{\mathrm{h}}^{\mathrm{pile}}$ to which the pile heads are subjected. The resulting expressions are

$$\mathbf{U}_{\mathrm{s}} = \mathbf{H}_{\mathrm{sh}}^{\mathrm{c}} \left(\mathbf{F}_{\mathrm{p}} + \mathbf{P}_{\mathrm{h}}^{\mathrm{pile}} \right) + \mathbf{H}_{\mathrm{sf}}^{\mathrm{c}} \mathbf{F}_{\mathrm{s}}, \tag{4.18a}$$

$$\mathbf{U}_{\mathrm{h}} = \mathbf{H}_{\mathrm{hh}}^{\mathrm{c}} \left(\mathbf{F}_{\mathrm{p}} + \mathbf{P}_{\mathrm{h}}^{\mathrm{pile}} \right) + \mathbf{H}_{\mathrm{hf}}^{\mathrm{c}} \mathbf{F}_{\mathrm{s}}. \tag{4.18b}$$

Finally, the kinematic and inertial interactions between the pile cap and the pile-group subsystems are satisfied when combining Eqs. (4.17) and (4.18). Thus, by combining those equations and after rearranging the resulting expression, the following system of equations for the coupled piles-cap system can be obtained

$$\begin{bmatrix} \mathbf{D}^{11} & \mathbf{D}^{12}\mathbf{W}_{\mathrm{b}} & \mathbf{0} \\ \mathbf{W}_{\mathrm{b}}^{\mathrm{T}}\mathbf{D}^{21} & \mathbf{W}_{\mathrm{b}}^{\mathrm{T}}\mathbf{D}^{22}\mathbf{W}_{\mathrm{b}} + (\mathbf{H}_{\mathrm{hh}}^{\mathrm{c}})^{-1} & \mathbf{0} \\ \mathbf{0} & -\mathbf{H}_{\mathrm{sh}}^{\mathrm{c}}(\mathbf{H}_{\mathrm{hh}}^{\mathrm{c}})^{-1} & \mathbf{I} \end{bmatrix} \begin{bmatrix} \mathbf{U}_{\mathrm{nb}}^{\mathrm{cap}} \\ \mathbf{U}_{\mathrm{h}} \\ \mathbf{U}_{\mathrm{s}} \end{bmatrix} = \begin{bmatrix} \mathbf{F}_{\mathrm{nb}}^{\mathrm{cap}} \\ \mathbf{F}_{\mathrm{p}} \\ \mathbf{0} \end{bmatrix} + \begin{bmatrix} \mathbf{0} \\ (\mathbf{H}_{\mathrm{hh}}^{\mathrm{c}})^{-1}\mathbf{H}_{\mathrm{hf}}^{\mathrm{c}} \\ \mathbf{H}_{\mathrm{sf}}^{\mathrm{c}} - \mathbf{H}_{\mathrm{sh}}^{\mathrm{c}}(\mathbf{H}_{\mathrm{hh}}^{\mathrm{c}})^{-1}\mathbf{H}_{\mathrm{hf}}^{\mathrm{c}} \end{bmatrix} \mathbf{F}_{\mathrm{s}}. \tag{4.19}$$

Eq. (4.19) is the system of equations that describes the dynamic response of the piles-cap model due to forces applied on the cap, on the pile heads or on the soil.

4.3 Numerical assessment of the pile-group model

In this section, the developed formulation for modelling the dynamic response of pile-group systems is numerically verified using two case studies. In the first one, the formulation presented in Section 4.1 is used to model a two-pile group embedded in an elastic half-space. In the second, the approach presented in Section 4.2 is used to add a pile cap to the previously considered two-pile group system. In both cases, the proposed approaches are verified by comparing their predictions against those obtained using a 3D FE-BE approach.

The geometric and mechanical parameters for the piles employed for the two case studies are given in Table 4.1 and correspond to the short pile employed in the validation of the single-pile model previously presented in Chapter 3. The piles are spaced between them for $s = 1.2$ m, and they are embedded in a soft soil modelled as a homogeneous half-space whose mechanical properties are also given in Table 4.1. Furthermore, the analysis is performed for frequencies between 1 Hz and 100 Hz, covering the frequency range where ground-borne vibration induced by railway traffic is usually significant [153].

When modelling both case studies using the developed formulations, the criteria described in Section 3.2.1 is used to define the number of cylindrical segments and collocation points required to represent each pile accurately. Thus, by considering the piles' geometry and the minimum wavelength of this problem, the criterion establishes that each pile should be modelled using $N_p = 47$ cylindrical segments with $N_s = 36$ collocation points each. Regarding the discretization scheme for 3D FE-BE models used for the verification, the piles and the pile cap structures are discretised using eight-noded hexahedral FEs, while the structure-soil boundary is discretised using four-noded quadrilateral BEs. Similar to the single-pile case, the FE-BE

model for the piles and cap employ nine nodes per wavelength to define the maximum distance between the nodes, which is 20 cm.

Finally, similar to the single-pile foundation model, the influence of neglecting the rotational motion and bending effect in the pile-soil coupling procedure of the proposed approach, carried through the transformation matrix $\mathbf{W}$, is also included in the comparison of results for the two case studies. Furthermore, it is worth mentioning that the torsional rotation has usually been neglected in previous works because of its low influence when the pile model is employed for modelling planar building foundations [5, 131] or when responses in low frequency range are accounted for in the analysis of pile-groups.

Description	Units	Soil	Piles	Pile cap
Density (ρ)	kg/m^3	1950	2860	2860
Young's modulus (E)	MPa	151.2	40000	40000
Poisson's ratio (ν)	-	0.35	0.25	0.25
Hysteretic damping ratio (D)	-	0.05	0.01	0.01
Speed of the P-waves (C_p)	m/s	352.8	-	-
Speed of the S-waves (C_s)	m/s	169.5	-	-
Pile length (L_p)	m	-	10	-
Pile radius (r_p)	m	-	0.3	-
Pile spacing (s)	m	-	1.2	-

TABLE 4.1: Soil, piles and pile cap parameters used in the case studies involving multi-pile foundations.

4.3.1 Case study 1: Two-pile group system

The numerical verification of the first case study is conducted by comparing the responses predicted by the proposed approach with those obtained using a 3D FE-BE approach when a harmonic point load is applied at the head of one pile. It is assumed that the pile subjected to the excitation (Pile 1) is located at the origin of a Cartesian system of coordinates. Three observation points are considered for this numerical verification: O_1, O_2 and O_3 located at position $(1.2, 0, 0)$ m, $(5, 0, 0)$ m and $(20, 0, 0)$ m, respectively; the first one evaluates the dynamic response at the second pile head and the other two are considering the response of the soil surface at the near and far field. The FRF due to unitary harmonic excitation at these evaluation points due to a unitary harmonic excitation at the head of Pile 1 $\mathbf{H}^{\mathrm{c}}_{k\mathrm{h}}$ are presented in Figs. 4.3 and 4.4 in dB with 1 m/N for the responses to unitary harmonic point loads and 1 m/N·m for the responses to unitary harmonic bending moments as references, respectively.

In the figures, the first, second and third columns are associated with responses at O_1, O_2 and O_3, respectively. Additionally, the subscript k depends on the observation point considered, being $k = h$ when the FRF at the pile head, computed using Eq. (4.9c), is considered, or $k = s$ when the FRF associated to a field point, computed using Eq. (4.9a), is required. For the 3D FE-BE approach, distributed loads were applied at the FE nodes located at the head of Pile 1. These distributions were designed to ensure that the resulting forces and moments acting on the pile head were equal to those applied in the case modelled using the new pile-group formulation.

The FRFs predicted by the proposed formulation agree well with those obtained using the 3D FE-BE approach, as shown in Fig. 4.3 and 4.4. On the contrary, when rotational motion and bending effects are neglected in the soil-pile coupling, discrepancies similar to those discussed in the single-pile studies presented in Section 3.2 are again observed. These discrepancies are are particularly notable in the displacements induced by bending moments in the y-direction, as shown in Fig. 4.4(a-i), (a-ii). Similar discrepancies are observed in the vertical responses induced by bending loads in the y-direction, as shown, for instance, in 4.4(c-i). In this case, the discrepancies can be explained by the assumption of imposing the rigid cylindrical segments solely to translation movements rather than to allow the rotational motion as the proposed model does. This trend is also observed in Fig. 4.4(c-ii), (c-iii) which suggests that neglecting the rotational motion effect in the pile-soil coupling increases the stiffness of the pile-group system associated to this motion, leading to predicted vibration levels that are lower than those predicted by the 3D FE-BE method.

Finally, the results presented in Figs. 4.4(d-i), (d-ii) and (d-iii) show another significant discrepancy between the presented approaches. While the results obtained for the case in which rotational and bending effects are considered agree well with those obtained using the FEM-BEM approach, no response is obtained when these effects are neglected in the proposed formulation. This result can be explained by the fact that, as piles are modelled using Euler-Bernouilli beam theory, a torsional moment applied at Pile head 1 will only cause torsional vibrations of Pile 1, i.e. no displacements of the pile centroid. Therefore, if torsional effects are neglected in the coupling, there is no pile-soil interaction and no transmission of SH waves through the ground. Consequently, the response at any observation point not located on Pile 1 is zero.

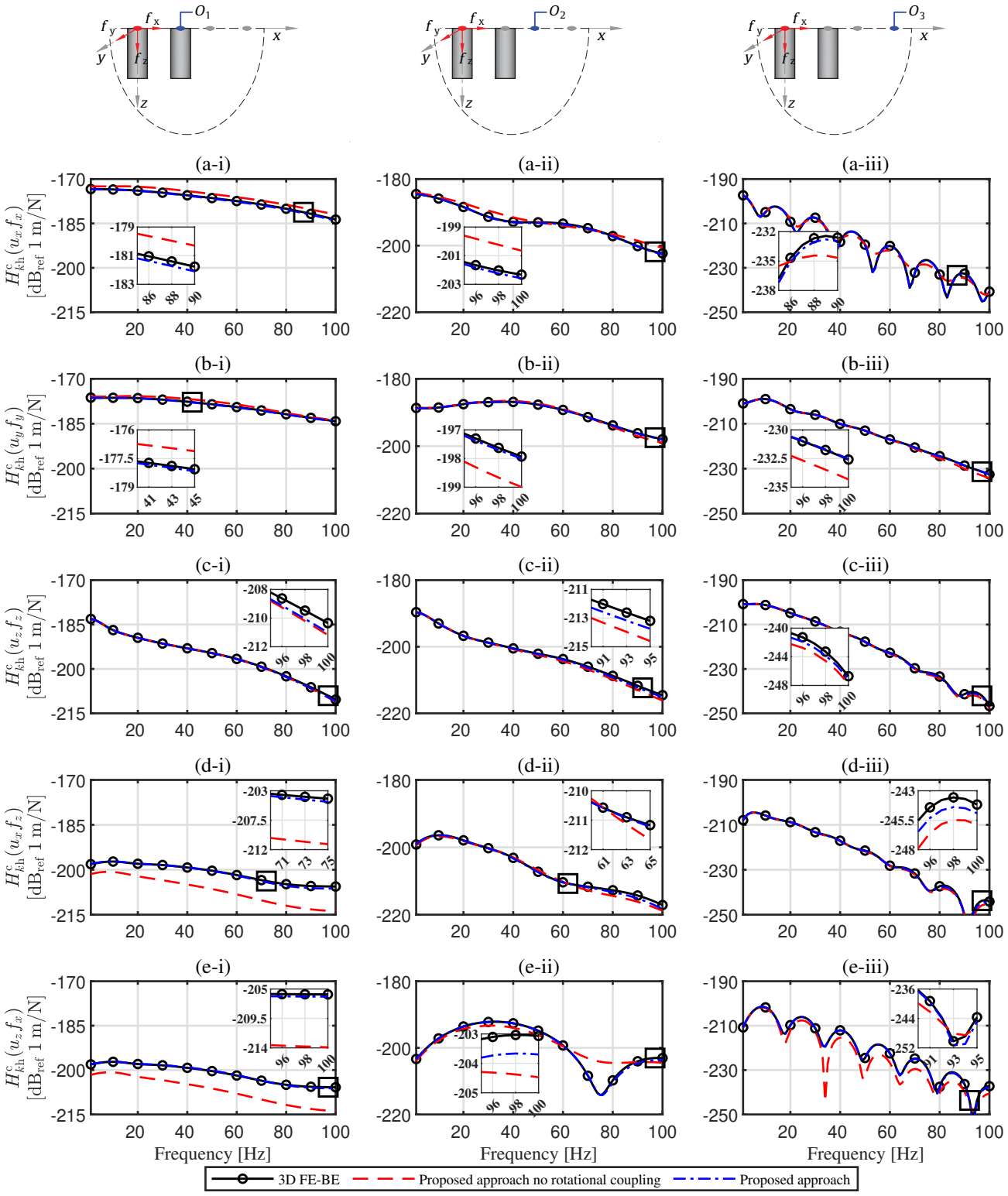

FIGURE 4.3: Receptance of a two-piled group system induced by harmonic point loads considering different approaches. Components of the receptance shown are xx (a), yy (b), zz (c), xz (d) and zx (e) and observation points considered are O_1 (i), O_2 (ii), O_3 (iii). Results in dB using $20\log_{10}(|H|)$, with 1 m/N as reference.

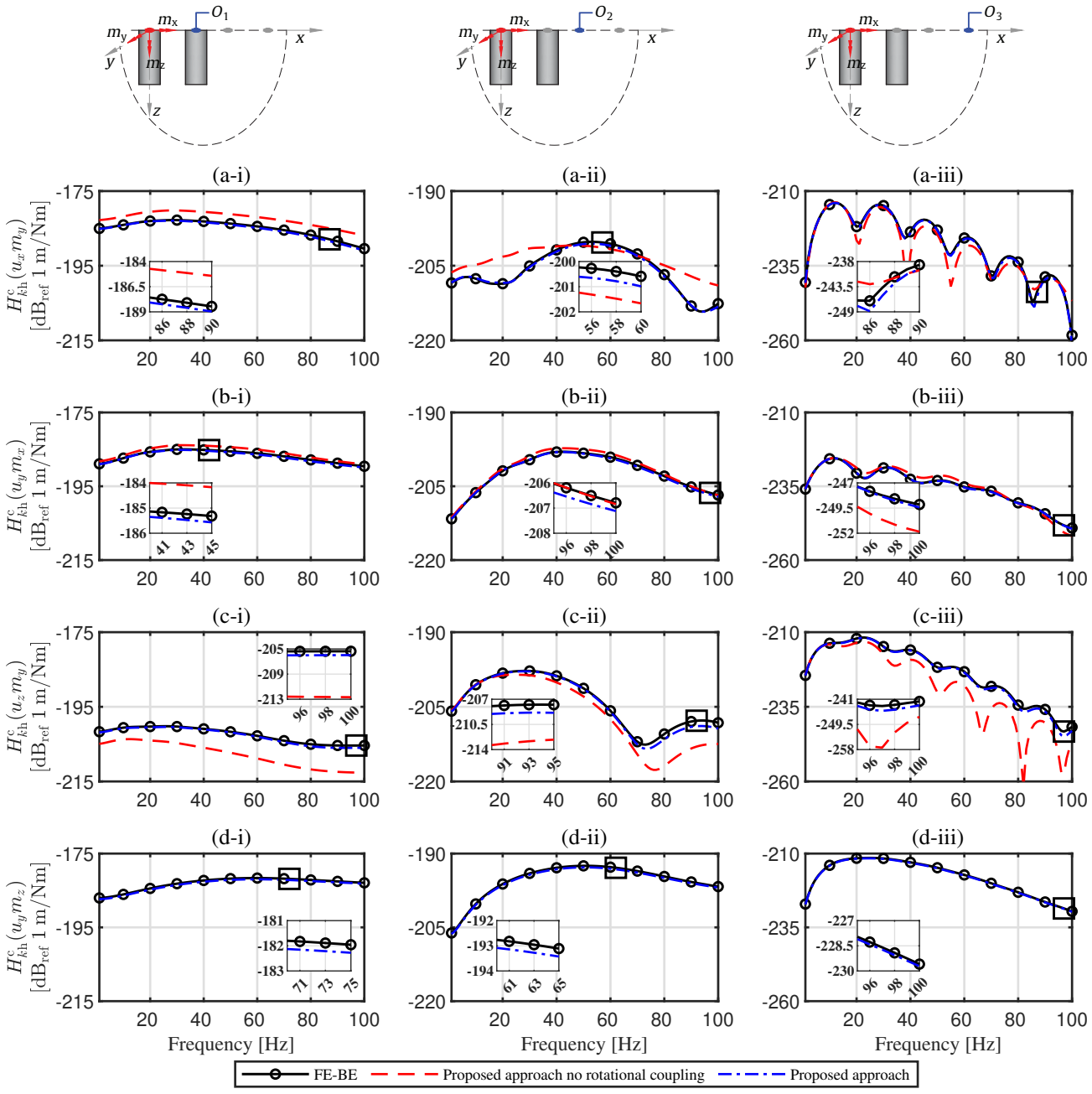

FIGURE 4.4: Receptance of a two-piled group system induced by harmonic bending moments considering different approaches. Components of the receptance shown are xy (a), yx (b), zy (c) and yz (d) and observation points considered are O_1 (i), O_2 (ii), O_3 (iii). Results in dB using $20\log_{10}(|H|)$, with 1 m/N·m as reference.

4.3.2 Case study 2: Two-pile group system with pile-cap

The second case study aims to study the performance of the proposed pile-cap foundation model developed in this chapter. The geometry of the piled foundation system considered in this second case study is presented in Fig. 4.5. As before, the FRFs obtained using the formulation presented in Section 4.2 are compared with those obtained by using a 3D FE-BE approach. Moreover, this case study is also used to study different coupling assumptions between the piles and the soil and between the piles and the pile cap, which it is assumed to have the same mechanical properties as those considered for the piles (see Table 4.1). The studied coupling conditions are classified into the following four coupling methodologies:

- **Methodology 1:** In this methodology, rotational and bending effects on the pile cylindrical segments are considered in the pile-soil coupling conditions, so the transformation matrix $\mathbf{W}$ is constructed as described in Appendix B. Similarly, the matrix $\mathbf{W}_b$ that relates the displacement and rotation of the pile heads with their corresponding FE nodes of the pile cap is constructed by considering the six degrees of freedom of each pile head. In this context, this methodology is referred to as fully coupled methodology in what follows.

- **Methodology 2:** Rotational and bending effects on the pile cylindrical segments are neglected in the pile-soil coupling conditions, so the transformation matrix $\mathbf{W}$, described in Appendix B, is modified accordingly. Whilst the piles-pile cap coupling conditions are equal to those considered in Methodology 1.

- **Methodology 3:** Rotational and bending effects on the pile cylindrical segments are neglected in the pile-soil coupling conditions, so the transformation matrix $\mathbf{W}$ is constructed accordingly as in Methodology 2. Whilst, torsional effects are neglected when considering the piles-pile cap coupling. Therefore, $\mathbf{W}_b$ is constructed accordingly.

- **Methodology 4:** Similar to Methodology 1, rotational and bending effects on the pile cylindrical segments are considered in this methodology for the construction of the transformation matrix $\mathbf{W}$, but torsional effects are neglected in the piles-pile cap coupling. Therefore, $\mathbf{W}_b$ is constructed accordingly.

The dynamic response of the system is initially assessed by considering a harmonic point load applied on the pile cap surface and just above the centroid line of Pile 1. This point is located at $(0, 0, -0.5)$ m in the Cartesian system of coordinates considered in this example, as shown

in Fig. 4.5. The considered excitation point ensures that the system is eccentrically loaded, inducing torsional motion. The comparison is performed at three evaluation points: O_1, O_2 and O_3 located at position $(1.2, 0, -0.5)$ m, $(5, 0, 0)$ m and $(20, 0, 0)$ m, respectively; the first one evaluates the dynamic response just above the centroid line of Pile 2, and the other two are considering the response of the soil surface at the near and far field.

Fig. 4.6 shows the receptances obtained at each evaluation point for the considered pile-cap loading scenario. The results show that the fully coupled approach (Methodology 1) predicts vibration levels that agree well with those predicted by the 3D FE-BE model. Slight discrepancies (of around 0.5 dB) are only observed at high frequencies and for the responses on the field, as shown in Fig. 4.6(c-ii) or (d-ii). However, when the studied alternative coupling conditions are considered, significant differences are observed between the predicted responses and those obtained using the FE-BE approach. These differences are particularly notorious in the lateral responses (u_y) due to lateral harmonic loads (f_y) presented in Figs. 4.6(b-i), (b-ii) and (b-iii). From these figures, it is clear that the alternative approaches (Methodologies 2, 3 and 4) cannot be used to predict the response of the system for the whole range of frequencies considered. However, it is worth highlighting that the discrepancies between the approaches are very small for frequencies between 1 and 25 Hz. This fact is consistent with the result previously reported by Novak et al. in [164], who stated that the error introduced by ignoring the twisting reaction of the piles in a group is usually small. A further observation regarding Methodology 4 denotes that even by employing a fully piles-soil coupling scheme (similar to Methodology 1), the dynamic response of the pile-cap system presents almost similar discrepancies to Methodology 3, for which the torsional motion is neglected in the piles-cap coupling. In contrast to what is observed for the other methodologies, the results obtained with Methodology 2 present unexpected troughs in the frequency range of 40 - 50 Hz when observed lateral responses (u_y) due to loads (f_y). These troughs can be explained by the fact that the pile cap transmits torsional motion to the pile-group, but this motion is not transferred to the soil since Methodology 2 does not consider it in the pile-soil coupling scheme.

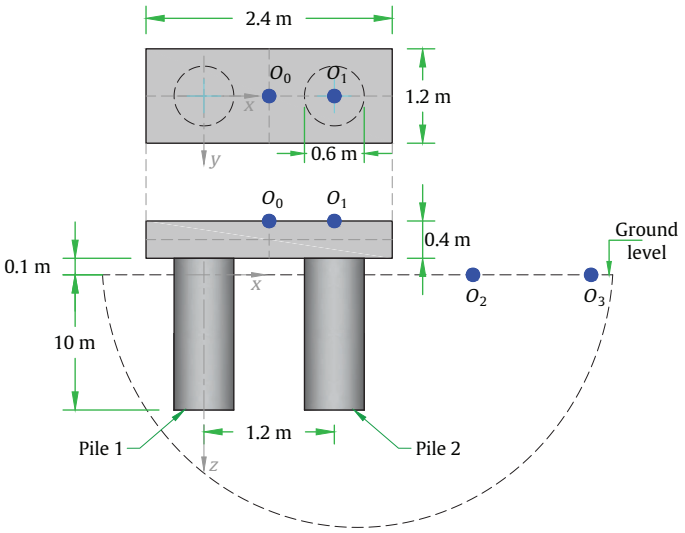

FIGURE 4.5: Schematic drawing of the pile cap system.

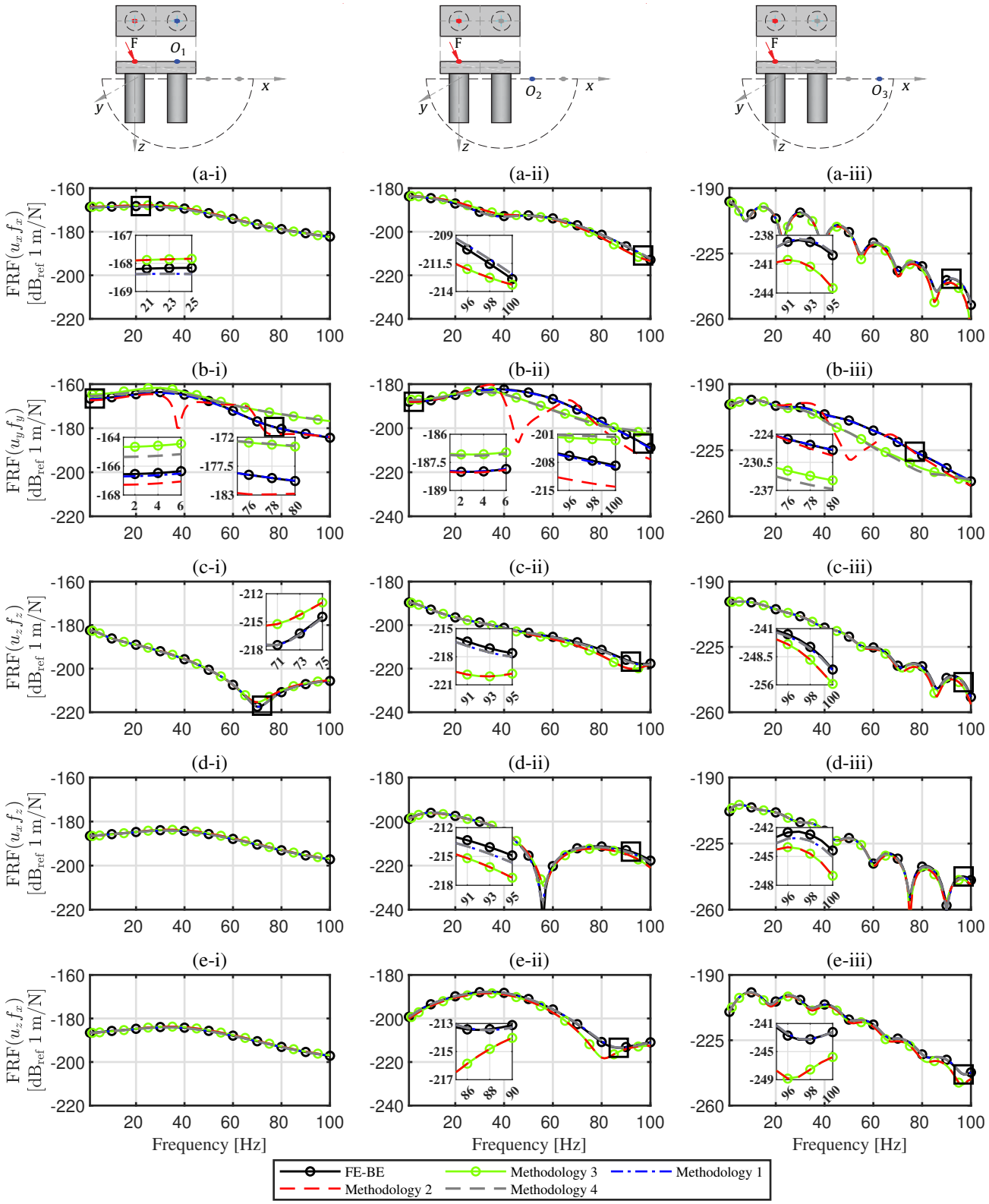

FIGURE 4.6: FRFs of the piles-cap system considering different coupling methodologies. Components of the FRFs matrices shown are xx (a), yy (b), zz (c), xz (d) and zx (e) and observation points considered are O_1 (i), O_2 (ii), O_3 (iii). Results in dB using $20\log_{10}(|H|)$, with 1 m/N as reference.

The proposed approach is also used in this case study to discuss whether the considered pile cap can be assumed to behave as a rigid body for the range of frequencies of interest. The study is performed by comparing the responses of the piled foundation system due to two different loading conditions. These loads are chosen so that the resultant forces and moments are equal in both cases, being equivalent to unit point forces and moments applied at point $O_0 = (0.6, 0, -0.5)$ m, which is located at the centre of the upper surface of the cap, as shown in Fig. 4.7. The first loading condition, referred to as P, considers combinations of point loads applied at the edges of the cap's upper surface as shown in Fig. 4.7(a). In contrast, the second one, referred to as D, consists of load distributions applied on the cap's upper surface, as shown in Fig. 4.7(b). Therefore, if applied to a rigid body, both loading conditions would cause the same dynamic response (translation and rotation) of that body. The responses of the system to both types of loading conditions predicted by the proposed approach are compared with the ones predicted by the FE-BE approach at three evaluation points: O_0, the location of the equivalent loads, O_2, located at $(5, 0, 0)$ m, and O_3, located at $(20, 0, 0)$ m; the first one is the location of the equivalent unit forces, and the other two are considering the response of the soil surface at the near and far field, as shown in Fig. 4.5. Moreover, the results obtained by the proposed approach correspond to the one referred to as a fully coupled system, which was previously detailed in Methodology 1.

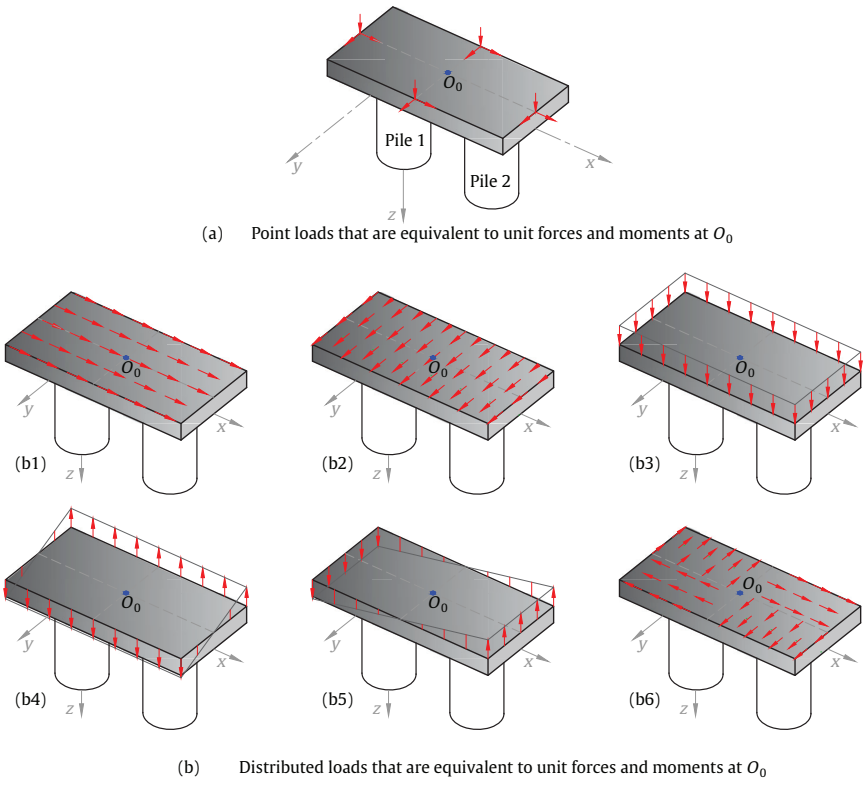

FIGURE 4.7: Considered (a) point and (b) distributed load configurations that are equivalent to unit forces and moments acting at the centre of the pile's cap upper surface.

Figs 4.8 and 4.9 show the displacements obtained when load distributions producing, respectively, unit forces and unit moments are applied at the pile cap of the pile foundation system. In general, the results obtained by the proposed approach agree very well with those predicted by the 3D FE-BE model. The results also indicate that the assumption of considering the assessed pile cap as a rigid body is valid for the whole range of frequencies studied since there are slight discrepancies between the vibration levels predicted for both loading cases in the whole range of frequencies of interest. For instance, the vibration levels in the x-direction due to a distributed load in the z-direction slightly differ (around 1 dB) from the one induced by the corresponding combination of point loads, as shown in Fig. 4.8(d-ii). Similar differences are observed for the displacements in the x-direction due to load distributions equivalent to a unit bending load in y-direction, as shown in Fig. 4.9(a-i). However, it is worth mentioning that this conclusion is limited to the specific piles-cap configuration adopted for the presented numerical assessment of the proposed approach because the behaviour of the current pile cap as a rigid body may no longer be valid for a system with other geometry configurations such as smaller pile cap thickness, bigger pile spacing, number of piles or pile distribution.

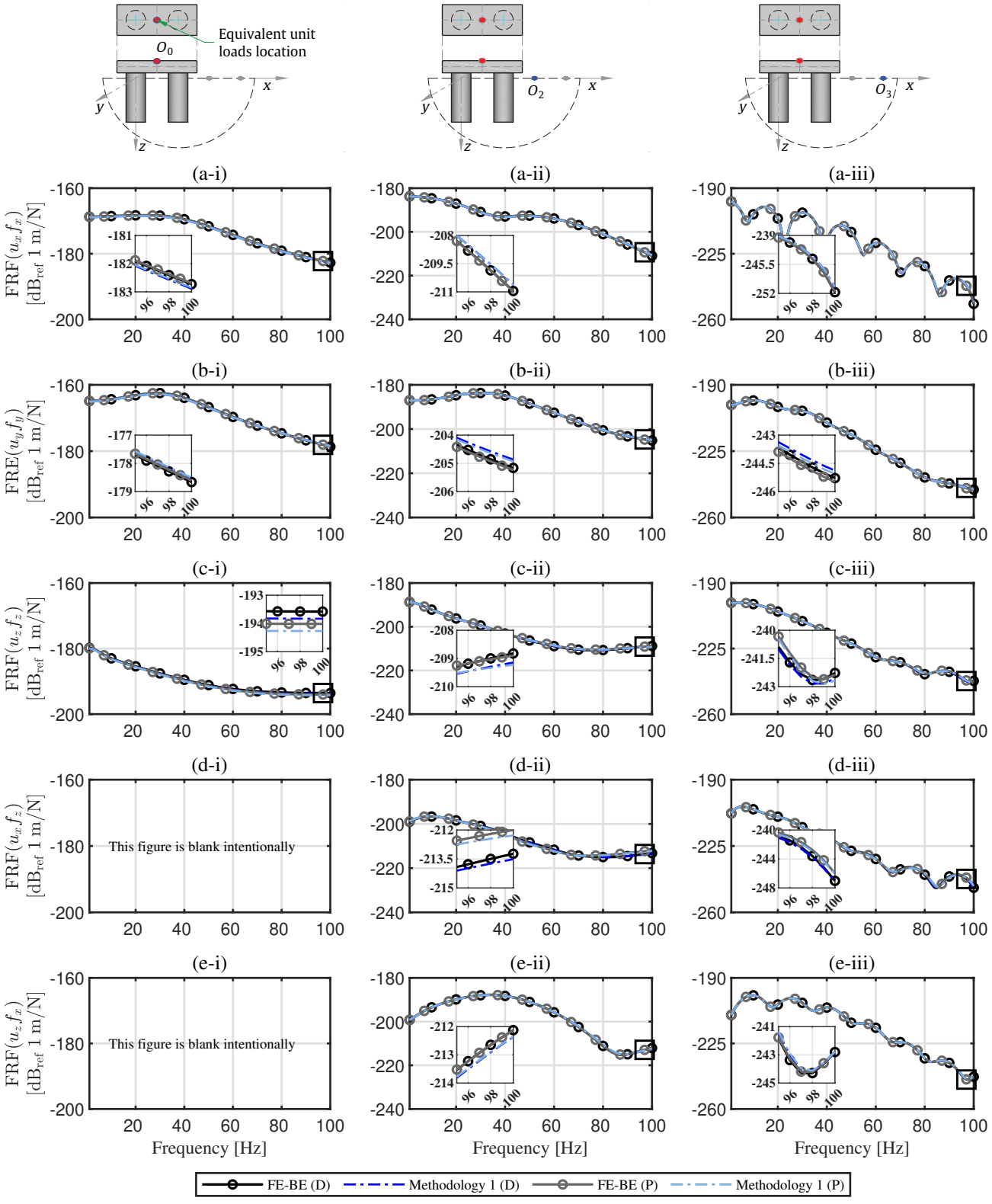

FIGURE 4.8: FRFs of the piles-cap system when subjected to equivalent unit forces. Components of the FRFs matrices shown are xx (a), yy (b), zz (c), xz (d) and zx (e) and observation points considered are O_0 (i), O_2 (ii), O_3 (iii). Results in dB using $20\log_{10}(|H|)$, with 1 m/N as reference.

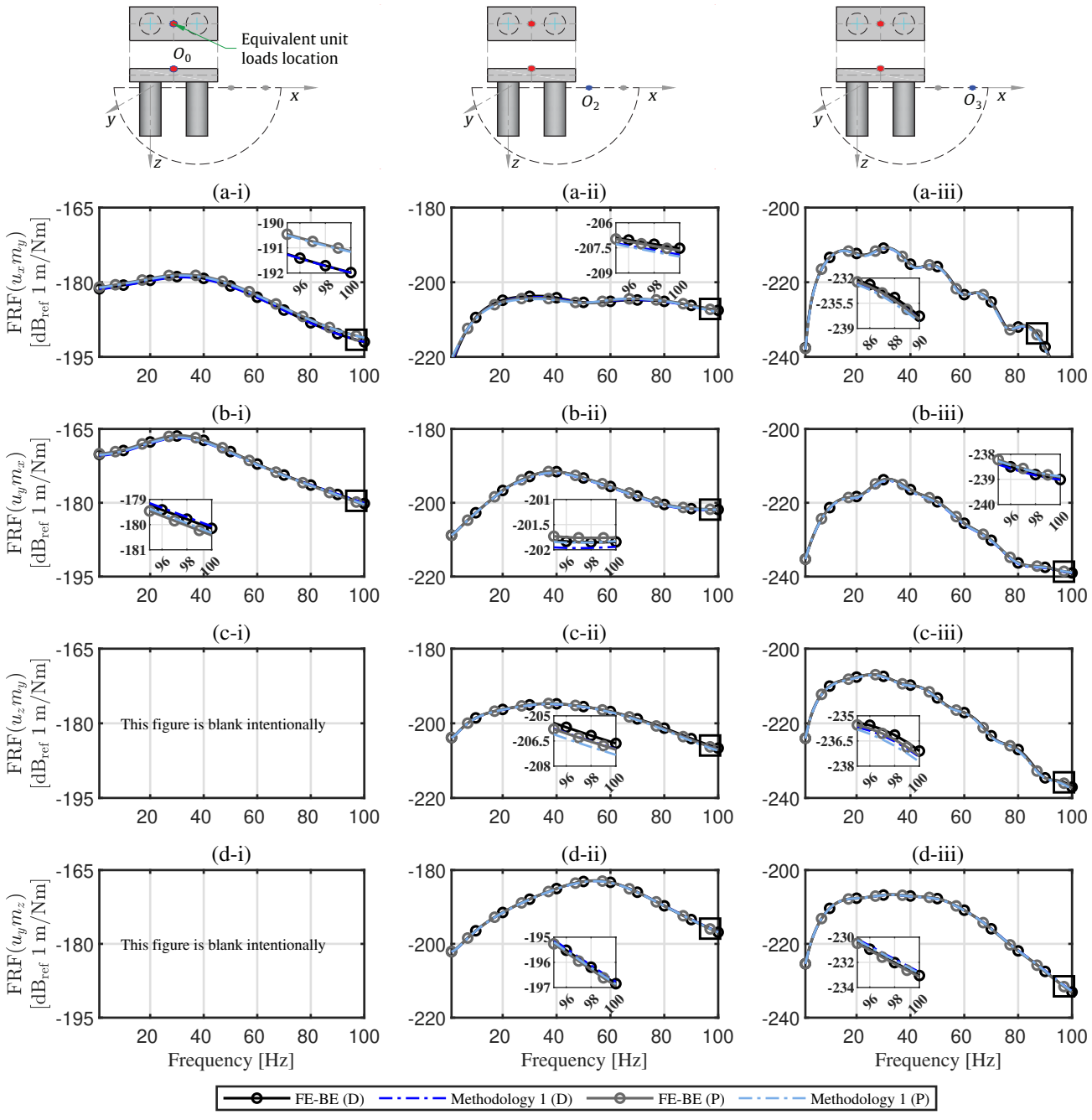

FIGURE 4.9: FRFs of the piles-cap system when subjected to equivalent unit moments. Components of the FRFs matrices shown are xy (a), yx (b), zy (c) and yz (d) and observation points considered are O_0 (i), O_2 (ii), O_3 (iii). Results in dB using $20\log_{10}(|H|)$, with 1 m/N·m as reference.

4.4 The effect of neighbouring piles in the calculation of the dynamic interaction factors

Despite the fact that the modelling approach for pile-groups presented in Section 4.1 is almost as accurate and much more efficient than the 3D FE-BE approach, its computational cost can still be significant when pile-groups with a large number of piles are considered. Because of this, an alternative solution scheme to reduce the computational effort or simplify the solution of a pile-group to smaller and simpler systems is highly desirable. The superposition method (firstly proposed by Poulos [116]) is a great alternative solution scheme that allows to avoid dealing with the large systems of equations involved in fully coupled systems. This method, which adopts the assumption that neighbouring piles do not significantly affect the motion of the two adjacent piles under consideration, solely employs the response of two isolated piles to construct a global flexibility matrix that relates forces and displacements only at the pile heads. Thus, for a system under static loads, the input in the global flexibility matrix is obtained from the solution of two piles, commonly referred to as the interaction factor, which is a function of the pile spacing and of the mechanical properties of the system. In order to employ the superposition method to solve a two-pile group subjected to unit harmonic load, Kaynia [3] defines the dynamic interaction factors of two piles in isolation α as

$$\alpha = \frac{H_{\mathrm{hh}}^{\mathrm{c}(2)}(\omega)}{H_{\mathrm{hh}}^{\mathrm{c}(1)}(\omega = 0)}, \tag{4.20}$$

where $H_{\mathrm{hh}}^{\mathrm{c}(2)}(\omega)$ is the receptance of Pile head 2 due to a harmonic load applied at Pile head 1 (which is given by Eq. (4.9c)), and $H_{\mathrm{hh}}^{\mathrm{c}(1)}(\omega = 0)$ is the static receptance of Pile head 1 due to a static load applied on it. This static receptance is computed considering a single-pile foundation, i.e. neglecting the existence of neighbouring piles. It is worth mentioning that although Poulos and Davis [165] presented an alternative solution for the static pile-head receptance of a single floating pile in a homogeneous half-space, the static receptance $H_{\mathrm{hh}}^{\mathrm{c}(1)}(\omega = 0)$ considered in this dissertation is approximated to the dynamic response of the system for an excitation frequency of 0,1 Hz. The results obtained for such excitation frequency are essentially the same to the ones obtained using the solution Poulus and Davis [165], as discussed in [131].

Existing comparisons between results obtained with fully coupled models and those obtained using the superposition method show that this methodology is valid for inertial loads for the

range of frequencies of interest in seismic applications with the accuracy improving as the pile spacing increases [3]. However, at high frequencies, it is expected that the interaction between two adjacent piles is increasingly affected by the existence of neighbouring piles. Thus, in order to evaluate this assumption, the definition of the dynamic interaction factor of two isolated piles is extended to a generic pile-group [166], which is given by

$$\alpha_{pq}^{(i,j)} = \frac{H_{\mathrm{hh},(pq)}^{\mathrm{c},(ij)}(\omega)}{H_{\mathrm{hh},(pq)}^{\mathrm{c},(ii)}(\omega = 0)}, \tag{4.21}$$

where $\alpha_{pq}^{i,j}$ is the dynamic interaction factor between Pile i (receiver) and Pile j (source). The subscript p denotes the component of the displacements ($p = 1, 2, 3$) or rotation ($p = 4, 5, 6$) at Pile head i, whilst q denotes the component of the force ($q = 1, 2, 3$) or moment ($q = 4, 5, 6$) acting at Pile head j. The FRF $H_{\mathrm{hh},(pq)}^{\mathrm{c},(ij)}(\omega)$ and the static receptance $H_{\mathrm{hh},(pq)}^{\mathrm{c},(ii)}(\omega = 0)$ are also calculated using Eq. (4.9c).

In this section, the approach for modelling pile-groups presented in Section 4.1 will be used to study the influence of neighbouring piles in the calculation of dynamic interaction factors of a generic pile-group in the framework of three different pile-group systems: a 2×1 pile-group, a 2×2 pile-group and a 3×3 pile-group. The dynamic interaction factors considered for each case are: $\alpha^{(2,1)}$ for Case 1, $\alpha^{(4,3)}$ for Case 2 and $\alpha^{(6,5)}$ for Case 3, as shown in Fig. 4.10.

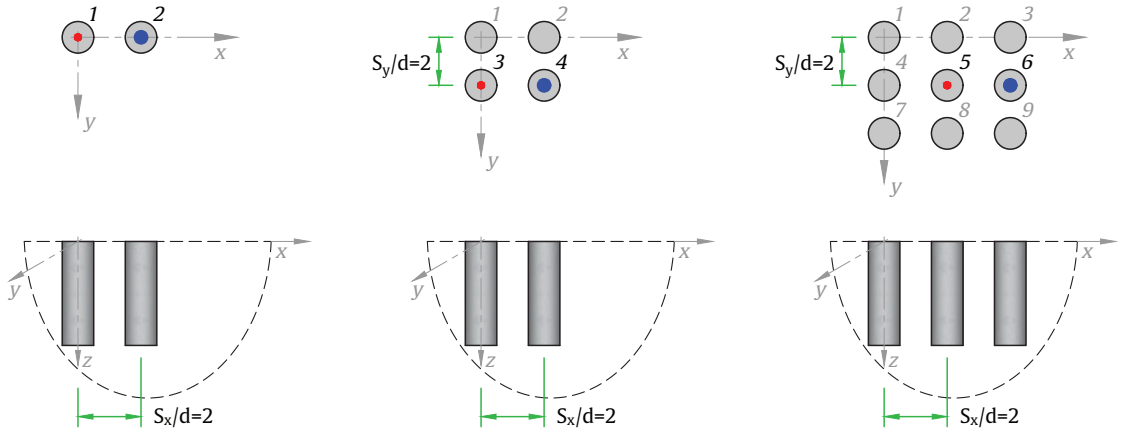

FIGURE 4.10: Pile-group systems with the same separation ratio $s/d = 2$ used for the calculation of the dynamic interaction factors. The unit harmonic loads are applied at Pile heads 1 (a), 3 (b) and 5 (c), while the responses are evaluated at Pile heads 2 (a), 4 (b) and 6 (c).

For verification purposes, the dynamic interaction factors calculated using the methodology proposed by Kaynia [3] for a 2×1 isolated pile-group, which were reproduced from [4], are also included in the comparison. Therefore, the mechanical and geometrical parameters used for the calculations presented in this section are consistent with the ones considered in [3]. In this study, the dimensionless parameters employed for the comparison are the ratio between the elastic modulus of the soil and pile $E_s/E_p = 1.0 \times 10^{-3}$ and the ratio of their densities $\rho_s/\rho_p = 0.7$. The Poisson's ratio for the soil and for the pile are $\nu_s = 0.4$ and $\nu_p = 0.25$, respectively. The hysteretic damping ratio for the soil is 0.05, whilst no damping ratio is considered for the pile. Regarding the pile-group geometry, the piles are all of diameter d and length L, with a pile aspect ratio of $L/d = 15$ and the pile spacing ratio is $s/d = 2$. The results are presented in terms of the dimensionless frequency $a_o = \omega d/C_s$. The number of collocation points employed to model all three pile-group cases is obtained by the criteria described in Section 3.2.1. Thus, in the current study, each pile is modelled using $N_p = 44$ cylindrical segments with $N_s = 44$ collocation points each.

Figs. 4.11 and 4.12 compare the dynamic interaction factors obtained using the proposed pile-group modelling approach to each one of the three pile-group cases. In general, the calculated dynamic interaction factors due to unit point loads (Fig. 4.11) and moments (Fig. 4.12) agree well at low frequencies with the ones presented in [3]. However, the results also show that the inclusion of neighbouring piles modifies the dynamic interaction factors for frequencies above 10 Hz. This effect is particularly clear, for instance, in Figs. 4.11(a) or 4.12(d) in which considerable discrepancies are observed between the 2×1 pile-group and 3×3 pile-group cases at high frequencies. These results indicate that the scattering of waves by neighbouring piles significantly influences the dynamic responses. The importance of this influence on systems with a pile spacing ratio of $s/d = 2$ is directly related to the number of neighbouring piles considered in the calculation of the dynamic interaction factors.

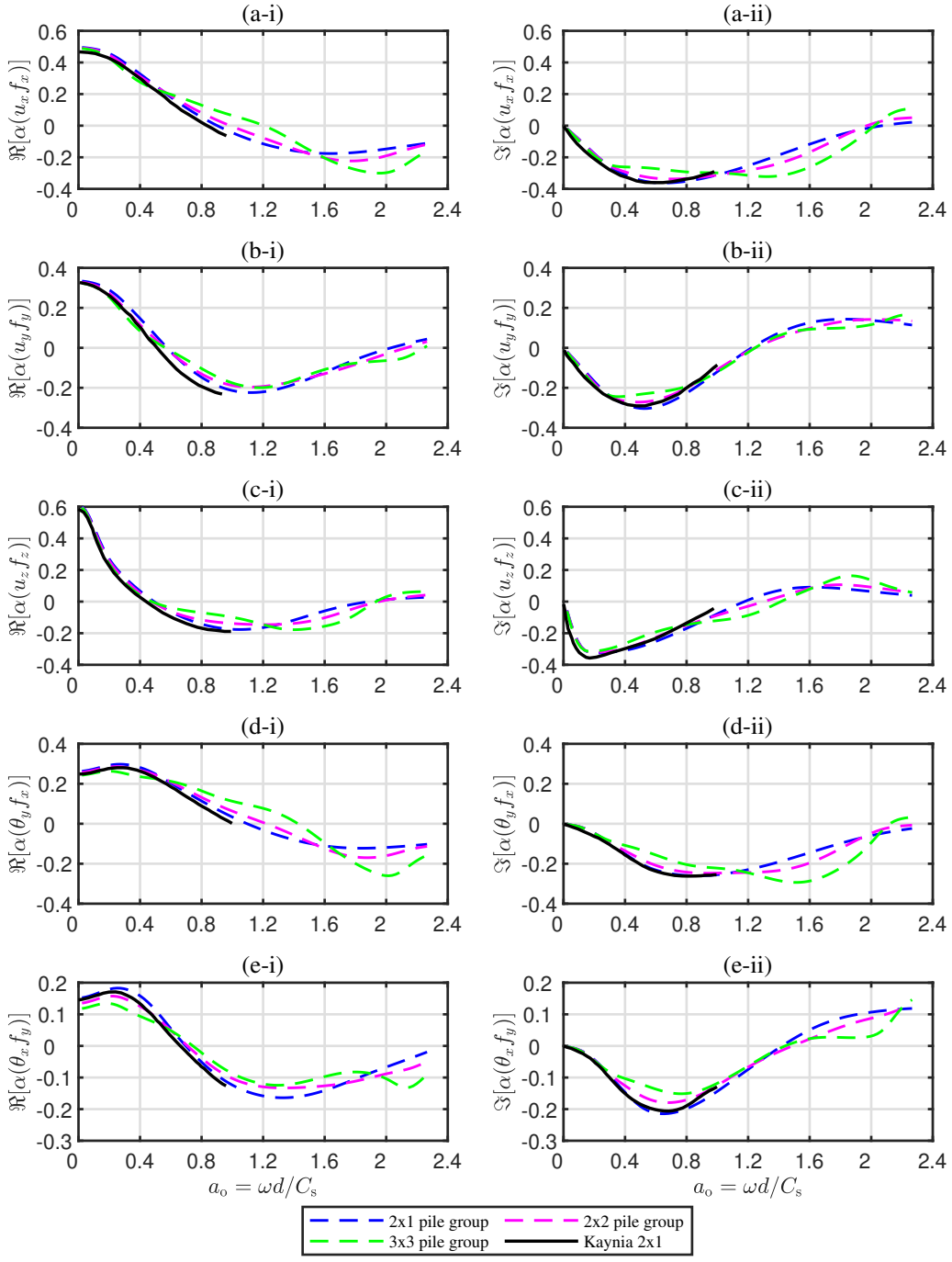

FIGURE 4.11: Comparison of the real ($\Re$) (i) and imaginary ($\Im$) (ii) parts of the dynamic interaction factor plotted against dimensionless frequency $a_o = \omega d/C_s$ for two adjacent piles in a 2×1, 2×2 and 3×3 pile-group system. Components of the dynamic interaction factor shown are $\alpha_{u_x f_x}$ (a), $\alpha_{u_y f_y}$ (b), $\alpha_{u_z f_x}$ (c), $\alpha_{\theta_y f_x}$ (d) and $\alpha_{\theta_x f_y}$ (e). The dynamic interaction factors associated with the Kaynia approach [3] were reproduced from [4].

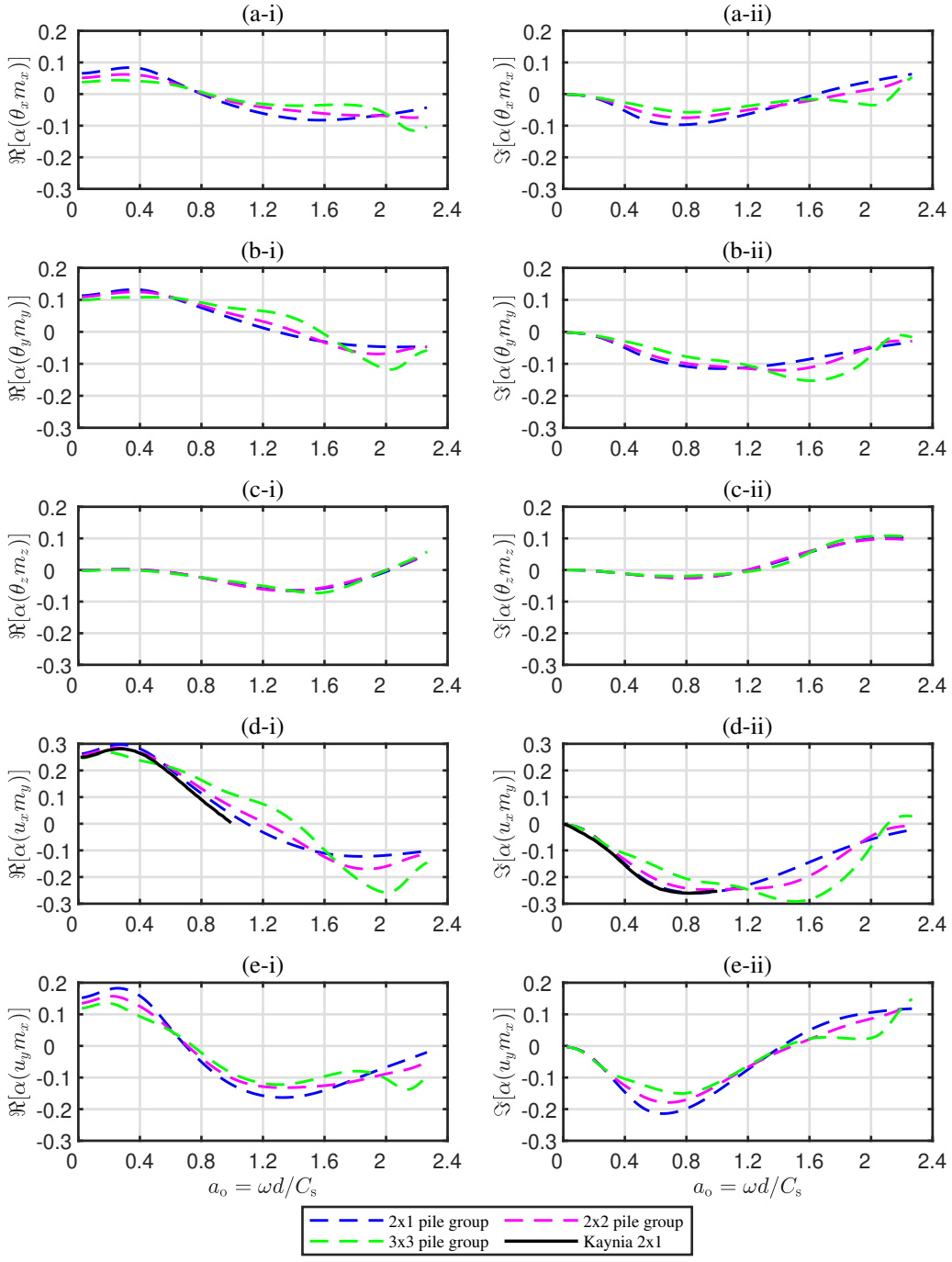

FIGURE 4.12: Comparison of the real ($\Re$) (i) and imaginary ($\Im$) (ii) parts of the dynamic interaction factor plotted against dimensionless frequency $a_o = \omega d/C_s$ for two adjacent piles in a 2×1, 2×2 and 3×3 pile-group system. Components of the dynamic interaction factor shown are $\alpha_{\theta_x m_x}$ (a), $\alpha_{\theta_y m_y}$ (b), $\alpha_{\theta_z m_z}$ (c), $\alpha_{u_x m_y}$ (d) and $\alpha_{u_y m_x}$ (e). The dynamic interaction factors associated with the Kaynia approach [3] were reproduced from [4].

The comparison between the results obtained when rotations and moments are included in the pile-soil coupling and those obtained when these effects are neglected (responses referred to as no rotational coupling (NRC) in the figures) for the three pile-group configurations considered in this section are also presented in Figs. 4.13 (point loads) and 4.14 (moments). The results are plotted in terms of the magnitude of the pile-head response in dB with 1 m/N or 1 m/N·m as references. The results are plotted up to 100 Hz, which corresponds to a dimensionless frequency $a_0 = 2.3$ for a soil system with the same mechanical properties described in Table 4.1, and piles with a pile radius of $r = 0.3$. The results show that, while the proposed approach and its simplified version predict similar responses for a 2×1 pile-group (see Figs. 4.13(i) and 4.14(i)), considerable discrepancies arise between them when a larger number of piles in the group is considered, as shown, for instance, in Figs. 4.13(iii) and 4.14(iii). However, both approaches still predict almost equal vertical responses due to vertical unit loads for all pile-group cases, as shown in Figs. 4.13(c-i), (c-ii) and (c-iii).

When the responses at Pile heads 2 (column i), 4 (column ii) and 6 (column iii) are compared, it can be noticed that differences in all components arise for excitation frequencies above 15 Hz, indicating that the scattering of waves by neighbouring piles becomes significant at higher frequencies.

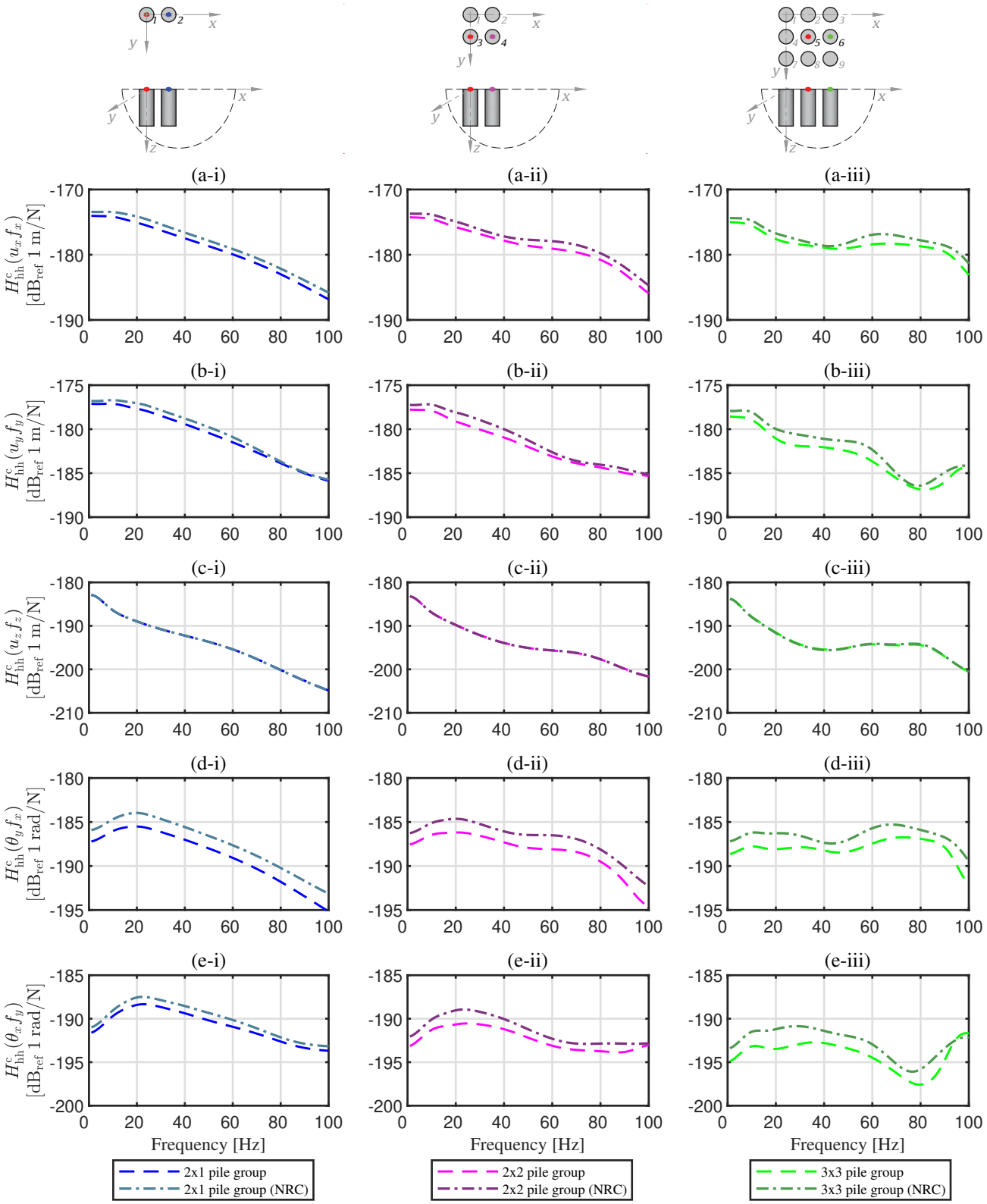

FIGURE 4.13: Comparison of the FRFs for two adjacent piles in a 2×1, 2×2 and 3×3 pile-group. External forces are applied in Pile heads 1, 3 and 5, whilst the dynamic response is evaluated, respectively, in Pile heads 2 (i), 4 (ii) and 6 (iii). Components of the FRFs matrices shown are $u_x f_x$ (a), $u_y f_y$ (b), $u_z f_x$ (c), $\theta_y f_x$ (d) and $\theta_x f_y$ (e). Results in dB using $20 \log_{10}(|H|)$, with 1 m/N as reference.

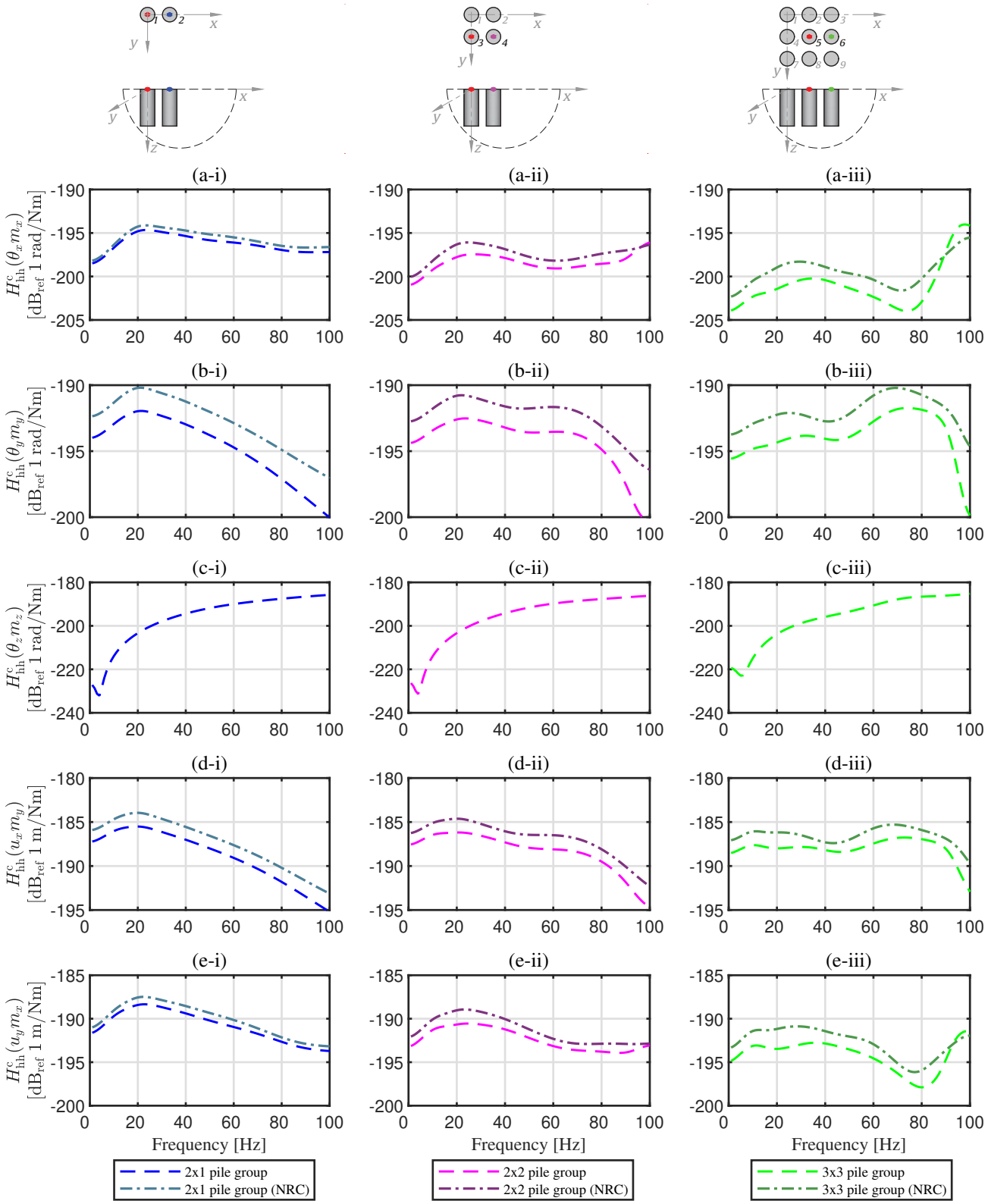

FIGURE 4.14: Comparison of the FRFs for two adjacent piles in a 2×1, 2×2 and 3×3 pile-group. External forces are applied in Pile heads 1, 3 and 5, whilst the dynamic response is evaluated, respectively, in Pile heads 2 (i), 4 (ii) and 6 (iii). Components of the FRFs matrices shown are $\theta_x m_x$ (a), $\theta_y m_y$ (b), $\theta_z m_z$ (c), $u_x m_y$ (d) and $u_y m_x$ (e). Results in dB using $20 \log_{10}(|H|)$, with 1 m/N·m as reference.

4.5 Conclusions

In this chapter, the proposed single-pile model, developed in Chapter 3, is extended to consider the dynamic response of the pile-group system embedded in half space. Furthermore, by employing the method of joining subsystems, the pile-group system is attached to a concrete block represented by 3D FEs to model a pile-cap system and study its dynamic behaviour at high frequencies. A 3D FE-BEM approach is employed for the numerical validation of the proposed piles-soil and pile-cap formulations. As in Chapter 3, the results of neglecting rotational motion and bending effects in the piles-soil coupling formulation, as well as of relaxing the torsional effects in the pile-cap coupling are also studied. The main outcomes of the studies performed in this chapter are:

- The proposed approach for modelling multi-pile foundations has been verified against a 3D FE-BE methodology in the context of a two-pile group system. The results obtained with the novel approach agree well with those obtained using the 3D FE-BE method when rotations and moments are accounted for in the piles-soil coupling. However, when these components are neglected, significant discrepancies arise between both models, as was previously observed when analysing single-pile foundations (see Chapter 3).
- The proposed approach for including pile caps in the multi-pile foundation model has also been verified against the 3D-FE method. Discrepancies between both approaches have only been observed when torsional effects have been neglected in the pile-cap coupling procedure, resulting in considerable discrepancies at high frequencies (above 30 Hz). This result is consistent with the previous work presented in [164], which states that the error introduced by ignoring the twisting reaction of the piles in a group is usually small at low frequencies.

The proposed methodology has also been employed to study the influence of neighbouring piles in the calculation of the dynamic interaction factor of two adjacent piles in 2×1, 2×2 and 3×3 pile-group scenarios, concluding that

- The dynamic interaction factors obtained for the three pile-group scenarios are very similar/almost equal at low frequencies (>10 Hz in the considered example). However, discrepancies due to the wave scattering of neighbouring piles arise when higher excitation frequencies are considered. Results showed that these discrepancies are more significant when considering higher excitation frequencies and/or larger pile-group systems.

- Inaccurate dynamic interaction factors (and, therefore, the response to point loads and moments) are obtained when the rotational motions and bending effects are neglected in the pile-soil coupling conditions. The results show that almost all components of the responses present discrepancies due to the assumption adopted in the piles-soil coupling, with the exception of the vertical responses due to vertical point loads.

Chapter 5

Experimental validation of the pile foundation model

This chapter presents an experimental measurement campaign that serves to validate the simulation approach presented in this dissertation in the framework of two scenarios: a single-pile and a 2×2 pile-group systems. To do so, an experimental site was constructed consisting of concrete casted-in-situ piles in a particular testing field dedicated to experimental studies regarding railway-induced vibration phenomenology. The existing soil was previously characterised by means of multichannel analysis of surface waves (MASW) and cross-hole testings, as well as laboratory analysis. For both single-pile and pile-group systems, employed measurement setups are based on several accelerometers distributed in the ground surface and the pile heads, while the system is excited using instrumented hammer impacts on the pile head as well as the ground surface. Comparisons between experimental and theoretical results confirm the validity of the approach proposed predicting the response of pile-soil systems in the vertical direction.

5.1 Description of the experimental test site

5.1.1 Location description

The experimental campaign developed to validate the approach proposed in this dissertation has been conducted at the testing facilities for experimental studies on railway-induced ground-borne noise and vibration of the Acoustical and Mechanical Engineering Laboratory (LEAM) of the Universitat Politècnica de Catalunya (UPC). The facilities are placed at the Institut Politècnic del Campus de Terrassa (IPCT), located 30 km northeast of Barcelona city and on the outskirts of Terrassa city town (carretera N-150 km 14.5 08227 Terrassa, Barcelona). The site where concrete cast-in-situ piles were installed is a field ground mainly composed of soft clays. Moreover, it is important to mention that the site is at a fairly remote location, with low exposure levels to environmental background vibration that make the site ideal for the planned studies. Fig. 5.1 presents the location of the mentioned testing facilities and distribution of piled foundation systems used for the study. Finally, from that figure, note that the locations of the piled foundation systems were selected to be far from other structures existing on the IPCT to avoid any dynamic interaction with the piles.

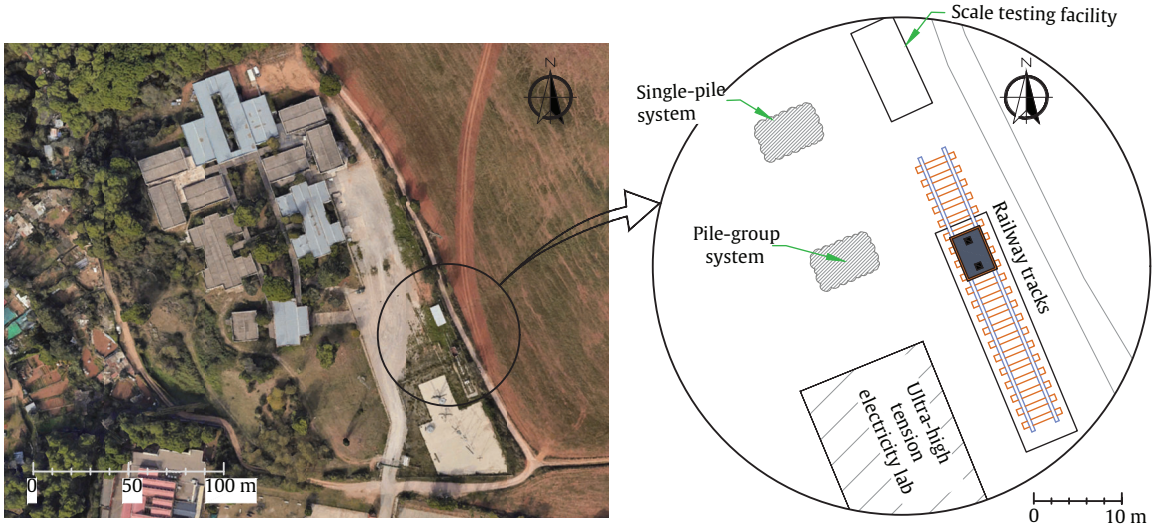

(a) IPCT facilites (UPC, Terrassa campus) (b) Railway-induced vibration test facilities

FIGURE 5.1: Overview of the site by an aerial photograph of the IPCT area (a) and a drawing of the facilities for railway-induced ground-borne vibration testing (b).

5.1.2 Soil condition

The soil composition has been obtained by conducting a geotechnical site investigation consisting of a MASW, cross-hole tests and laboratory analysis of undisturbed soil samples (ground retrieved with minimal disturbance to its structure, density, water contains and stress state) collected from the drilled boreholes. Cross-hole tests were conducted according to the standard ASTM D 4428/D 4428M–00 [167]. The survey consisted of two drilled boreholes of 30 m depth referred to as S_1 and S_2 and located between the measured lines used for the MASW tests, as shown in Fig. 5.2(a). By releasing energy from the first source at S_1 to the soil, the train of the seismic waves is recorded by a transducer located at the receiver S_2, as shown in Fig.5.2(b). This procedure has been repeated at different probe depths, with a spacing of 1 meter between each one, to determine the speed of the horizontally travelling P- and S-waves, resulting in obtaining at different depths the shear modulus, Young's modulus and Poisson's ratio of the soil. The soil density at different depths has been obtained by laboratory analysis of the undisturbed soil samples, as shown in Fig. 5.2(d), that were retrieved from the drilled boreholes used for the cross-hole test. Additionally, the MASW test was performed along three measurement lines, referred to as L_1, L_2 and L_3, distributed as shown in Figs. 5.2(a) and (c) and based on geophones spaced at intervals of 5 meters to record the particle vibration velocity, in the vertical direction, induced by Rayleigh-type surface waves. To produce the surface waves, a 5 kg weight sledgehammer has been used as an external source. The excitation point of the sledgehammer was selected to be located 10 m away from the first geophone for each measurement line. From the MASW test, S-wave speed profiles are estimated, and results showed that all soil conditions just below the three measured lines consist of dense or medium-dense sand, gravel or stiff clay. This first layer corresponds to a ground with a S-wave speed between 200-400 m/s. The thickness of this first layer varies according to the measured line location, being 6, 10 and 14 m of thickness associated with the measured lines L_3, L_2 and L_1, respectively. A second soil layer of 30 m depth for measured lines L_2 and L_3 and of 18 m depth for the L_1 were identified and consisted of very dense sand, gravel or very stiff clay with a S-wave speed between 400-750 m/s. Rock or other rock-like geological formations with an S-wave speed exceeding 750 m/s appear after the second layer in all measurement lines. The P-wave speeds obtained from both MASW and cross-hole tests have been found to be in agreement. Results are synthesised in Table 5.1.

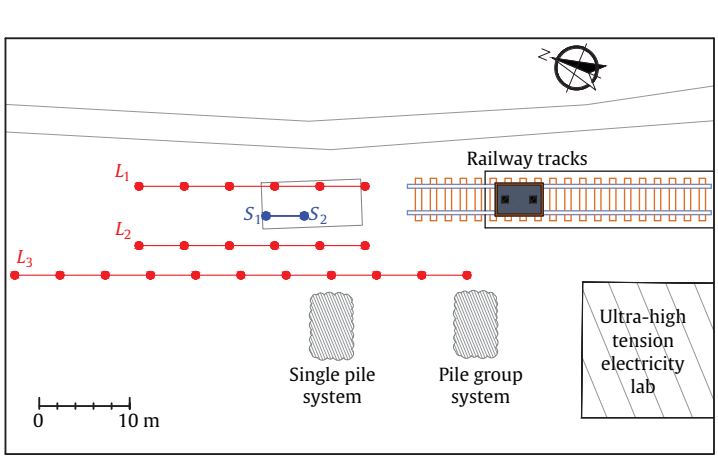

(a) Location of the measurements lines (L) for the MASW test and points (S) selected for the cross-hole test

(b) Equipments for the cross-hole test.

(c) Measurement line L_3 for the MASW test

(d) Undisturbed soil samples retrieved from the drilled boreholes S_1

FIGURE 5.2: Measurement setup for the MASW and cross-hole tests (a-c). Soil samples obtained from borehole drilling (d).

5.1.3 Pile systems design and installation

The experimental setup was designed to accommodate two cast-in-place piled foundations, including a single piled foundation and a 2×2 pile-group system. The borehole drilling was conducted in December 2020 and cast with concrete to create piles of 10 cm radius and total length of 5.5 m, from which only a length of 5.3 m is embedded in the soil, as shown in Fig. 5.3(a). This free 20 cm of the piles was adopted to facilitate future experimental studies in which lateral excitations would be applied, or other structural systems, such as concrete pile caps, could be incorporated. The spacing between the piles for the pile-group system is 1 m horizontally and $1,5$ m vertically, as shown in Fig. 5.3(b). Moreover, the single-pile is located long enough from the pile-group system (around 18 m away) to avoid any dynamic interaction between the two systems.

Depth	C_s	C_p	ν	ρ	G	E	Ground
(m)	(m/s)	(m/s)	(-)	(kg/m^3)	(GPa)	(GPa)	type
1	180	532	0.44	2260	0.07	0.21	Dense or medium-dense sand, gravel or stiff clay
2	241	721	0.44	2260	0.13	0.38	
3	303	809	0.42	2260	0.21	0.59	
4	371	933	0.41	2260	0.31	0.88	
5	419	1038	0.40	2260	0.40	1.11	
6	452	1133	0.41	2260	0.46	1.30	Very dense sand, gravel or very stiff clay
7	494	1308	0.42	2130	0.52	1.47	
8	537	1480	0.42	2130	0.61	1.75	
9	547	1672	0.44	2130	0.64	1.84	
10	602	1899	0.44	2130	0.77	2.23	
11	637	1966	0.44	2080	0.84	2.43	
12	603	1925	0.45	2080	0.76	2.18	
13	530	1818	0.45	2080	0.58	1.70	
14	467	1714	0.46	2080	0.45	1.33	
15	442	1740	0.47	2080	0.41	1.19	
16	470	1796	0.46	2080	0.46	1.35	
17	526	1920	0.46	2080	0.58	1.68	
18	558	2040	0.46	2080	0.65	1.89	
19	599	2075	0.45	2080	0.75	2.17	
20	619	2138	0.45	2080	0.80	2.32	
21	644	2142	0.45	2080	0.86	2.51	
22	720	2128	0.44	2080	1.08	3.09	
23	757	2135	0.43	2080	1.19	3.40	Rock or other rock-like geological formations
24	748	2096	0.43	2080	1.16	3.32	
25	755	2055	0.42	2080	1.19	3.37	
26	770	2074	0.42	2080	1.23	3.51	
27	785	2119	0.42	2080	1.28	3.64	
28	783	2109	0.42	2080	1.27	3.62	
Inf	779	2086	0.42	2080	1.26	3.58	

TABLE 5.1: Experimentally estimated soil properties.

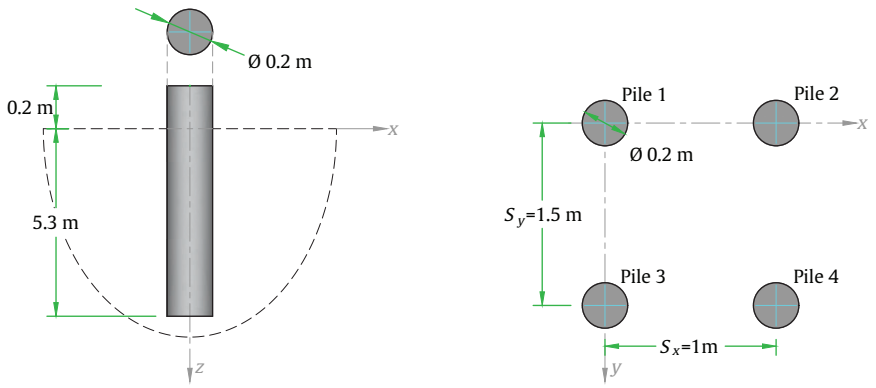

(a) Pile dimensions (b) Top view of the pile group system

FIGURE 5.3: Geometrical definition of the piled foundations systems constructed for the validation of the proposed simulation approach.

5.2 Experimental setups and testing procedures

The experimental investigations were conducted using two measurement setups for which hammer impacts at the pile heads and the surrounding ground were employed to determine experimentally the receptances of the system. The impact hammer used in both experimental campaigns is a PCB Piezotronics 086D50 with a hammer mass of 5.5 kg. Both setups are based on a set of accelerometers PCB 393B12 and PCB 393B31 placed on the piles and on the ground surface, as shown in Fig 5.4. The accelerometers and instrumented hammer are connected to the 24-channel data acquisition system LMS SCADAS.

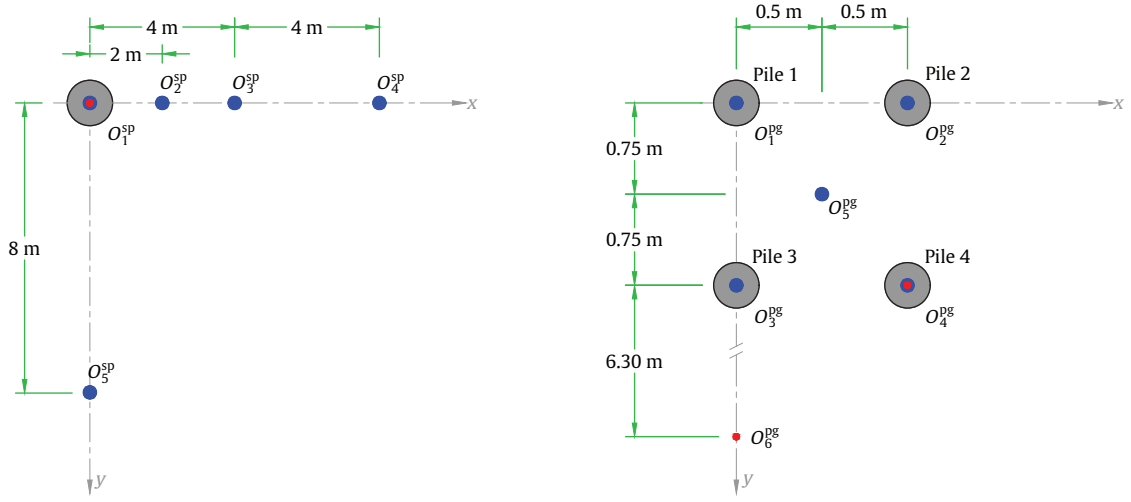

FIGURE 5.4: Experimental setup for the single-pile case (a) and for the pile-group system (b). The locations of the accelerometers are denoted by blue dots, while the application of hammer the hammer excitation is marked with red ones.

The first phase of the measurement campaign took place in August 2021, nine months after the installation of the piles. This timing was chosen to ensure sufficient soil consolidation, mitigating the impact of the weak boundary zone resulting from the borehole drilling [141]. In this first setup, only the single-pile foundation is considered. Fig. 5.4(a) and Fig. 5.5 show various illustrations of the measurement setup adopted. Since only vertical responses of the system are intended to be obtained, accelerometers are all directed to the vertical direction and the hammer impacts are only applied in the vertical direction. Acceleration levels were measured by accelerometers placed at the following points: O_1^{sp}, O_2^{sp}, O_3^{sp}, O_4^{sp} and O_5^{sp} located at the positions 5.4(a), being the first one placed at the pile head to retrieve the driving-point response of the pile, while the other four are distributed on the ground surface. Points O_4^{sp}

and O_5^{sp} are specifically employed to account for the variability of the ground composition in different horizontal directions.

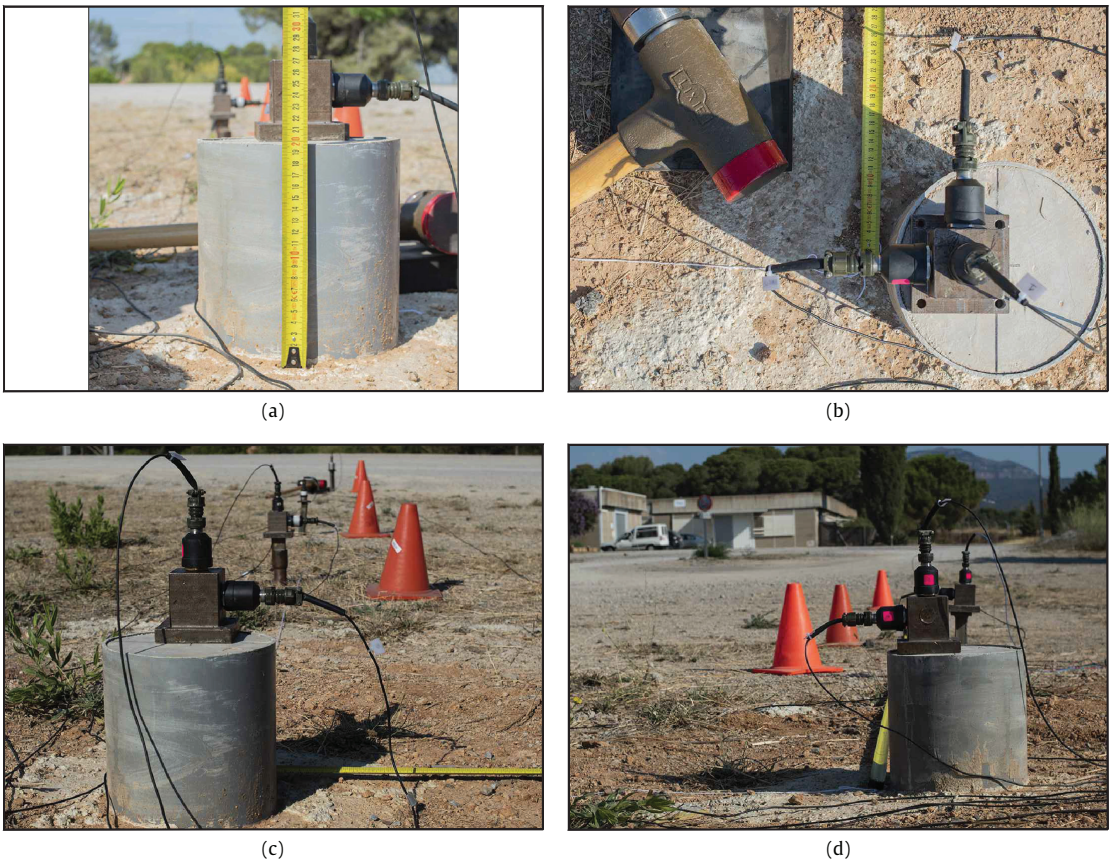

FIGURE 5.5: Single-pile setup. Measurement equipment: (a) accelerometers placed on the pile head, (b) impact hammer and accelerometers distribution along (c) the x- and (d) y-directions with respect to the single-pile system local coordinates.

The second test was conducted in October 2021, and it aimed to study the pile-group system and, especially, the dynamic interaction between piles. Again, hammer impacts in the vertical direction were used to excite the system. Two different dynamic loading schemes were considered in this case. In the first one, the excitation is applied at the pile head of Pile 4, as depicted in Fig. 5.4(b), while in the other one, the excitation is applied on the ground surface, at the point O_6^{pg}. For both loading scenarios, the response is evaluated at points O_1^{pg}, O_2^{pg}, O_3^{pg}, O_4^{pg} and O_5^{pg} located at $(0, 0, -0.2)$ m, $(1, 0, -0.2)$ m, $(0, 1.5, -0.2)$ m, $(1, 1.5, -0.2)$ m and $(0.5, 0.75, 0)$ m, respectively; the first four ones correspond to accelerometers located at the pile head of Piles 1, 2, 3 and 4, respectively, and the remaining one lies on the free field, in central point of the pile-group system. Note that the response at the accelerometer placed

in Pile 4 was discarded in the first dynamic loading scenario because the recorded signals were saturated due to the proximity of that accelerometer to the impact loads. The first loading scenario aimed to study the dynamic interaction between the piles and the radiation pattern of a pile-group system. The second one, instead, was adopted to analyse the response of a pile group to an incident wave field, as well as the scattering of waves through this system. Fig. 5.6 illustrates the setup employed in the second test.

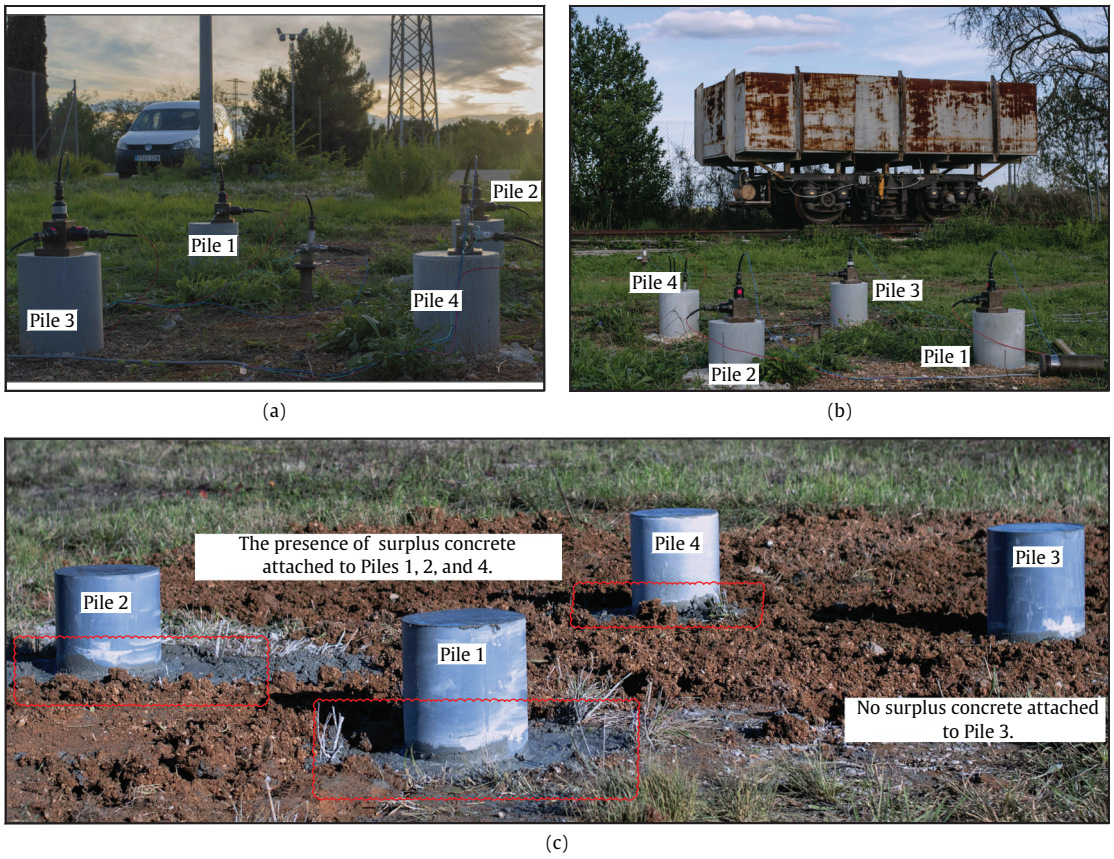

FIGURE 5.6: Experimental setup for the pile-group system shown in (a) and (b). The presence of surplus concrete specimens attached to Piles 1,2 and 4 are depicted in (c).

For all described test setups, various measurements were conducted to ensure the correctness of the results obtained. For each measurement, 50 impacts of the instrumented hammer are carried out. This procedure is adopted to ensure that the output FRFs are not highly affected by background noise. To post-process the gathered data, all recorded signals from each measurement are initially divided into 50 blocks of the same length (specifically, a block size of 2^{11} samples is adopted). Each block contains the acceleration and force time histories corresponding to one hammer impact. Welch's method [168] is then employed to determine the FRFs of the system, which will be compared in Section 5.4 with the numerical model results, aiming to

validate the approach proposed in this dissertation. Coherence functions have also been calculated to demonstrate the correctness of the FRF estimations within the frequency range of interest. The coherence function is a measure that statistically validates the frequency content of estimated transfer functions, where a zero value denotes no causal relationship between the input and output, and a value of 1 indicates the existence of a linear noise-free relation between the input and the output [140].

Finally, it is worth mentioning that although each measured point in both loading schemes was implemented with three accelerometers to record the dynamic responses in the three directions of the local Cartesian coordinate, as shown in Figs. 5.5 and 5.6, only vertical responses are presented in this study because of the complexity of applying horizontal inertial excitations at the pile head due to its cylindrical surface.

5.3 Numerical model

A numerical model of the two piled foundation systems of the experimental site has been constructed employing the approach proposed in Chapters 3 and 4. Thus, both assumptions of the proposed model, namely the hypotheses of low strains and the absence of relative motion between the pile and the soil, are also adopted here. From the data gathered in the construction process of the experimental site, the concrete piles are supposed to have a density of 2860 kg/m^3, modulus of elasticity of 40 GPa and a Poisson's ratio of 0.25. The soil is modelled as a homogeneous, horizontally layered elastic media with mechanical properties similar to as obtained from the soil characterisation and outlined in Table 5.1. The soil is modelled as a homogeneous, horizontally layered elastic media with mechanical properties similar to as obtained from the soil characterisation and outlined in Table 5.1. Due to the lack of experimental evidence about soil damping, all numerical results have been computed using assumed soil damping values ranging from those associated with soft soils (0.03) to hard soils (0.07). The analysis is performed for frequencies between 1 Hz and 100 Hz, covering the frequency range where ground-borne vibration induced by railway traffic is usually significant [153].

Regarding the details of the numerical computation, both numerical models were constructed by adopting the criteria described in Section 3.2.1 that suggests the number of cylindrical segments and collocation points required to represent each pile foundation system accurately. In this context, and employing 10 collocation points per wavelength in the longitudinal direction of the pile, each pile is modelled by $N_p = 30$ cylindrical segments with $N_s = 16$ collocation

points each. Furthermore, the corresponding Green's functions for a layered half-space required for computing the FRFs of the system using the proposed approach are calculated with the EDT toolbox [154].

5.4 Comparison of results

In this section, the experimentally obtained FRFs are compared to the results delivered by the proposed numerical model on the basis of the parameters described in previous sections. It is worth mentioning that the results shown correspond to the vertical frequency response function of the system due to dynamic loads exciting the system also in the vertical direction. Results are presented in terms of the magnitude (in dB with 1 m/N as references) and phase of the pile head and free-field FRFs. For the experimental data, two different measurements denoted by T_1 and T_2 are presented. Results of the numerical model are presented for soil damping values ranging from 0.03 to 0.07, while results for a damping of 0.05 are especially highlighted.

5.4.1 Response of the single-pile system

This section presents the results associated with the single-pile system. Fig. 5.7 presents the experimentally and numerically obtained direct FRFs at the pile head. On the one hand, experimental results show high coherence values above 20 Hz, ensuring its correctness above this frequency. On the other hand, numerical results are found to be not affected by the soil damping at all. In this context, it can be said that experimental and numerical results agree well since discrepancies between them only reach 1.5 dB at 80 Hz, as shown in Fig. 5.7(i). Although the proposed numerical approach tends to overestimate the predicted vibration levels slightly, it can be stated that the proposed pile-soil model developed in the current dissertation can accurately predict vertical driving point responses. Moreover, the phase of the resulting experimental and the numerical FRFs also agree quite accurately. The phase of the numerical result tends to zero at low frequencies due to the similarity to the static case, while this tendency cannot be observed in the experimental results because of the poor estimation of the FRFs below 20 Hz pointed out by the coherence results. Low coherence values at low frequencies can be explained by the fact that the hammer impact excitation does not have significant energy content at this frequency range, a problem that is encountered all along the

present study. However, the main focus of this dissertation lies upon the proper evaluation of the response of piled foundation at high frequencies, a frequency range generally excited by the employed hammer [140].

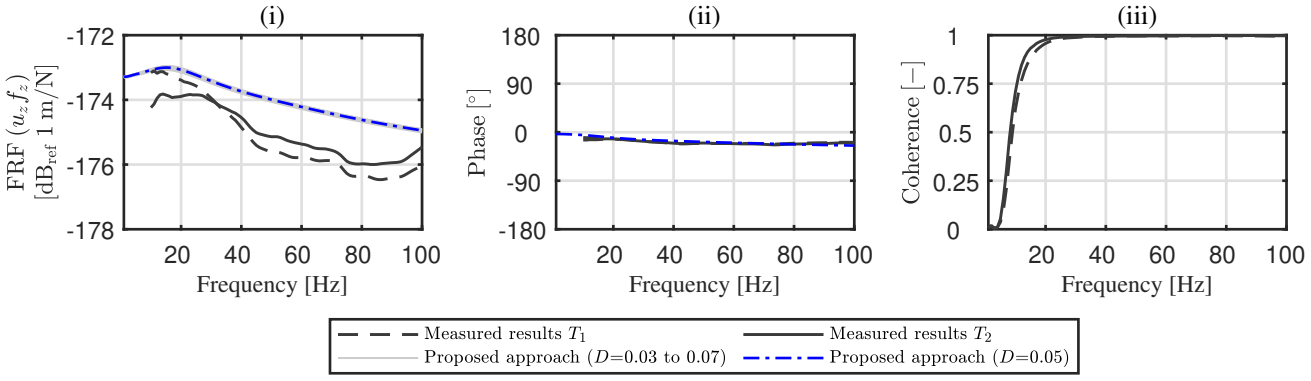

FIGURE 5.7: Comparison of experimentally and numerically predicted driving-point receptances of the single-pile system. Vertical external forces are applied at the pile head, whilst the dynamic response is also evaluated at the pile head. The magnitude of the responses (i) and their phases (ii) are presented for the vertical direction, as well as the coherence function (iii) of the measured results. Only the phase associated with FRF of the numerical model solution with soil damping $D = 0.05$ is plotted. FRF results are displayed in dB using $20\log_{10}(|H|)$, with 1 m/N as reference.

The results obtained for the free-field responses at the four evaluation points O_2^{sp}, O_3^{sp}, O_4^{sp} and O_5^{sp} are depicted in Fig. 5.8. In general, the experimental vertical FRFs are very similar to the ones numerically predicted. As expected, in contrast with the pile head FRF, the free-field response is much more sensitive to the variation of soil damping values at high frequencies and when the distance between the evaluation and source points is large. It is worth mentioning that, above 30 Hz, the measured FRFs are contained in the envelope of the predicted ones, which were calculated using the previously stated range of soil damping values $(0.03 - 0.07)$. The soil damping value of 0.05 can be adopted as a good approximation to represent the real soil damping since their corresponding FRFs are very similar to the experimentally determined receptances.

Theoretically speaking, a single circular pile foundation system embedded in a horizontally layered elastic half-space is a fully axisymmetric system. This could not be true in real cases if the heterogeneity of the ground horizontal directions is strong. Thus, a notable observation arises when comparing the experimental free-field responses at points $O_4^{sp} = (8, 0, 0)$ m and $O_5^{sp} = (0, 8, 0)$ m. In contrast to the predicted results, which depict the same vibration levels

in those cases, the experimental results indicate that the soil is actually slightly heterogeneous horizontally speaking, since both exhibit variations along the frequency range of interest. Although too much effort was invested in determining the mechanical properties of the soil underneath, those discrepancies in the experimental results were expected, to some extent, since the soil, in the real world, is a complex heterogeneous medium, and their properties not only vary with depth but also in other directions. In contrast to the phase of the pile head response, which varies smoothly with frequency and possesses values near zero, the phases associated with the free-field responses show the influence of the damping of the soil since the phase curves denote complex values of the FRFs.

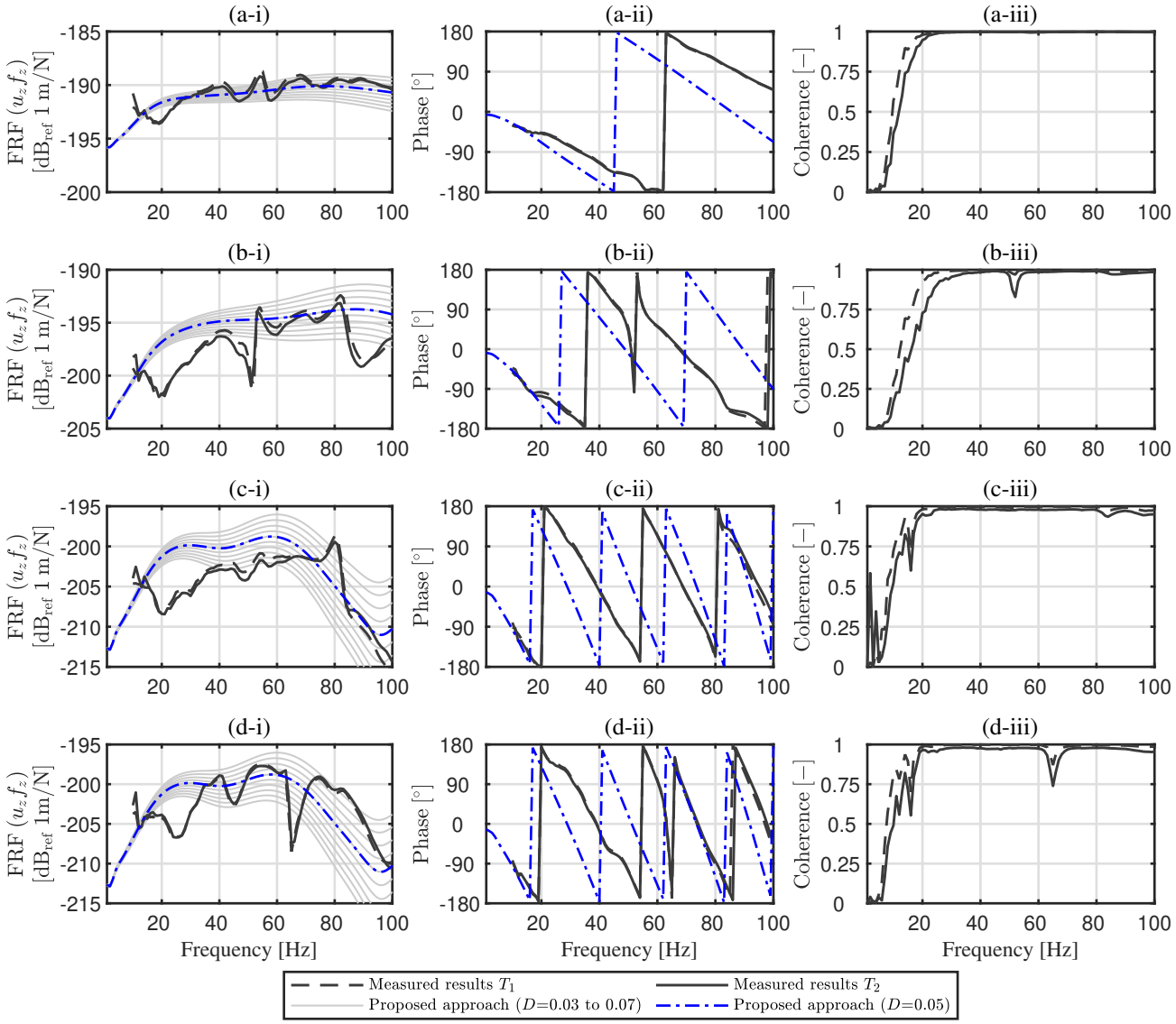

FIGURE 5.8: Comparison of experimentally and numerically predicted driving-point receptances of the single-pile system. Vertical external forces are applied at the pile head, whilst the dynamic responses are evaluated in the field at points O_2^{sp} (a), O_3^{sp} (b), O_4^{sp} (c) and O_5^{sp} (d). The magnitude of the responses (i) and their phases (ii) are presented for the vertical direction, as well as the coherence function (iii) of the measured results. Only the phase associated with FRF of the numerical model solution with soil damping $D = 0.05$ is plotted.

FRF results are displayed in dB using $20\log_{10}(|H|)$, with 1 m/N as reference.

5.4.2 Response of the pile-group system

The comparison of experimentally and numerically predicted receptances of the 2×2 pile-group system in its first loading configuration is presented in Figs. 5.9 and 5.10, which plot

the receptances associated with the pile-soil-pile interaction and the free-field responses, respectively. When comparing the PSPI results, it is shown that reasonable agreement of the FRFs for the one associated with Pile 3 for which discrepancies between the experimentally and the numerically predicted FRFs reach up to 2 dB over the frequency range of interest. On the contrary, although the numerical model predicts similar levels of FRFs for Piles 1 and 2, those predicted receptances are slightly overestimated, mostly at high frequencies, with the worst scenario being the one associated with Pile 2, for which the discrepancies reach up to 12 dB at 100 Hz with respect to the measured ones. Although this behaviour can be explained by the fact that the soil properties have not been well characterised along the exact local area where the pile-group has been installed, this assumption ceases to be valid since the predicted FRF values on the ground at the point O_5^{pg} reasonable agree well with respect the measured results, except for the frequency range of 62-80 Hz in which the coherence function considerably decay up to unreliable experimental data. Then, the discrepancies found for the FRFs associated with Piles 1 and 2 do not come from a wrongly experimental soil characterisation. However, a visual inspection of the pile-group system area reveals the existence of surplus concrete attached to the piles, as shown in Fig. 5.6(c). These leftovers of concrete result from the concrete poured on the ground on the concrete-casted day, and they can be pointed out as the cause of the discrepancies in the comparison of results. From that visual inspection, it can be highlighted that the largest amount of surplus concrete appears to be attached to Piles 1 and 2, which are also associated with significant discrepancies at high frequencies between the predicted and measured results. Similarly, it is noticed that the presence of surplus concrete in Pile 3 represents a small amount of spread concrete attached to its interface. This is the reason why the results associated with the Pile 3 are more in agreement with the numerical ones. A further observation of these results is the low influence of the different soil damping range values on the results presented, as plotted in Figs. 5.9(i) and 5.10(i), which was expected due to the proximity of the evaluation points with respect to the excitation.

Finally, results for the second loading case in which the excitation is applied to the ground surface are presented in Figs. 5.11 and 5.12. In general, the numerical model predicts reasonably similar vibration levels with respect to the measured ones at frequencies below 70 Hz. As discussed in the first loading case, the numerical model tends to overestimate the system's dynamic response for frequencies above 70 Hz, in which discrepancies between them can reach up to 12 dB at high frequencies. The disagreements found can be explained by the surplus concrete attached to the piles. Additionally, it is worth mentioning that the FRF associated with Piles 2 and 4, as well as the FRF on the ground at the point O_6^{pg}, present unstable values

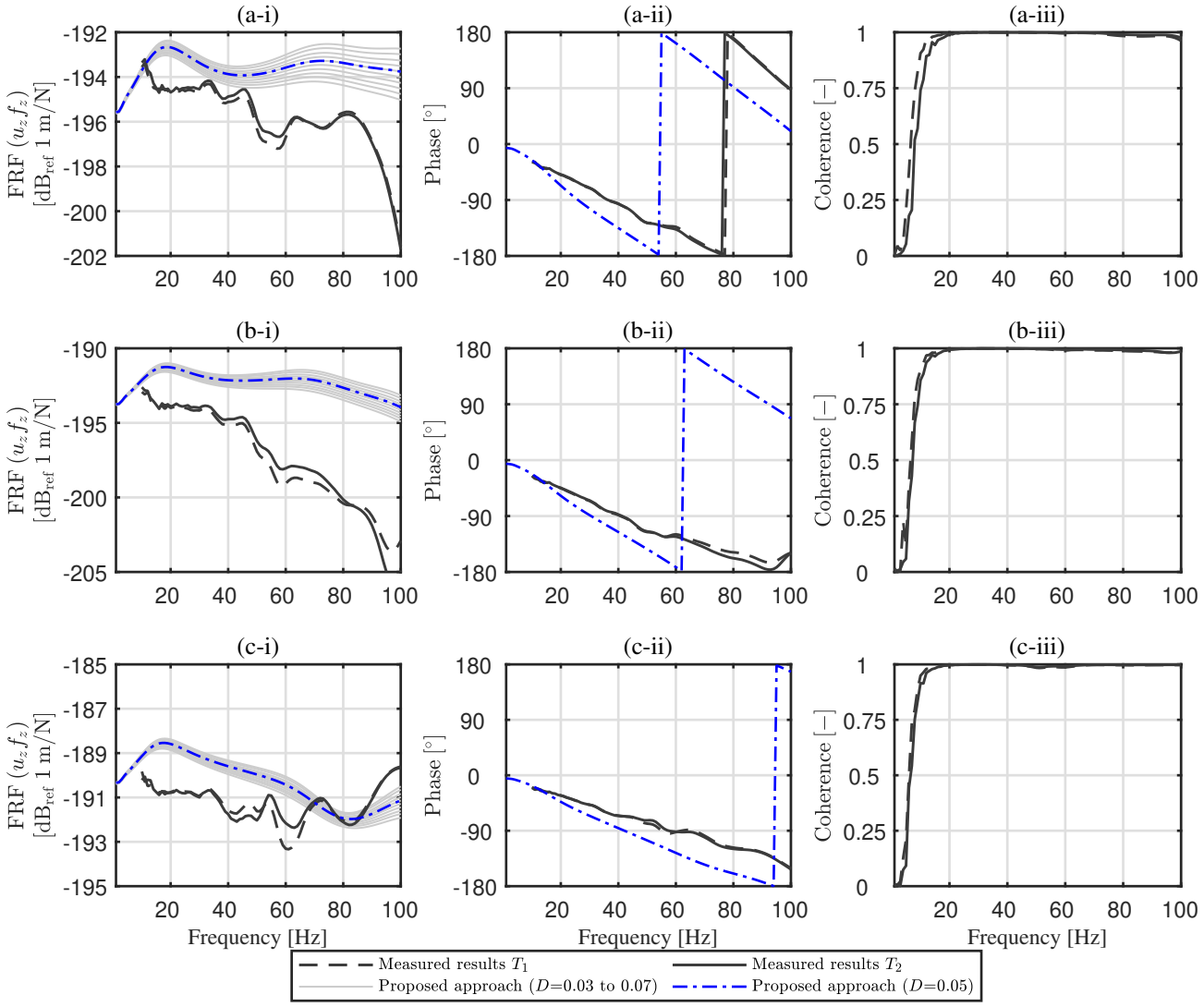

FIGURE 5.9: Comparison of experimentally and numerically predicted receptances of the 2×2 pile-group system. Vertical external forces are applied at Pile head 4, whilst the dynamic responses are evaluated at Pile heads 1 (a), 2 (b) and 3 (c). The magnitude of the responses (i) and their phases (ii) are presented for the vertical direction, as well as the coherence function (iii) of the measured results. Only the phase associated with FRF of the numerical model solution with soil damping $D = 0.05$ is plotted. FRF results are displayed in dB using $20\log_{10}(|H|)$, with 1 m/N as reference.

for the coherence function that could affect the correctness of the obtained FRF.responses.

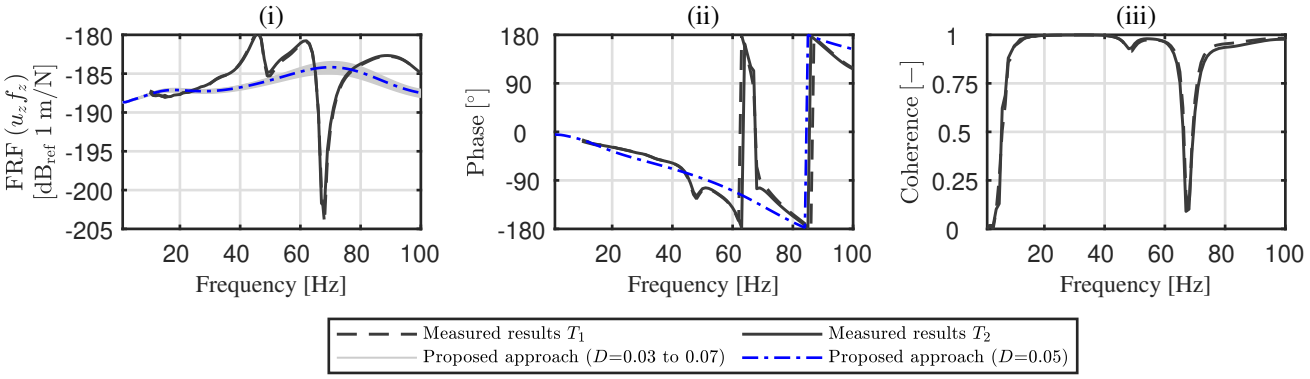

FIGURE 5.10: Comparison of experimentally and numerically predicted receptances of the 2×2 pile-group system. Vertical external forces are applied at Pile head 4, whilst the dynamic responses are evaluated on the field at the point O_5^{pg}. The magnitude of the responses (i) and their phases (ii) are presented for the vertical direction, as well as the coherence function (iii) of the measured results. Only the phase associated with FRF of the numerical model solution with soil damping $D = 0.05$ is plotted. FRF results are displayed in dB using $20 \log_{10}(|H|)$, with 1 m/N as reference.

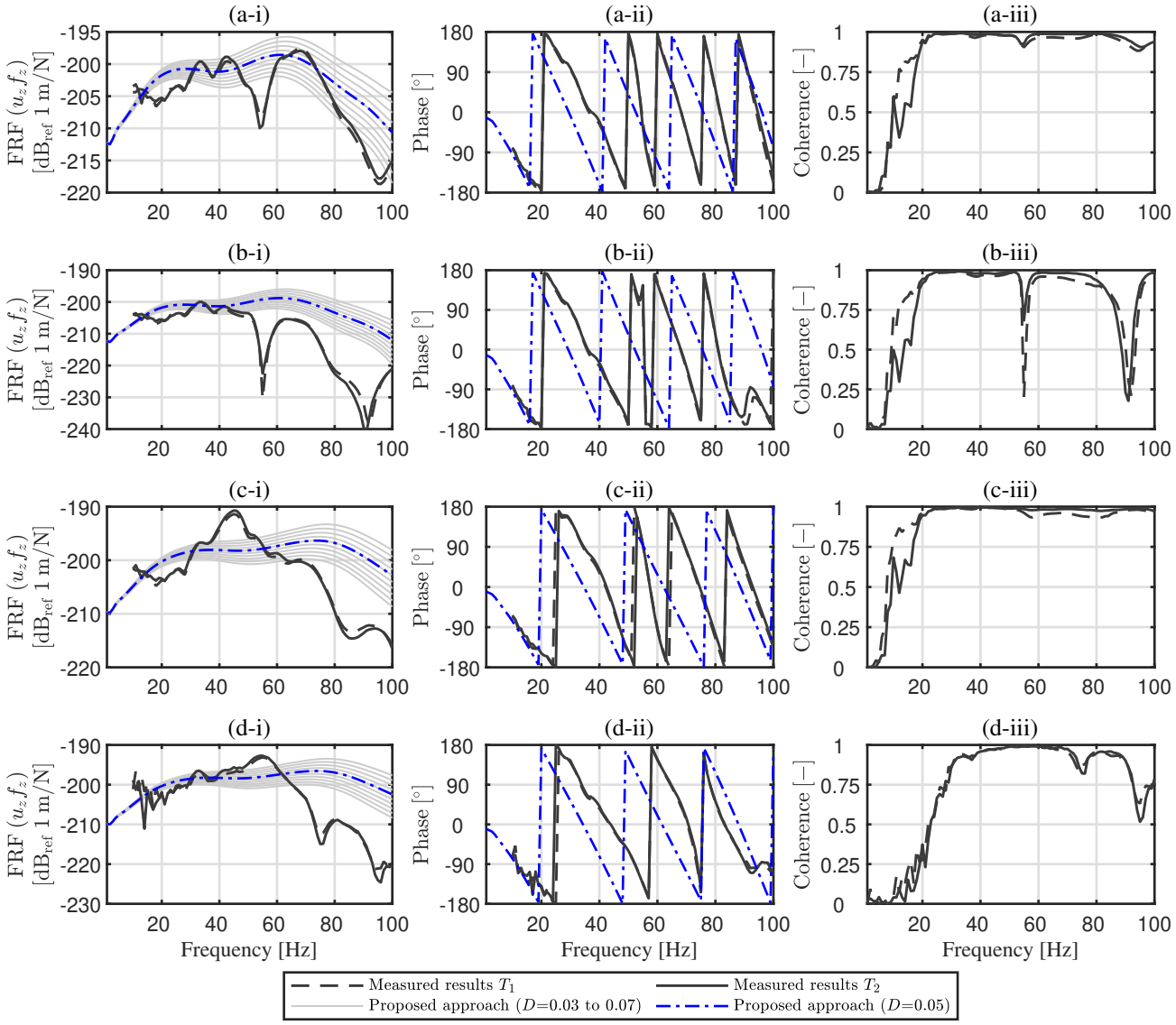

FIGURE 5.11: Comparison of experimentally and numerically predicted receptances of the 2×2 pile-group system. Vertical external forces are applied on the field at the point O_6^{pg}, whilst the dynamic responses are evaluated at the Pile heads 1 (a), 2 (b), 3 (c) and 4 (d). The magnitude of the responses (i) and their phases (ii) are presented for the vertical direction, as well as the coherence function (iii) of the measured results. Only the phase associated with FRF of the numerical model solution with soil damping $D = 0.05$ is plotted. FRF results are displayed in dB using $20 \log_{10}(|H|)$, with 1 m/N as reference.

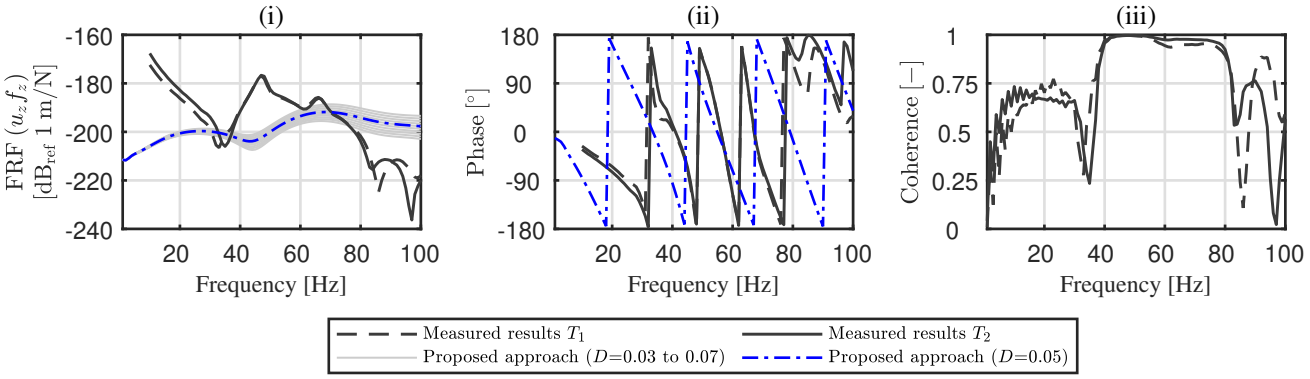

FIGURE 5.12: Comparison of experimentally and numerically predicted receptances of the 2×2 pile-group system. Vertical external forces are applied on the field at the point O_6^{pg}, whilst the dynamic responses are evaluated on the field at the point O_5^{pg}. The magnitude of the responses (i) and their phases (ii) are presented for the vertical direction, as well as the coherence function (iii) of the measured results. Only the phase associated with FRF of the numerical model solution with soil damping $D = 0.05$ is plotted. FRF results are displayed in dB using $20 \log_{10}(|H|)$, with 1 m/N as reference.

5.5 Conclusions

This chapter presents a comparison of experimentally and numerically predicted FRF of a single-pile and 2×2 pile-group. The full-scale cast-in-situ piles were installed in layered soil, which has been characterised by means of the MASW and cross-hole tests and laboratory analysis of undisturbed soil samples. The experimental results were obtained in two experimental campaigns. The first one corresponds to the experimental campaign for the single-pile system, which is subjected to inertial excitation, whilst the second campaign evaluates the dynamic response of the 2×2 pile-group system under inertial excitation and indecent wave fields due to vertical hammer impacts on the ground. The measured results, in terms of magnitude and phase, are compared with the ones numerically predicted by the proposed methodology. Furthermore, because the hysteretic soil damping has not been experimentally characterised, a range of assumed soil damping values associated with soft soils (0.03) to hard soils (0.07) was employed in the numerical model to evaluate the sensitivity of the FRF to those values. Thus, the outcomes of the comparison of the results obtained for the single-pile system can be summarised in the following list:

- In general, the numerically predicted and measured responses in the vertical direction agree very well when comparing the driving-point responses. Moreover, it has shown that discrepancies between them only reach 1.5 dB at 80 Hz and that the adopted values of the damping soil for the numerical model do not significantly affect the driving-point response.

- A comparison of the experimentally free-field responses against the ones numerically predicted shows that the measured FRFs are contained in the envelope of predicted ones, which were calculated by assuming a range of soil damping values between $0.03 - 0.07$. In contrast with the point-driving responses, which are less sensitive to the assumed soil-damping values, the free-field responses are more susceptible to those damping values at high frequencies or when the distance between the source and receiver increases. Furthermore, the predicted FRF with soil damping of 0.05 can be adopted as a good approximation to represent the real soil damping since their corresponding FRFs agree very well with the experimental ones.

Although the proposed numerical approach tends to overestimate the predicted vibration levels at the pile head and on the free field, it can be stated that the proposed single-pile model

can accurately predict their dynamic responses. Thus, given the robustness of the proposed approach, in conjunction with the computational efficiency discussed in the previous chapter, this methodology was also employed to predict the FRF of the full-scale 2×2 pile-group system. From the comparison of results, the following outcomes can be summarised in the following:

- When the pile-group considered inertial excitation, the comparison of the FRF at the pile heads shows that the numerical response can reasonably predict similar vibration levels up to 70 Hz. Above this frequency, the numerical model slightly tends to overestimate the dynamic response. A visual inspection of the experimental setup shows that these discrepancies can be explained by the added effect of surplus concrete attached to the pile surface. Thus, it was found that the significant discrepancies at high frequencies come from the Pile head 3, which also has the biggest surplus concrete attached to its surface.

- When the pile-group considered incident wave field due to vertical hammer impacts on the ground, similar discrepancies to the first loading case were obtained. Although acceptable agreement of results was obtained up to 70 Hz, the added effect of those surplus concrete specimens also appears at high frequencies where considerable discrepancies arise between the experimentally and numerically predicted results.

Chapter 6

Conclusions and further work recommendations

This dissertation has presented a new approach to model piled foundation systems under inertial and kinematic excitation. The proposed method employs the SBM to model the soil as a half-space, whilst the pile is represented by an Euler-Bernoulli bean and a rod for accounting for flexural and axial motions, respectively. Both soil and pile are modelled in the space-frequency domain, and they are coupled by imposing geometry compatibility and traction equilibrium at the pile-soil interface. Therefore, the pile is divided into circular segments, each of them involving a set of collocation points placed at their soil-pile interface. Thus, assuming that each circular segment behaves as a rigid body, the pile reaction at the collocation points is obtained by considering a transformation matrix that relates the pile response computed at the centre of each circular segment (pile's centroid) with their corresponding collocation points. This transformation matrix is constructed according to both translational and rotational motions of the pile segments, as well as forces and bending moments. This new approach has been assessed in terms of assumptions, accuracy and computational effort against existing methods. Special focus is placed on the study of the influence of different pile-soil coupling conditions. This chapter summarises the main findings of this research and also provides some recommendations for further work based on the experience acquired by the author during the course of the doctoral studies.

6.1 Conclusions

As mentioned, this dissertation presents a novel three-dimensional, fully-coupled pile-soil model to deal with ground-borne noise and vibration problems. To successfully achieve this goal, a number of objectives were outlined in Section 1.2, which are now reviewed to evaluate the extent to which they have been met.

In Chapter 3, the novel approach is developed in the context of single-pile foundation systems. A convergence analysis conducted for the proposed single-pile model has provided a criterion for defining the minimum number of collocation points required to ensure an acceptable trade-off between robustness, accuracy and numerical performance of the scheme. Furthermore, an extensive numerical assessment of the proposed approach is also conducted to verify its accuracy against a 3D FE-BE methodology, an axisymmetric FE-PML approach and Novak's method. These assessments have demonstrated that the proposed approach can predict similar vibration levels to the ones obtained by the 3D FE-BE methodology. Moreover, the SBM typically involves fewer Green's function evaluations with respect to BEM per collocation point, allowing for the conclusion that the method is more computationally efficient than a standard 3D FE-BE. Another pile-soil coupling condition that neglects the rotational motions and bending moments in the coupling procedure has also been accounted for in the numerical assessment of the proposed method. Results show that some discrepancies in the dynamic response with respect to the proposed fully-coupled approach and the 3D FE-BE method can arise, especially at high frequencies and when estimating the lateral response of the free field due to lateral or vertical loading patterns.

Given the robustness of the proposed fully coupled single-pile model, its formulation has been extended in Chapter 4 to deal with pile-group systems with or without a concrete cap. Similar to the single-pile case, the comparison of results shows that the proposed pile-group model predicts similar vibration levels to the 3D FE-BE method when both rotational motions and torques are accounted for in the pile-soil coupling scheme. Otherwise, significant discrepancies, as in the single-pile case, have been found for the crossed responses, mostly at high frequencies. Furthermore, the accuracy of the approach with the presence of a concrete pile cap in the context of piles-soil and piles-cap coupling conditions is also verified against the 3D FE-BE approach. This study has highlighted that a fully piles-soil coupled system attached to a pile cap, by considering the six-degree-of-freedom of the pile heads in its formulation, can predict accurate vibration levels with respect to ones modelled by a 3D FE-BE model. However, it was observed that if the rotational motion and bending effects are all neglected in the

piles-soil coupling, or the torsional motion is relaxed in the pile-cap coupling procedure, then discrepancies arise at frequencies above 30 Hz when compared with the proposed fully coupled or the 3D FE-BE model. This result was expected since it is consistent with previous works, which stated that the error introduced by ignoring the twisting reaction of the piles in a group is usually small at low frequencies. Moreover, the proposed formulation was employed to study the influence of considering neighbouring piles in the calculation of the dynamic interaction factor of two adjacent piles in 2×1, 2×2 and 3×3 pile-group scenarios. These dynamic interaction factors agree very well between them and with the ones obtained by Kaynia [3], but only at low frequencies. It has shown that the wave-scattering feedback between the considered two adjacent piles and the remaining neighbouring piles of each pile-group scenario affects the dynamic response of the system as the frequency of analysis and the number of neighbouring piles increase, as well as by the piles-soil coupling assumption adopted for the transformation matrix.

This dissertation also includes an experimental validation of the proposed novel approach. The experimental tests are conducted over full-scale cast-in-situ single pile 2×2 pile-group systems constructed on the testing facilities for experimental studies in railway-induced vibration of the Acoustical and Mechanical Engineering Laboratory. The soil has been characterised by means of the MASW and cross-hole tests, as well as laboratory analysis of undisturbed soil samples. The experimental results in the vertical direction due to vertical hammer impacts are compared with the ones numerically predicted using the approach presented in this dissertation. Because the hysteretic soil damping has not been experimentally characterised, it is assumed to be ranging between typical damping ratios for soft (0.03) and stiff (0.07) soils. On the one hand, it has been observed that the numerically predicted results for the single-pile system, when considering inertial excitation, agree very well with respect to the experimental results, for which discrepancies between them only reach 1.5 dB at 80 Hz and that the adopted values of the damping soil for the numerical model do not significantly affect the driving-point response. The last statement is not true for the numerically predicted free-field responses since they are obviously more sensitive to those damping values, especially at high frequencies and large distances away from the pile. However, a comparison of the experimentally free-field responses against those numerically predicted shows that the measured results are contained in the envelope of the predicted ones. Moreover, the numerical results associated with a soil damping of 0.05 can be adopted as a good approximation to represent the real soil damping since their corresponding FRFs agree very well with the experimental ones. On the other hand, the comparison of experimental and numerical results in the context of the tested pile-group

system shows that the pile-soil-pile interaction can be well-predicted using the proposed approach up to frequencies of 70 Hz. Above this frequency, the numerical model is found to be slightly overestimating the dynamic response. Similar patterns are found when comparing numerical and measured responses of the system under incident wave fields due to vertical hammer impacts on the ground. A visual inspection of the experimental setup shows that these discrepancies can be explained by the influence of the surplus concrete resulting from the construction process of the cast-in-situ piles.

6.2 Further work recommendations

The piled foundation model outlined in this dissertation provides an interesting alternative to predict building vibration levels based on this foundation system type when subjected to ground vibration. This model represents a valuable contribution towards the field of soil-structure interaction research, as the model offers an interesting trade-off between robustness, accuracy and numerical performance, as discussed in the current dissertation. The results presented correspond to two generic piled foundation cases, a single-pile system and a 2×2 pile-group one, on the basis of a set of hypotheses that have been found to be valid for the majority of situations. However, there are many scenarios for which the proposed hypothesis could not be valid. Furthermore, the influence of other structural systems could induce important changes on the dynamic behaviour of piled foundation systems. In such a sense, the following topics for further investigation on the present topic are proposed and listed below:

- When deploying the SBM in the context of the proposed approach, the origin intensity factor for the Neumann boundary condition involves the calculation of the term $\mathbf{B}_{\text{cc}}$, given in Eq. (3.9). However, as discussed in Chapter 3, this term has been neglected in all calculations presented in this dissertation because it has been found to be very small with respect to the other terms computed for the smooth geometry of a circular pile. Although the relevancy of this term in the context of circular piles is clearly low, this omission may not be directly extrapolated to arbitrarily shaped boundaries. Thus. the importance of the term $\mathbf{B}_{\text{cc}}$, can be of high interest for structures with complex geometries, allowing thus to extend the applicability of the SBM to any 3D soil-structure interaction problem.

- Although the hypothesis of considering the concrete cap as a solid rigid at high frequencies in a pile-cap system was revisited for a specific cap thickness, it cannot be concluded

that this hypothesis can be applied to caps with lower thickness than the assumed in this dissertation. In such a sense, an extensive analysis of pile-cap systems with different cap thicknesses can provide an efficient and versatile means to establish new guidelines to determine for which thicknesses the concrete cap behaves as a solid rigid and its influence in piled-buildings subjected to ground vibration sources. Furthermore, the formulation developed for the pile-cap coupling assumes the cap as a floating subsystem since no contact with the soil is considered. In this context, comparing the dynamic response between the previous analysis and those obtained by considering cap-soil coupling is also an interesting topic to study.

- Further work is required to assess the relevancy of accounting for the rotational motion and the interaction torques in the pile-soil coupling conditions when a superstructure (e.g. a residential building) is considered.

- Another interesting topic for further research is to study efficient approaches to include the effect of a near-at-grade or underground railway system. In such a sense, a comprehensive and efficient model for track-soil-foundation-building systems in situations of high proximity between the two structures could be a very interesting outcome.

- In its present form, the proposed approach models pile-soil coupling considering perfect contact (no relative motion between the two sub-systems). However, relative motion could occur between the pile and the soil in the real world, especially at low depths. Including a model for the pile-soil interaction that accounts for this possibility of motion could result in a better representation of the actual physical problem.

References

[1] A. M. Kaynia, E. Kausel, Dynamics of piles and pile groups in layered soil media, Soil Dynamics and Earthquake Engineering 10 (1991) 386–401.

[2] G. Mylonakis, G. Gazetas, Vertical vibration and additional distress of grouped piles in layered soil, Soils and Foundations 38 (1998) 1–14.

[3] A. M. Kaynia, Dynamic stiffness and seismic response of pile groups, Ph.D. thesis, Massachusetts Institute of technology, 1982.

[4] T. L. Edirisinghe, J. P. Talbot, Inertial interaction in pile-groups: A study of the influence of coupling via an iterative wave-scattering approach, Computers and Geotechnics 128 (2020) 103804.

[5] J. P. Talbot, H. E. M. Hunt, A computationally efficient piled-foundation model for studying the effects of ground-borne vibration on buildings, Proceedings of the Institution of Mechanical Engineers, Part C: Journal of Mechanical Engineering Science 217 (2003) 975–990.

[6] J. H. Hyde, H. R. Lintern, The vibrations of roads and structures., Minutes of the Proceedings of the Institution of Civil Engineers 227 (1929) 187–199.

[7] D. Thompson, Railway noise and vibration: mechanisms, modelling and means of control, Elsevier, 2008.

[8] J. F. Semblat, A. Pecker, Waves and vibrations in soils: earthquakes, traffic, shocks, construction works, IUSS Press, 2009.

[9] Z. Zhu, B. Mohanty, H. Xie, Numerical investigation of blasting-induced crack initiation and propagation in rocks, International Journal of Rock Mechanics and Mining Sciences 44 (2007) 412–424.

[10] M. Lak, S. François, G. Degrande, G. Lombaert, Development and experimental validation of a numerical model for the prediction of ground vibration generated by pavement breaking, Soil Dynamics and Earthquake Engineering 79 (2015) 199–210.

[11] A. Colaço, P. A. Costa, C. M. Parente, A. S. Cardoso, Ground-borne noise and vibrations in buildings induced by pile driving: An integrated approach, Applied Acoustics 179 (2021) 108059.

[12] T. V. Sofiste, L. Godinho, P. A. Costa, D. Soares, A. Colaço, Numerical modelling for prediction of ground-borne vibrations induced by pile driving, Engineering Structures 242 (2021) 112533.

[13] D. M. Hiller, V. S. Hope, and, Groundborne vibration generated by mechanized construction activities., Proceedings of the Institution of Civil Engineers - Geotechnical Engineering 131 (1998) 223–232.

[14] H. E. M. Hunt, Measurement and modelling of traffic-induced ground vibration., Ph.D. thesis, University of Cambridge, 1988.

[15] G. Watts, The generation and propagation of vibration in various soils produced by the dynamic loading of road pavements, Journal of Sound and Vibration 156 (1992) 191–206.

[16] M. Lak, G. Degrande, G. Lombaert, The effect of road unevenness on the dynamic vehicle response and ground-borne vibrations due to road traffic, Soil Dynamics and Earthquake Engineering 31 (2011) 1357–1377.

[17] International Organization for Standardization, ISO 2631-2. Mechanical vibration and shock. Evaluation of human exposure to whole-body vibration. Part 2: Continuous and shock-induced vibration in buildings (1-80Hz), 2003.

[18] Swiss Association for Standardization, SN 640-312A:1992 Vibrations - Vibrations effects in buildings, 1992.

[19] M. Crispino, M. D'apuzzo, Measurement and prediction of traffic-induced vibrations in a heritage building, Journal of Sound and Vibration 246 (2001) 319–335.

[20] K. Korkmaz, Z. Ay, S. Keskin, D. Ceditoglu, Investigation of traffic-induced vibrations on masonry buildings in turkey and countermeasures, Journal of Vibration and Control 17 (2011) 3–10.

[21] G. Bongiovanni, P. Clemente, D. Rinaldis, F. Saitta, Traffic-induced vibrations in historical buildings, in: Proceedings of the 8th International Conference on Structural Dynamics, Leuven, Belgium, 2011, pp. 812–819.

[22] M. Novak, State-of-the-art in analysis and design of machine foundations, in: A. Cakmak (Ed.), Soil-Structure Interaction, volume 43 of *Developments in Geotechnical Engineering*, Elsevier, 1987, pp. 171–192.

[23] M. H. E. Naggar, K. J. Bentley, Dynamic analysis for laterally loaded piles and dynamic p-y curves, Canadian Geotechnical Journal 37 (2000) 1166–1183.

[24] D. P. Connolly, G. P. Marecki, G. Kouroussis, I. Thalassinakis, P. K. Woodward, The growth of railway ground vibration problems - A review, Science of The Total Environment 568 (2016) 1276–1282.

[25] M. Heckl, G. Hauck, R. Wettschureck, Structure-borne sound and vibration from rail traffic, Journal of Sound and Vibration 193 (1996) 175–184.

[26] G. Lombaert, G. Degrande, S. François, D. J. Thompson, Ground-borne vibration due to railway traffic: A review of excitation mechanisms, prediction methods and mitigation measures, in: Noise and Vibration Mitigation for Rail Transportation Systems, Springer Berlin Heidelberg, Berlin, Heidelberg, 2015, pp. 253–287.

[27] V. V. Krylov, On the theory of railway-induced ground vibrations, Le Journal de Physique IV 4 (1994) C5–769.

[28] V. V. Krylov, Generation of ground vibrations by superfast trains, Applied Acoustics 44 (1995) 149–164.

[29] V. V. Krylov, C. C. Ferguson, Recent progress in the theory of railway-generated ground vibrations, Loughborough University (1995).

[30] H. Dieterman, A. Metrikine, The equivalent stiffness of a half-space interacting with a beam. Critical velocities of a moving load along the beam, European Journal of Mechanics Series A Solids 15 (1996) 67–90.

[31] H. A. Dieterman, A. Metrikine, Critical velocities of a harmonic load moving uniformly along an elastic layer, Journal of Applied Mechanics 64 (1997) 596–600.

[32] C. Madshus, A. Kaynia, High-speed railway lines on soft ground: Dynamic behaviour at critical train speed, Journal of Sound and Vibration 231 (2000) 689–701.

[33] D. Thopmson, C. Jones, A review of the modelling of wheel/rail noise generation, Journal of Sound and Vibration 231 (2000) 519–536.

[34] G. Kouroussis, D. Connolly, O. Verlinden, Railway-induced ground vibrations - A review of vehicle effects, International Journal of Rail Transportation 2 (2014) 69–110.

[35] D. Connolly, G. Kouroussis, O. Laghrouche, C. Ho, M. Forde, Benchmarking railway vibrations – track, vehicle, ground and building effects, Construction and Building Materials 92 (2015) 64–81. Railway Engineering-2013.

[36] Z. Zhu, L. Wang, P. A. Costa, Y. Bai, Z. Yu, An efficient approach for prediction of subway train-induced ground vibrations considering random track unevenness, Journal of Sound and Vibration 455 (2019) 359–379.

[37] J. C. O. Nielsen, A. Pieringer, D. J. Thompson, P. T. Torstensson, Wheel–rail impact loads, noise and vibration: A review of excitation mechanisms, prediction methods and mitigation measures, in: Noise and Vibration Mitigation for Rail Transportation Systems, Springer International Publishing, Cham, 2021, pp. 3–40.

[38] K. Knothe, S. Grassie, Modelling of railway track and vehicle/track interaction at high frequencies, Vehicle System Dynamics 22 (1993) 209–262.

[39] J. Nielsen, A. Igeland, Vertical dynamic interaction between train and track influence of wheel and track imperfections, Journal of Sound and Vibration 187 (1995) 825–839.

[40] T. Wu, D. Thompson, On the parametric excitation of the wheel/track system, Journal of Sound and Vibration 278 (2004) 725–747.

[41] L. Auersch, The excitation of ground vibration by rail traffic: theory of vehicle–track–soil interaction and measurements on high-speed lines, Journal of Sound and Vibration 284 (2005) 103–132.

[42] N. Triepaischajonsak, The influence of various excitation mechanisms on ground vibration from trains, Ph.D. thesis, University of Southampton, 2012.

[43] P. Galvín, A. Romero, J. Domínguez, Fully three-dimensional analysis of high-speed train–track–soil-structure dynamic interaction, Journal of Sound and Vibration 329 (2010) 5147–5163.

[44] J. N. Varandas, P. Hölscher, M. A. Silva, Dynamic behaviour of railway tracks on transitions zones, Computers and Structures 89 (2011) 1468–1479.

[45] P. Fiala, G. Degrande, F. Augusztinovicz, Numerical modelling of ground-borne noise and vibration in buildings due to surface rail traffic, Journal of Sound and Vibration 301 (2007) 718–738.

[46] E. Kausel, Advanced Structural Dynamics, Cambridge University Press, 2017.

[47] W. Thomson (Lord Kelvin), On the equations of equilibrium of an elastic solid, Cambridge–Dublin Mathematical Journal 3 (1884) 87 – 89. A reprint of this paper is included in "Mathematical and Physical Papers by Sir William Thomson", Collected from Different Scientific Periodicals from May 1841 to the present time, vol. I, Cambridge: At the University Press, 1882.

[48] G. G. Stokes, On the dynamical theory of diffraction, Transactions of the Cambridge Philosophical Society 9 (1849) 1–48.

[49] G. Eason, J. Fulton, I. N. Sneddon, L. Rosenhead, The generation of waves in an infinite elastic solid by variable body forces, Philosophical Transactions of the Royal Society of London. Series A, Mathematical and Physical Sciences 248 (1956) 575–607.

[50] J. Boussinesq, Équilibre d'élasticité d'un sol isotrope sans pesanteur, supportant différents poids, Comptes Rendus, Paris, Gauthier-Villars 86 (1878) 1260–1263.

[51] V. Boussinesq, Sur la dépression que produit, à la surface d'un sol horizontal élastique et isotrope, un poids qu'on dépose, et sur la répartition de ce poids entre ses divers point d'appui, Comptes Rendus, Paris, Gauthier-Villars (1878) 402–405.

[52] V. Boussinesq, Sur la manière dont se distribue entre ses points d'appui le poids d'un corps dur, posé sur un sol poli, horizontal et élastique: identité de ce mode de répartition, pour une base de sustentation plane et horizontale, avec celui d'une charge électrique en équilibre dans une plaque mince de même forme, Comptes Rendus, Paris, Gauthier-Villars 87 (1878) 519–522.

[53] V. Cerruti, Ricerche intorno all'equilibrio de'corpi elastici isotropi, Salviucci, 1882.

[54] H. Lamb, I. On the propagation of tremors over the surface of an elastic solid, Philosophical Transactions of the Royal Society of London. Series A, Containing Papers of a Mathematical or Physical Character 203 (1904) 1–42.

[55] E. Kausel, Early history of soil–structure interaction, Soil Dynamics and Earthquake Engineering 30 (2010) 822–832. Special Issue in honour of Prof. Anestis Veletsos.

[56] R. D. Mindlin, Force at a point in the interior of a semi-infinite solid, Physics 7 (1936) 195–202.

[57] E. Kausel, An explicit solution for the Green functions for dynamic loads in layered media, Department of Civil Engineering, School of Engineering, Massachusetts, 1981.

[58] E. Kausel, R. Peek, Dynamic loads in the interior of a layered stratum: An explicit solution, Bulletin of the Seismological Society of America 72 (1982) 1459–1481.

[59] J. Boussinesq, Application des potentiels à l'étude de l'équilibre et du mouvement des solides élastiques, volume 4, Paris, Gauthier-Villars, Imprimeur-Libraire, 1885.

[60] F. Schleicher, Zur theorie des baugrundes, Bauingenieur 48 (1926) 931–935.

[61] H. Borowicka, Über ausmittig belastete, starre platten auf elastisch-isotropem untergrund, Ingenieur-Archiv 14 (1943) 1–8.

[62] E. Reissner, H. Sagoci, Forced torsional oscillations of an elastic half-space. I, Journal of Applied Physics 15 (1944) 652–654.

[63] H. F. Sagoci, Forced torsional oscillations of an elastic half-space. II, Journal of Applied Physics 15 (1944) 655–662.

[64] R. D. Mindlin, Compliance of elastic bodies in contact, Journal of Applied Mechanics 16 (2021) 259–268.

[65] W. Steinbrenner, Tafeln zur setzungsberechnung, Die Strasse 1 (1934) 121–124.

[66] K.-i. Terazawa, On the elastic equilibrium of a semi-infinite solid under given boundary conditions, Journal of the College of Science (1916) 14–24.

[67] A. E. H. Love, The stress produced in a semi-infinite solid by pressure on part of the boundary, Philosophical Transactions of the Royal Society of London. Series A, Containing Papers of a Mathematical or Physical Character 228 (1929) 377–420.

[68] E. Reissner, Stationäre, axialsymmetrische, durch eine schüttelnde masse erregte schwingungen eines homogenen elastischen halbraumes, Ingenieur-Archiv 7 (1936) 381–396.

[69] E. Reissner, Freie und erzwungene torsionsschwingungen des elastischen halbraumes, Ingenieur-Archiv 8 (1937) 229–245.

[70] R. J. Apsel, J. E. Luco, Torsional response of rigid embedded foundation, Journal of the Engineering Mechanics Division 102 (1976) 957–970.

[71] P. Chadwick, E. A. Trowbridge, Oscillations of a rigid sphere embedded in an infinite elastic solid: I. Torsional oscillations, Mathematical Proceedings of the Cambridge Philosophical Society 63 (1967) 1189–1205.

[72] P. Chadwick, E. A. Trowbridge, Oscillations of a rigid sphere embedded in an infinite elastic solid: II. Rectilinear oscillations, Mathematical Proceedings of the Cambridge Philosophical Society 63 (1967) 1207–1227.

[73] K. A. Kuo, H. E. M. Hunt, Dynamic models of piled foundations, Applied Mechanics Reviews 65 (2013). 031003.

[74] J. Lysmer, F. E. Richart, Dynamic response of footings to vertical loading, Journal of the Soil Mechanics and Foundations Division 92 (1966) 65–91.

[75] J. Lysmer, R. L. Kuhlemeyer, Finite dynamic model for infinite media, Journal of the Engineering Mechanics Division 95 (1969) 859–877.

[76] V. A. Baranov, On the calculation of excited vibrations of an embedded foundation (in Russian), Vopr. Dynamiki Prochnocti 14 (1967) 195–209.

[77] M. Novak, Y. O. Beredugo, Vertical vibration of embedded footings, Journal of the Soil Mechanics and Foundations Division 98 (1972) 1291–1310.

[78] Y. O. Beredugo, M. Novak, Coupled horizontal and rocking vibration of embedded footings, Canadian Geotechnical Journal 9 (1972) 477–497.

[79] M. Novak, Dynamic stiffness and damping of piles, Canadian Geotechnical Journal 11 (1974) 574–598.

[80] T. Nogami, M. Novak, Soil-pile interaction in vertical vibration, Earthquake Engineering & Structural Dynamics 4 (1976) 277–293.

[81] T. Nogami, M. Novak, Resistance of soil to a horizontally vibrating pile, Earthquake Engineering & Structural Dynamics 5 (1977) 249–261.

[82] M. Novak, T. Nogami, Soil-pile interaction in horizontal vibration, Earthquake Engineering & Structural Dynamics 5 (1977) 263–281.

[83] E. Ntotsios, W. Hamad, D. Thompson, M. Hussein, H. Hunt, J. Talbot, Predictions of the dynamic response of piled foundations in a multi-layered half-space due to inertial and railway induced loadings, in: 5th International Conference on Computational Methods in Structural Dynamics and Earthquake Engineering (COMPDYN) (24/05/15 - 26/05/15), 2015, pp. 133–145.

[84] M. Novak, Vertical vibration of floating piles, Journal of the Engineering Mechanics Division 103 (1977) 153–168.

[85] R. Y. S. Pak, P. C. Jennings, Elastodynamic response of pile under transverse excitations, Journal of Engineering Mechanics 113(7) (1987) 1101–1116.

[86] J. P. Wolf, Foundation vibration analysis using simple physical models, Prentice-Hall, London, United Kingdom (1995).

[87] R. K. N. D. Rajapakse, A. H. Shah, On the longitudinal harmonic motion of an elastic bar embedded in an elastic half-space, International Journal of Solids and Structures 23(2) (1987) 267–285.

[88] R. K. N. D. Rajapakse, A. H. Shah, On the lateral harmonic motion of an elastic bar embedded in an elastic half-space, International Journal of Solids and Structures 23(2) (1987) 287–303.

[89] G. Anoyatis, R. Di Laora, A. Mandolini, G. Mylonakis, Kinematic response of single piles for different boundary conditions: Analytical solutions and normalization schemes, Soil Dynamics and Earthquake Engineering 44 (2013) 183–195.

[90] G. Anoyatis, R. Di Laora, G. Mylonakis, Axial kinematic response of end-bearing piles to p waves, International Journal for Numerical and Analytical Methods in Geomechanics 37 (2013) 2877–2896.

[91] R. D. Laora, E. Rovithis, Kinematic bending of fixed-head piles in nonhomogeneous soil, Journal of Geotechnical and Geoenvironmental Engineering 141 (2015) 04014126.

[92] R. D. Laora, E. Rovithis, Kinematic bending of fixed-head piles in nonhomogeneous soil, Journal of Geotechnical and Geoenvironmental Engineering 141 (2015) 04014126.

[93] K. Kuo, H. Hunt, An efficient model for the dynamic behaviour of a single pile in viscoelastic soil, Journal of Sound and Vibration 332 (2013) 2549–2561.

[94] J. Forrest, H. Hunt, A three-dimensional tunnel model for calculation of train-induced ground vibration, Journal of Sound and Vibration 294 (2006) 678–705.

[95] J. Forrest, H. Hunt, Ground vibration generated by trains in underground tunnels, Journal of Sound and Vibration 294 (2006) 706–736.

[96] R. Kuhlemeyer, Static and dynamic laterally loaded floating piles, Journal of the Geotechnical Engineering Division 105 (1979) 289–304.

[97] R. Kuhlemeyer, Vertical vibration of piles, Journal of the Geotechnical Engineering Division 105 (1979) 273–287.

[98] K. Syngros, Seismic response of piles and pile-supported bridge piers evaluated through case histories, Ph.D. thesis, The City University of New York, 2004.

[99] A. F. Homayoun Rooz, A. Hamidi, A numerical model for continuous impact pile driving using ale adaptive mesh method, Soil Dynamics and Earthquake Engineering 118 (2019) 134–143.

[100] R. Krishnan, G. Gazetas, A. Velez, Static and dynamic lateral deflexion of piles in non-homogeneous soil stratum, Geotechnique 33 (1983) 307–325.

[101] A. Velez, G. Gazetas, R. Krishnan, Lateral dynamic response of constrained-head piles, Journal of Geotechnical Engineering 109 (1983) 1063–1081.

[102] G. Wu, W. D. Finn, Dynamic nonlinear analysis of pile foundations using finite element method in the time domain, Canadian Geotechnical Journal 34 (1997) 44–52.

[103] B. K. Maheshwari, K. Z. Truman, M. H. El Naggar, P. L. Gould, Three-dimensional finite element nonlinear dynamic analysis of pile groups for lateral transient and seismic excitations, Canadian Geotechnical Journal 41 (2004) 118–133.

[104] B. K. Maheshwari, K. Z. Truman, P. L. Gould, M. H. El Naggar, Three-dimensional nonlinear seismic analysis of single piles using finite element model: Effects of plasticity of soil, International Journal of Geomechanics 5 (2005) 35–44.

[105] K. J. Bentley, M. H. E. Naggar, Numerical analysis of kinematic response of single piles, Canadian Geotechnical Journal 37 (2000) 1368–1382.

[106] D. E. Beskos, Boundary element methods in dynamic analysis, Applied Mechanics Reviews 40 (1987) 1–23.

[107] D. E. Beskos, Boundary element methods in dynamic analysis: Part II (1986-1996), Applied Mechanics Reviews 40 (1987) 1–23.

[108] S. E. Kattis, D. Polyzos, D. E. Beskos, Vibration isolation by a row of piles using a 3-D frequency domain BEM, International Journal for Numerical Methods in Engineering 46 (1999) 713–728.

[109] L. A. Padrón, J. J. Aznárez, O. Maeso, BEM-FEM coupling model for the dynamic analysis of piles and pile groups, Engineering Analysis with Boundary Elements 31 (2007) 473–484.

[110] P. Coulier, The vibration response of piled foundations to inertial and underground railway induced loadings, 2010.

[111] W. Chen, F. Z. Wang, A method of fundamental solutions without fictitious boundary, Engineering Analysis with Boundary Elements 34 (2010) 530–532.

[112] Y. Gu, W. Chen, C.-Z. Zhang, Singular boundary method for solving plane strain elastostatic problems, International Journal of Solids and Structures 48 (2011) 2549–2556.

[113] Y. Gu, W. Chen, Z. J. Fu, B. Zhang, The singular boundary method: Mathematical background and application in orthotropic elastic problems, Engineering Analysis with Boundary Elements 44 (2014) 152–160.

[114] L. Sun, W. Chen, A. H. Cheng, Singular boundary method for 2D dynamic poroelastic problems, Wave Motion 61 (2016) 40–62.

[115] H. Liravi, R. Arcos, A. Clot, K. F. Conto, J. Romeu, A 2.5D coupled FEM–SBM methodology for soil–structure dynamic interaction problems, Engineering Structures 250 (2022) 113371.

[116] H. G. Poulos, Behavior of laterally loaded piles: II-pile groups, Journal of the Soil Mechanics and Foundations Division 97 (1971) 733–751.

[117] M. Novak, R. F.Grigg, Dynamic experiments with small pile foundations, Canadian Geotechnical Journal 13 (1976) 372–385.

[118] M. Sheta, M. Novak, Vertical vibration of pile groups, Journal of the Geotechnical Engineering Division 108 (1982) 570–590.

[119] J. Wolf, G. Von Arx, Impendance function of a group of vertical piles, in: From Volume I of Earthquake Engineering and Soil Dynamics–Proceedings of the ASCE Geotechnical Engineering Division Specialty Conference, June 19-21, 1978, Pasadena, California. Sponsored by Geotechnical Engineering Division of ASCE in cooperation with:, Proceeding, 1978, pp. p. 1024–1041.

[120] T. Nogami, Dynamic group effect of multiple piles under vertical vibration, in: Engineering mechanics, ASCE, 1979, pp. 750–754.

[121] T. Nogami, Flexural responses of grouped piles under dynamic loading, Earthquake Engineering & Structural Dynamics 13 (1985) 321–336.

[122] T. Nogami, Dynamic stiffness and damping of pile groups in inhomogeneous soil, Special Technical Publication on Dynamic Response of Pile Foundations: Analytical Aspects (1980) 31–52.

[123] T. Nogami, Dynamic group effect in axial responses of grouped piles, Journal of Geotechnical Engineering 109 (1983) 228–243.

[124] T. Nogami, H. L. Chen, Simplified approach for axial pile group response analysis, Journal of Geotechnical Engineering 110 (1984) 1239–1255.

[125] R. Dobry, G. Gazetas, Simple method for dynamic stiffness and damping of floating pile groups, Géotechnique 38 (1988) 557–574.

[126] G. Gazetas, N. Makris, Dynamic pile-soil-pile interaction. Part I: Analysis of axial vibration, Earthquake Engineering & Structural Dynamics 20 (1991) 115–132.

[127] N. Makris, G. Gazetas, Dynamic pile-soil-pile interaction. Part II: Lateral and seismic response, Earthquake Engineering & Structural Dynamics 21 (1992) 145–162.

[128] R. Cairo, E. Conte, G. Dente, Analysis of pile groups under vertical harmonic vibration, Computers and Geotechnics 32 (2005) 545–554.

[129] R. Cairo, E. Conte, G. Dente, Interaction factors for the analysis of pile groups in layered soils, Journal of Geotechnical and Geoenvironmental Engineering 131 (2005) 525–528.

[130] E. Kausel, J. M. Roësset, Stiffness matrices for layered soils, Bulletin of the Seismological Society of America 71 (1981) 1743–1761.

[131] J. P. Talbot, On the performance of base-isolated buildings: a generic model, Ph.D. thesis, University of Cambridge, 2002.

[132] L. Brillouin, M. Parodi, Wave propagation in periodic structures, international series in pure and applied physics, éd: McGraw-Hill, New York (1946).

[133] P. J. Meymand, Shaking table scale model tests of nonlinear soil-pile-superstructure interaction in soft clay, University of California, Berkeley, 1998.

[134] B. E. Sharnouby, M. Novak, Dynamic experiments with group of piles, Journal of Geotechnical Engineering 110 (1984) 719–737.

[135] M. Novak, B. E. Sharnouby, Evaluation of dynamic experiments on pile group, Journal of Geotechnical Engineering 110 (1984) 738–756.

[136] H. El-Marsafawi, Y. C. Han, M. Novak, Dynamic experiments on two pile groups, Journal of Geotechnical Engineering 118 (1992) 576–592.

[137] A. Boominathan, R. Ayothiraman, Dynamic behaviour of laterally loaded model piles in clay, Proceedings of the Institution of Civil Engineers - Geotechnical Engineering 158 (2005) 207–215.

[138] W. Finn, W. B. Gohl, Response of model pile groups to strong shaking, in: Piles under Dynamic Loads, ASCE, 1992, pp. 27–55.

[139] J. P. Burr, M. J. Pender, T. J. Larkin, Dynamic response of laterally excited pile groups, Journal of Geotechnical Engineering 123 (1997) 1 – 8.

[140] H. Masoumi, G. Degrande, A. Holeyman, Pile response and free field vibrations due to low strain dynamic loading, Soil Dynamics and Earthquake Engineering 29 (2009) 834–844.

[141] M. Elkasabgy, M. H. El Naggar, Dynamic response of vertically loaded helical and driven steel piles, Canadian Geotechnical Journal 50 (2013) 521–535.

[142] M. Novak, M. Sheta, L. El-Hifnawy, H. El-Marsafawi, O. Ramadan, Dyna5: A computer program for calculation of foundation response to dynamic loads, Geotechnical Research Centre, University of Western Ontario, London (1999).

[143] M. C. Capatti, F. Dezi, S. Carbonari, F. Gara, Full-scale experimental assessment of the dynamic horizontal behavior of micropiles in alluvial silty soils, Soil Dynamics and Earthquake Engineering 113 (2018) 58–74.

[144] Y. Han, H. Vaziri, Dynamic response of pile groups under lateral loading, Soil Dynamics and Earthquake Engineering 11 (1992) 87–99.

[145] S. Biswas, B. Manna, Experimental and theoretical studies on the nonlinear characteristics of soil-pile systems under coupled vibrations, Journal of Geotechnical and Geoenvironmental Engineering 144 (2018) 04018007.

[146] S. S. Choudhary, S. Biswas, B. Manna, Effect of pile arrangements on the dynamic coupled response of pile groups, Geotechnical and Geological Engineering 39 (2021) 1963–1978.

[147] F. Theland, G. Lombaert, S. François, C. Pacoste, F. Deckner, P. Blom, J.-M. Battini, Dynamic response of driven end-bearing piles and a pile group in soft clay: an experimental validation study, Engineering Structures 267 (2022) 114629.

[148] J. Lin, W. Chen, C. S. Chen, Numerical treatment of acoustic problems with boundary singularities by the singular boundary method, Journal of Sound and Vibration 333 (2014) 3177–3188.

[149] M. Bonnet, Boundary integral equation methods for solids and fluids, John Wiley and Sons, Chichester, United Kingdom (1995).

[150] E. Kausel, Fundamental solutions in elastodynamics: A compendium, Cambridge University Press, 2006.

[151] W. Chen, Y. Gu, An improved formulation of singular boundary method, Advances in Applied Mathematics and Mechanics 4 (2012) 543–558.

[152] Z. Fu, W. Chen, J. Chen, W. Qu, Singular boundary method: Three regularization approaches and exteriorwave applications, CMES - Computer Modeling in Engineering and Sciences 100 (2014) 59–84.

[153] International Organization for Standardization, ISO 14837-1. Mechanical vibration. Ground-borne noise and vibration arising from rail systems. Part 1: General Guidance, 2005.

[154] M. Schevenels, S. François, G. Degrande, EDT: An ElastoDynamics Toolbox for MATLAB, Computers & Geosciences 35 (2009) 1752–1754.

[155] J. Domínguez, R. Abascal, On fundamental solutions for the boundary integral equations method in static and dynamic elasticity, Engineering Analysis 1 (1984) 128–134.

[156] U. Basu, A. K. Chopra, Perfectly matched layers for time-harmonic elastodynamics of unbounded domains: theory and finite-element implementation, Computer Methods in Applied Mechanics and Engineering 192 (2003) 1337–1375.

[157] S. François, M. Schevenels, G. Lombaert, G. Degrande, A 2.5 D displacement-based PML for elastodynamic wave propagation, in: Proceedings of the 4th European Conference on Computational Mechanics, 2010.

[158] Z.-J. Fu, W. Chen, J. Lin, A. H.-D. Cheng, Singular boundary method for various exterior wave applications, International Journal of Computational Methods 12 (2015) 1550011.

[159] M. J. Tomlinson, R. Boorman, Foundation design and construction, Pearson Education, 2001.

[160] M. Tomlinson, J. Woodward, Pile design and construction practice, CRC press, 2014.

[161] EN 1992-1-1:2004, Eurocode 2: Design of concrete structures, Standard, The European Union, 2004.

[162] EN 1997-1:2004, Eurocode 7: Geotechnical design - Part 1: General rules, Standard, The European Union, 2004.

[163] EN 1997-2:2007, Eurocode 7: Geotechnical design - Part 2: Ground investigation and testing, Standard, The European Union, 2007.

[164] M. Novak, J. F. Howell, Torsional vibration of pile foundations, Journal of the Geotechnical Engineering Division 103 (1977) 271–285.

[165] H. G. Poulos, E. H. Davis, Pile foundation analysis and design, volume 397, Wiley New York, 1980.

[166] T. Edirisinghe, J. Talbot, A parametric study of the train-induced vibration of a single pile near an underground railway tunnel, Soil Dynamics and Earthquake Engineering 158 (2022) 107274.

[167] American Society for Testing and Materials, ASTM, D 4428/D 4428M–00. Standard test methods for cross-hole seismic testing. Gd, 2000.

[168] P. Welch, The use of fast Fourier transform for the estimation of power spectra: A method based on time averaging over short, modified periodograms, IEEE Transactions on Audio and Electroacoustics 15 (1967) 70–73.

Appendix A

Unknown-constant values for a pile with free-free ends

This appendix presents the expressions for the constants A_j (for $j = 1, 2, 3, 4$), B_j (for $j = 1, 2, 3, 4$), and C_j (for $j = 1, \ldots, 8$) associated to the pile model adopting free-free boundary conditions and under external unitary point loads and bending moments located at $z = z_1$, as shown in Fig. 3.2. The coefficients A_j are given by

$$\begin{aligned} A_1 &= -\frac{\cos(\alpha z_1)\cos(\alpha L_\mathrm{p}) + \sin(\alpha z_1)\sin(\alpha L_\mathrm{p})}{\alpha A_\mathrm{p} E_\mathrm{p} \sin(\alpha L_\mathrm{p})}, \\ A_2 &= 0, \\ A_3 &= -\frac{\cos(\alpha z_1)\cos(\alpha L_\mathrm{p})}{\alpha A_\mathrm{p} E_\mathrm{p} \sin(\alpha L_\mathrm{p})}, \\ A_4 &= -\frac{\cos(\alpha z_1)}{\alpha A_\mathrm{p} E_\mathrm{p}}. \end{aligned} \tag{A.1}$$

The coefficients B_j associated with the torsional response due to a unitary torsional moment are given by

$$
\begin{aligned}
B_1 &= -\frac{\cos(\gamma z_1)\cos(\gamma L_\mathrm{p}) + \sin(\gamma z_1)\sin(\gamma L_\mathrm{p})}{\gamma J_\mathrm{p} G_\mathrm{p} \sin(\gamma L_\mathrm{p})},\\
B_2 &= 0,\\
B_3 &= -\frac{\cos(\gamma z_1)\cos(\gamma L_\mathrm{p})}{\gamma J_\mathrm{p} G_\mathrm{p} \sin(\gamma L_\mathrm{p})},\\
B_4 &= -\frac{\cos(\gamma z_1)}{\gamma J_\mathrm{p} G_\mathrm{p}}.
\end{aligned}
\tag{A.2}
$$

Finally, the expressions for the coefficients C_j associated with the flexural response of the pile due to a unitary point load are

$$
\begin{aligned}
C_1 = C_3 &= b_1[a_4 \sinh(\beta z_1) + a_3 \cosh(\beta z_1) + a_5 \sin(\beta z_1) + a_3 \cos(\beta z_1)],\\
C_2 = C_4 &= b_1[a_2 \sinh(\beta z_1) + a_5 \cosh(\beta z_1) + a_2 \sin(\beta z_1) + a_4 \cos(\beta z_1)],\\
C_5 &= b_1[a_4 \sinh(\beta z_1) + a_3 \cosh(\beta z_1) + a_4 \sin(\beta z_1) + a_3 \cos(\beta z_1)],\\
C_6 &= b_1[a_2 \sinh(\beta z_1) + a_5 \cosh(\beta z_1) + a_2 \sin(\beta z_1) + a_5 \cos(\beta z_1)],\\
C_7 &= b_1[a_5 \sinh(\beta z_1) + a_3 \cosh(\beta z_1) + a_5 \sin(\beta z_1) + a_3 \cos(\beta z_1)],\\
C_8 &= b_1[a_2 \sinh(\beta z_1) + a_4 \cosh(\beta z_1) + a_2 \sin(\beta z_1) + a_4 \cos(\beta z_1)].
\end{aligned}
\tag{A.3}
$$

where $b_1 = (a_1\beta^3)^{-1}$ and

$$
\begin{aligned}
a_1 &= 4E_\mathrm{p}I_\mathrm{p}[\cos(\beta L_\mathrm{p})\cosh(\beta L_\mathrm{p}) - 1],\\
a_2 &= \sin(\beta L_\mathrm{p})\cosh(\beta L_\mathrm{p}) + \sinh(\beta L_\mathrm{p})\cos(\beta L_\mathrm{p}),\\
a_3 &= \sin(\beta L_\mathrm{p})\cosh(\beta L_\mathrm{p}) - \sinh(\beta L_\mathrm{p})\cos(\beta L_\mathrm{p}),\\
a_4 &= \cos(\beta L_\mathrm{p})\cosh(\beta L_\mathrm{p}) - \sin(\beta L_\mathrm{p})\sinh(\beta L_\mathrm{p}) - 1,\\
a_5 &= -\cos(\beta L_\mathrm{p})\cosh(\beta L_\mathrm{p}) - \sin(\beta L_\mathrm{p})\sinh(\beta L_\mathrm{p}) + 1.
\end{aligned}
\tag{A.4}
$$

In the case that the flexural motion is induced by a unitary external bending moment, the coefficients C_j (for $j = 1, \ldots, 8$) become

$$\begin{aligned}
C_1 &= C_3 = b_2[a_3 \sinh(\beta z_1) + a_4 \cosh(\beta z_1) - a_3 \sin(\beta z_1) + a_5 \cos(\beta z_1)], \\
C_2 &= C_4 = b_2[a_5 \sinh(\beta z_1) + a_2 \cosh(\beta z_1) - a_4 \sin(\beta z_1) + a_2 \cos(\beta z_1)], \\
C_5 &= b_2[a_3 \sinh(\beta z_1) + a_4 \cosh(\beta z_1) - a_3 \sin(\beta z_1) + a_4 \cos(\beta z_1)], \\
C_6 &= b_2[a_5 \sinh(\beta z_1) + a_2 \cosh(\beta z_1) - a_5 \sin(\beta z_1) + a_2 \cos(\beta z_1)], \\
C_7 &= b_2[a_3 \sinh(\beta z_1) + a_5 \cosh(\beta z_1) - a_3 \sin(\beta z_1) + a_5 \cos(\beta z_1)], \\
C_8 &= b_2[a_4 \sinh(\beta z_1) + a_2 \cosh(\beta z_1) - a_4 \sin(\beta z_1) + a_2 \cos(\beta z_1)],
\end{aligned} \tag{A.5}$$

where $b_2 = (a_1 \beta^2)^{-1}$.

Appendix B

Pile-soil transformation matrix

The pile-soil interaction modelling strategy is based on the assumption that the pile is divided into N_{p} segments, each one of them behaving as a rigid solid. Therefore, the displacement of one of these segments at the collocation points located at its perimeter can be defined in terms of the translational and rotational motions of the segment centroid. Thus, the response at the n_{s}-th collocation point of the n-th segment, located at the position

$$\mathbf{x}^{n,n_{\mathrm{s}}} = \left\{ x^{n,n_{\mathrm{s}}} \quad y^{n,n_{\mathrm{s}}} \quad z^{n,n_{\mathrm{s}}} \right\}^{\mathrm{T}}, \tag{B.1}$$

can be written as a function of the pile centroid point motion of the corresponding segment $\mathbf{U}_{\mathrm{p}}^{n}$ as

$$\mathbf{U}_{\mathrm{b}}^{\mathrm{p},n,n_{\mathrm{s}}} = \begin{Bmatrix} U_{\mathrm{b}x}^{n,n_{\mathrm{s}}} \\ U_{\mathrm{b}y}^{n,n_{\mathrm{s}}} \\ U_{\mathrm{b}z}^{n,n_{\mathrm{s}}} \end{Bmatrix} = \begin{bmatrix} 1 & 0 & 0 & 0 & 0 & -y^{n,n_{\mathrm{s}}} \\ 0 & 1 & 0 & 0 & 0 & x^{n,n_{\mathrm{s}}} \\ 0 & 0 & 1 & y^{n,n_{\mathrm{s}}} & -x^{n,n_{\mathrm{s}}} & 0 \end{bmatrix} \begin{Bmatrix} U_{\mathrm{p}x}^{n} \\ U_{\mathrm{p}y}^{n} \\ U_{\mathrm{p}z}^{n} \\ \theta_{\mathrm{p}x}^{n} \\ \theta_{\mathrm{p}y}^{n} \\ \theta_{\mathrm{p}z}^{n} \end{Bmatrix} = \mathbf{W}^{n,n_{\mathrm{s}}} \mathbf{U}_{\mathrm{p}}^{n}. \tag{B.2}$$

The matrix that relates the displacement at all collocation points with the six-component motions of all pile centroid points is given by

$$\mathbf{W} = \begin{bmatrix} \mathbf{W}^{1,1} & & & & \\ \mathbf{W}^{1,2} & & & & \\ \vdots & & & & \\ \mathbf{W}^{1,N_\mathrm{s}} & & & & \\ & \mathbf{W}^{2,1} & & & \\ & \mathbf{W}^{2,2} & & & \\ & \vdots & & & \\ & \mathbf{W}^{2,N_\mathrm{s}} & & & \\ & & \ddots & & \\ & & & \mathbf{W}^{N,1} & \\ & & & \mathbf{W}^{N,2} & \\ & & & \vdots & \\ & & & \mathbf{W}^{N,N_\mathrm{s}} & \\ & & & \mathbf{W}^{N,N_\mathrm{s}+1} & \end{bmatrix}. \tag{B.3}$$

It can be demonstrated that the transpose of this matrix can also be used to determine the equivalent forces applied to the segment centroid as a result of the forces at the collocation points, having that

$$\mathbf{P}_\mathrm{p} = -\mathbf{W}^\mathrm{T}\mathbf{P}_\mathrm{b}^\mathrm{s}. \tag{B.4}$$

In the case that neither the rotations nor the bending and torsion moments associated with each segment are not desired to be accounted for in the coupling procedure, the right 3×3 matrix of $\mathbf{W}^{n,n_\mathrm{s}}$ should be replaced by a null matrix.

Appendix C

Vertical and lateral soil reaction equations

In the approximate formulation presented by Baranov [76], the soil reactions are described by

$$\begin{aligned} N_x &= GS_x u(z), \\ N_z &= GS_z w(z), \end{aligned} \tag{C.1}$$

where N_x and N_z are, respectively, the soil reactions to lateral and vertical motions, G is the shear modulus of the soil and S_x and S_z are given by

$$\begin{aligned} S_x(a_0,\nu) &= 2\pi a_0 \frac{\frac{1}{\sqrt{q}} H_2^{(2)}(a_0)H_1^{(2)}(x_0) + H_2^{(2)}(x_0)H_1^{(2)}(a_0)}{H_0^{(2)}(a_0)H_2^{(2)}(x_0) + H_0^{(2)}(x_0)H_2^{(2)}(a_0)}, \\ S_z(a_0) &= 2\pi a_0 \frac{J_1(a_0)J_0(a_0) + Y_1(a_0)Y_0(a_0)}{J_0^2(a_0) + Y_0^2(a_0)} + \frac{4\mathrm{i}}{J_0^2(a_0) + Y_0^2(a_0)}, \end{aligned} \tag{C.2}$$

where $H_n^{(2)}$ is the Hankel function of the second kind and order n, J_0 and J_1 are the Bessel functions of the first kind of order zero and one, respectively, and Y_0 and Y_1 are the Bessel functions of the second kind of order zero and one, respectively. The dimensionless frequency a_0 and the parameters q and x_0 are given by

$$a_0 = r_\mathrm{p}\omega\sqrt{\frac{\rho}{G}}, \quad q = \frac{(1-2\nu)}{2(1-\nu)}, \quad x_0 = a_0\sqrt{q}, \tag{C.3}$$

where r_p is the pile radius, ω the angular frequency, ρ is the density of the soil and ν its Poisson's ratio.